UNIVERSITY OF GENOVA

PHD PROGRAM IN BIOENGINEERING AND ROBOTICS

Advancing Knowledge of Upper Limb Motor Control Through Electromyography

by

Indya Ceroni

Thesis submitted for the degree of *Doctor of Philosophy* (38° cycle)

May 2026

Marianna Semprini	Supervisor
Paolo Massobrio	Head of the PhD program

Thesis Jury:

Ioannis Delis, *University of Leeds*	External examiner
Silvia Muceli, *Chalmers University of Technology*	External examiner
Matteo Moro, *University of Genoa*	Internal examiner

Dibris

Department of Informatics, Bioengineering, Robotics and Systems Engineering

Declaration

I hereby declare that except where specific reference is made to the work of others, the contents of this dissertation are original and have not been submitted in whole or in part for consideration for any other degree or qualification in this, or any other university. This dissertation is my own work and contains nothing which is the outcome of work done in collaboration with others, except as specified in the text and Acknowledgements. This dissertation contains fewer than 65,000 words including appendices, bibliography, footnotes, tables and equations and has fewer than 150 figures.

Indya Ceroni
April 2026

Abstract

The rehabilitation of motor functions of subjects affected by neurological disorders and amputation will benefit from any advance in our knowledge of the neuromechanical principles of motor control. Electromyography (EMG) holds the possibility to record the electrical activity originating with muscle contraction, thus offering the opportunity to quantify the mechanical direct consequences of the motor command. This project aims to characterize motor production starting from EMG signals in order to: 1) Quantitatively and objectively assess the impact of upper limb assistive devices on motor production and their potential benefits in the rehabilitation of individuals with neuromotor impairments; 2) Explore EMG-driven models that holds potential for the control of rehabilitative devices.

The first objective is addressed through a use case employing the muscle synergy framework to investigate the modular organization of motor control during a standardized reaching task performed both with and without robotic assistance from the Float upper-limb exoskeleton. The analysis is initially conducted on healthy participants to establish baseline synergy structures and to examine the extent to which these patterns are altered by robotic assistance. Subsequently, the same approach is applied to chronic post-stroke individuals to assess whether robotic assistance could induce short term modulation that could promote the restoration of physiological motor modules. This analysis provides insight into the effects of robotic assistance on the modular organization of anterior reaching movements and highlights promising influences of the Float exoskeleton on motor modularity in post-stroke individuals. Importantly, these findings have the potential to inform clinical practice by introducing objective, physiologically grounded metrics for evaluating the effectiveness of technology-assisted rehabilitation. This represents a meaningful advancement over conventional clinical scales, which are predominantly observer-dependent and are often limited by poor inter- and intra-rater reliability, as well as by floor and ceiling effects.

The second objective is addressed through another experimental framework aimed at leveraging EMG decomposition techniques and their capability of reconstructing single

motor unit activity from global surface EMG recordings. The resulting motor neuron activity patterns represent promising command signals for the control of rehabilitative devices, as they encode the central motor commands conveyed by innervating alpha-motoneurons. Within this context, the activity of individual motor units from the wrist extensors was tracked during goal-oriented reaching, grasping, and object repositioning tasks involving differently shaped objects. In parallel, the feasibility of a hand-gesture classifier based on motor unit activity was explored.
The results obtained from these analyses support the feasibility of leveraging motor neuron activity as a physiologically meaningful control signal. At the same time, they highlight the current technological and methodological limitations that hinder the immediate translation of these approaches into clinical practice.

Together, the findings of this PhD work delineate both the potential and the challenges of EMG–based tools for neurorehabilitation, providing a foundation for future investigations aimed at bridging the gap between experimental neuroengineering solutions and clinically deployable rehabilitation technologies.

Table of contents

List of figures

List of tables

Chapter 1

Introduction

1.1 Motivation

The restoration of upper limb motor function represents one of the major challenges in neurorehabilitation. Motor impairments caused by neurological injuries such as stroke, or by limb loss, often compromise the ability to perform activities of daily living and therefore significantly affect the autonomy and quality of life of affected individuals. Understanding how motor commands are generated and how they are altered by pathology is therefore a central objective for the development of effective rehabilitative interventions and assistive technologies. In this context, physiological signals that reflect neuromuscular activation provide a valuable source of information on the mechanisms underlying motor production.

Surface electromyography (EMG) provides a non-invasive window into the neural strategies underlying motor production. By capturing the electrical activity generated by muscles during movement, EMG enables the extraction of neurophysiological metrics that reflect how the central nervous system (CNS) organizes muscle activation to produce functional actions. These metrics can provide insights into both normal and pathological motor control, and can therefore play an important role in the design, evaluation, and control of rehabilitation technologies.

This PhD thesis focuses on the development and application of EMG-based methods to characterize upper limb motor production in tasks that are functionally relevant for rehabilitation. In particular, the work targets complex motor behaviors such as reaching and grasping, which represent fundamental components of many activities of daily living and are therefore frequently addressed during rehabilitative treatments.

Damage to any component of the neuromusculoskeletal system may lead to abnormal motor patterns. In neurological populations, these alterations often manifest as changes in muscle coordination, impaired motor unit recruitment, or compensatory activation strategies. Quantifying such alterations is essential both for understanding the mechanisms underlying motor impairment and for assessing the effectiveness of therapeutic interventions.

This research was conducted within the Rehab Technologies Lab of the Istituto Italiano di Tecnologia (IIT), which has long-standing expertise in the development of robotic devices for rehabilitation, with particular emphasis on active upper-limb exoskeletons and robotic prostheses. Within this context, investigating motor control is not only relevant from a neurophysiological perspective but also directly linked to the practical development and deployment of assistive robotic systems designed for neurological patients and individuals with limb amputation.

1.2 Objectives

In relation to the robotic technologies developed in the laboratory, two main research directions were identified in which EMG-derived metrics could provide a meaningful contribution:

1. Objective assessment of robotic rehabilitation devices, by quantifying how robotic assistance influences motor control strategies during functional tasks.

2. Development of EMG-driven models for the control of assistive technologies, particularly in the context of intuitive interfaces for robotic prostheses or rehabilitation devices.

Accordingly, this PhD project aims to develop and investigate reliable methods to characterize motor production from EMG signals in order to:

1. Quantitatively and objectively assess the impact of upper-limb assistive devices on motor control, and to evaluate their potential benefits for the rehabilitation of individuals with neuromotor impairments.

2. Explore EMG-derived representations of neuromuscular activity that may serve as control signals for assistive robotic systems.

1.3 Structure of the Thesis

This thesis is organized into two main parts addressing complementary aspects of EMG-based characterization of motor control:

1. Part I focuses on the use of muscle synergy analysis (1) to characterize the impact of robotic assistance on the modular structure of reaching movements. Using the Float upper limb exoskeleton developed by the Rehab Technologies Lab (2) as a case study, this part examines how modular muscle coordination is modulated by robotic assistance in healthy individuals and in post-stroke patients.

2. Part II adopts a more exploratory perspective and investigates the use of high-density EMG (hdEMG) to study the activity of individual motor units (3) during grasping tasks in healthy individuals. By analyzing the neural drive to muscles at the motor unit level, this work aims to explore potential neural features that could be exploited for the control of assistive devices such as robotic prostheses.

Each part presents a set of studies framed within the relevant literature and designed to address specific research questions related to the two PhD objectives (Sec 1.2).

Across both parts of the thesis, particular attention is devoted to the use or development of standardized experimental frameworks that enable reproducible and comparable characterization of motor control across populations and robotic platforms. Establishing such frameworks is essential to facilitate the translation of neurophysiological metrics into practical tools for rehabilitation assessment and assistive technology development (4).

1.4 Overview of Part I: Muscle synergy based characterization of exoskeleton-assisted reaching

1.4.1 Motivation

Substantial evidence indicates that motor recovery after neurological injuries is enhanced by intensive, repetitive, and task-oriented training (5). This evidence has supported the integration of robotic devices into neurorehabilitation practice. In recent years, many different robotic devices have been introduced to support the rehabilitation of upper-limb motor function (6; 7). Robot-assisted arm training has demonstrated promising effects in improving activities of daily living (ADLs), upper limb motor function, and muscle strength in individuals post-stroke (8; 9; 10).

Currently the assessment of the effectiveness of technology-assisted interventions rely mainly on clinical scales. Clinical scores are intrinsically observer-based and have poor inter-rater and intra-rater reliability, and floor and ceiling effects (11).

EMG signals, on the contrary, allow the extraction of neurophysiological metrics that are independent of the observer and have shown potential as biomarkers to objectively assess the impact of assistive devices (10; 12).

Over the last two decades, it has been proposed that the key organizational principle of the central nervous system (CNS) could be modularity, and that the diverse motor outputs could be generated by the combination of a small number of structural modules. A prominent model for such modularity is the muscle synergy model (1).

Synergy-based analyses have been widely used to investigate differences in motor coordination between healthy individuals and neurological patients (13). Moreover, several studies have shown that muscle synergy analysis can provide clinically relevant information that complements traditional clinical scales and kinematic analyses, enabling researchers to quantify the effects of rehabilitative interventions and to investigate how such interventions influence the organization of motor control (10; 14). These insights can also inform the design and clinical application of robotic devices by highlighting how robotic assistance interacts with the underlying neuromuscular control strategies.

Nevertheless, despite the growing body of evidence supporting the relevance of muscle synergy analysis, its adoption as a systematic tool for the evaluation of rehabilitation technologies remains limited (14).

1.4.2 Objective

The objective of this part of the thesis is to investigate whether muscle synergy analysis can provide a meaningful framework to characterize how robotic assistance influences the modular organization of muscle activity during reaching movements.

In particular, this work aims to evaluate the feasibility of using synergy-derived metrics to quantify the effects of the Float upper-limb exoskeleton developed at the Rehab Technologies

Lab of the Istituto Italiano di Tecnologia (2). Furthermore, it explores the potential of these metrics as objective biomarkers for assessing the effects of robotic rehabilitation interventions on motor coordination.

1.4.3 Structure

To address the above mentioned objective, the studies presented in this part of the thesis were conducted using a standardized benchmarking framework named NeBULA (Neuromechanical Biomarkers for Upper Limb Assessment). NeBULA implements a structured reaching task paradigm designed to extract neuromechanical biomarkers derived from electromyography (EMG) and electroencephalography (EEG), enabling reliable and repeatable quantification of the effects of robotic assistance on motor control during functional tasks (4; 15). The NeBULA framework is described in detail in Chapter 2.

Pilot studies conducted in healthy populations represent an important step in the development and validation of rehabilitation technologies. They allow researchers to refine experimental paradigms and provide reference baselines that can later be used to interpret results obtained in clinical populations (7; 16; 17). Following this approach, the first stage of the research focused on characterizing the impact of the Float exoskeleton on motor coordination in healthy individuals.

Within the context of this PhD project, two studies were conducted on healthy participants to preliminarily assess the effects of Float assistance on the organization of muscle synergies during reaching movements. The first study, presented in Chapter 3, investigates how assistance provided by the Float exoskeleton influences the synergistic organization of muscle activation during reaching. The results of this study also provide insights that may inform future iterations of exoskeleton design.

The second study, described in Chapter 4, aims to establish a reliable reference set of muscle synergies characterizing reaching movements in both unassisted and assisted conditions in healthy individuals. This reference set is intended to serve as a baseline for comparison with neurological populations. It aims to establish a reliable reference set of synergies from healthy individuals to be used as a baseline for comparison with neurological patients. It also explores the potential influence of age as a contributing factor to the high degree of inter-subject differences in muscle synergies structure observed across healthy individuals.

Finally, the muscle synergy framework was applied in a preliminary study involving post-stroke subjects to explore whether assistance provided by the Float exoskeleton may promote the emergence of more physiological patterns of muscle coordination, as suggested in previous rehabilitation studies (10; 18). As part of this effort, I contributed to the collection of experimental data from post-stroke participants performing anterior reaching tasks before and after receiving assistance from the Float exoskeleton. A preliminary analysis was conducted to compare the muscle synergies of the paretic arm of five post-stroke subjects with the reference synergies derived from the healthy population. The results of this exploratory study are presented in Chapter 5.

1.5 Overview of Part II: Motor units based characterization of grasping

1.5.1 Motivation

Motor units constitute the fundamental elements through which the central nervous system (CNS) controls muscle contraction. The discharge of motor units reflects the activity of spinal motor neurons, which represent the final neural pathway through which voluntary motor commands are transmitted to the muscles before being translated into force production and movement (19). For this reason, the analysis of motor unit discharge patterns provides direct access to the neural drive to muscles and has been proposed as a promising source of control signals for human–machine interfaces and assistive technologies.

Recent advances in myoelectric upper-limb prosthetics have enabled the control of devices with multiple degrees of freedom (DoFs) (20). Among the different approaches, pattern recognition techniques have become one of the most widely explored strategies to allow intuitive multi-DoF control and have recently been implemented in commercial prosthetic systems (21). Despite these technological advances, current myoelectric control strategies often suffer from limited robustness and generalization, which contributes to high rates of prosthesis abandonment among users (22).

One of the most widely reported limitations of pattern recognition–based control is the degradation of classification performance across different arm configurations (23). Changes in limb posture can significantly alter the surface EMG signals used by control algorithms, leading to reduced reliability during everyday use. Previous studies have mainly investigated these effects at the level of global EMG features (24). However, it remains unclear how variations in arm configuration influence the activity of individual motor units, which represent the fundamental contributors to the surface EMG signal.

Advances in hdEMG decomposition techniques now make it possible to estimate the discharge patterns of multiple motor units non-invasively (3). By reconstructing motor unit activity, these methods allow the investigation of the neural drive to muscles during voluntary movement. However, reliable motor unit decomposition during dynamic and functional movements remains challenging, as most studies have been conducted under highly controlled isometric conditions.

1.5.2 Objective

Within this context, the studies presented in this part of the thesis aim to explore the feasibility and potential benefits of analyzing motor unit activity during goal-directed movements that are relevant for daily life, such as reaching and grasping. Characterizing the neural drive to muscles during these functional behaviors could provide valuable insights for the development of more physiologically grounded control strategies for assistive technologies.

1.5.3 Structure

To support the systematic investigation of such movements, a standardized experimental framework was developed to characterize goal-directed upper-limb behaviors including reaching, grasping, and object transport. Inspired by the NeBULA framework described in Chapter 2, this protocol integrates structured grasp and manipulation tasks within a scalable and reproducible assessment platform and is named ReGULA (Reach and Grasp for Upper Limb Assessment). The development of ReGULA was carried out in collaboration with two other PhD researchers and provides a foundation for future investigations into both prosthetic control strategies and neurophysiological mechanisms of motor control.

Within this framework, the study presented in Chapter 7 investigates how variations in arm configuration influence motor unit activity during grasping tasks and examines the neural mechanisms underlying the well-documented degradation of pattern recognition performance across limb postures (24).

The study described in Chapter 8 extends this analysis by evaluating whether features derived from motor unit discharge patterns can enhance traditional EMG-based pattern recognition approaches. In particular, this work explores whether neural-level descriptors extracted from motor unit activity can provide improved robustness and physiological interpretability for the control of upper-limb prostheses.

Part I

Muscle synergy based characterization of exoskeleton-assisted reaching

Chapter 2

NeBULA Experimental framework

2.1 NeBULA: Neuromechanical Biomarkers for Upper Limb Assessment

All the studies included in Part I are based on a standardized framework named NeBULA (Neuromechanical Biomarkers for Upper Limb Assessment), developed by our research group as a reliable and reproducible assessment tool to quantify the effects of robotic rehabilitation devices across different neurological populations. NeBULA was conceived to address the need for reliable biomarkers (25), i.e. objective, accurate, and repeatable quantitative measures of motor function, that reflect neuromechanical aspects of upper-limb control enabling objective comparisons across subjects, conditions, and interventions. These biomarkers are derived from task execution and include motor-control–relevant metrics such as muscle synergies.

To this end, NeBULA relies on a standardized reaching task implemented through an adjustable and programmable sensorized panel, which guides task execution while adapting the workspace to individual anthropometric characteristics. This framework enables the extraction of reliable biomarkers, under controlled and repeatable experimental conditions.

The application of the NeBULA framework to the assessment of the Float exoskeleton represents a first use case aimed at demonstrating the feasibility and usefulness of the framework.

Although both the NeBULA paradigm and the use case involving the Float exoskeleton were conceived prior to the start of my PhD program, this Chapter provides a comprehensive description of them to establish a clear and unified context for the studies presented in Chapters 3, 4, and 5.

2.2 Rationale

In the last decades, the employment of robotic devices in the rehabilitation process has been widely explored (26), as they own the potential to increase the intensity of the rehabilitative treatment and improve its outcomes (5). As interest in robotic rehabilitation technologies continues to grow, the objective assessment of their performance from the early stages of design and development has become increasingly important (27).

In this context, the ultimate goal of the NeBULA paradigm is to provide an objective framework for assessing the performance and potential clinical benefits of rehabiliative robots, thereby enabling systematic evaluation and comparison across different technologies. To pursue this goal, NeBULA implements the standardized execution of anterior reaching, identified as one of the motor skill relevant to neurorehabilitation in the taxonomy by Magill and Anderson (28) and applied in the clinical benchmarking scheme proposed by Longatelli and colleagues (11).

2.3 Sensorized platform for standardized reaching

The standardized execution of the motor skill anterior reaching is enabled and guided by an adaptable touch panel. This panel acts as the central interface for participants, who can be seated or standing, to undertake self-paced reaching tasks. It is endowed with multiple targets that can be moved to adjust different anthropometric measures. It can accommodate both the patient's and any accompanying robotic aids' spatial requirements, ensuring targets are within a full arm's reach. This configuration balances the need for standardized movement and the emulation of natural motion.

Each target has a LED indicator used to cue the participant to reach that target and a capacitive cover that allow the precise identification of the time instant in which the participant reaches the target. The panel can be programmed to customize the target activation sequences and timings. Each reaching trial is initiated through a push button which also acts as a physical TTL trigger that can synchronize different measurement systems, enabling a comprehensive and multimodal characterization of the anterior reaching motor skill. The platform is also designed to record time-related events, capturing both the sequence of movements and the participant's behavioral responses. The main features of the adjustable touch panel are shown in Figure 2.1.

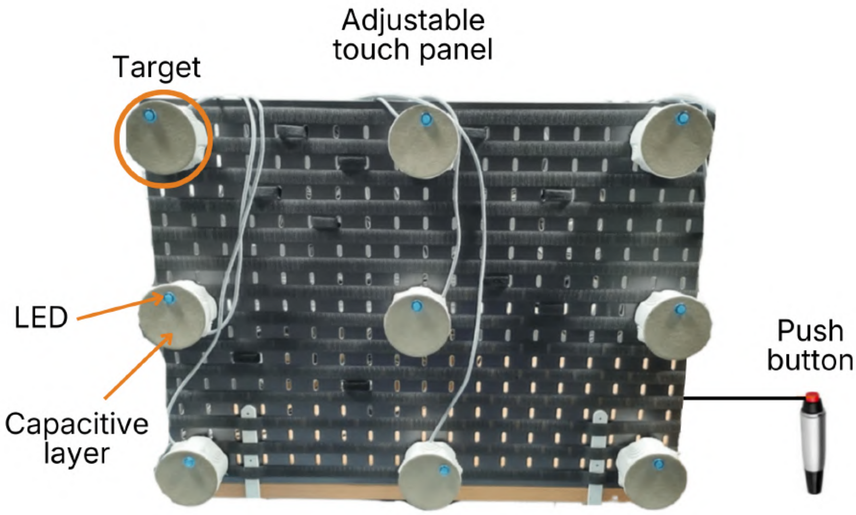

Figure 2.1 Main features of the adjustable touch panel used to standardize reaching in the NeBULA framework.

2.4 Assessment of Float upper limb exoskeleton

The first use case that allowed us to test the efficacy of the NeBULA framework in a real-life scenario was the assessment of the impact of the Float upper limb exoskeleton on the neurophysiology of reaching.

2.4.1 Float upper limb exoskeleton

The Float exoskeleton has been developed by Rehab Technologies Lab of IIT for the rehabilitation of the shoulder complex in orthopaedic and neurological subjects (2). It features 5 rotational joints that reproduce all the degrees of freedom of the shoulder complex. A corset and a passive upper-limb orthosis are integrated in the exoskeleton to ensure a stable and safe connection between the user and the robot. The links of the exoskeleton can be adjusted to align the motors to the right shoulder of the user. The control modality used in our studies implements a model-based compensation of friction at each joint while providing active feed-forward assistance at the level of joint J4 acting to flex the shoulder (Figure 2.2). In this modality the user should not perceive the weight and the inertia of the robot and should perceive a reduced effort when performing upward movements of the arm. The feed-forward assistance provided at joint J4 to flex the shoulder can be set at two levels (low or high), which have been tuned empirically as described in (2).

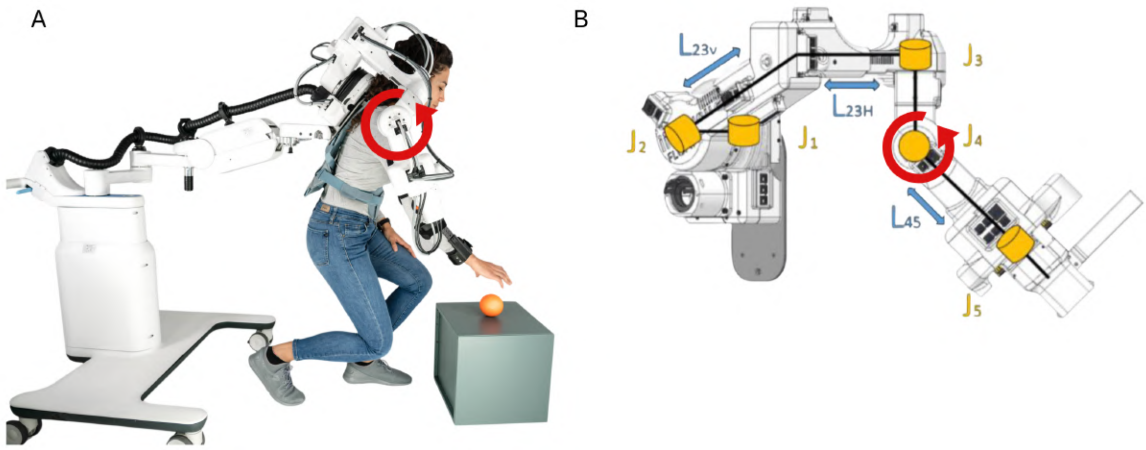

Figure 2.2 A) Float upper limb exoskeleton worn by a healthy subject. B) Mechanical structure of Float. The red arrow indicates the direction of the assistance provided by J4 which act to facilitate shoulder flexion.

2.4.2 Data collections

Healthy subjects

A first data collection on 40 healthy individuals has been conducted and is described in detail in (15). The protocol was designed to characterize the impact of Float's assistance on motor control and it involved the execution of standardized reaching first without Float and subsequently with Float providing low and high assistance in a randomized order. The experimental procedures were approved by the local ethical committee (Comitato Etico Regionale della Liguria: 784/2022 - DB id 12044) and the data acquisition was split into two parts:

1. The first 20 subjects were collected prior to the beginning of my PhD program. The panel was programmed to guide the execution of 10 pseudorandomized repetition of reaching towards 9 targets arranged as in Figure 2.1. This data have been analyzed in the study presented in Chapter 3, which explores the impact of Float on the modularity of anterior reaching.

2. During the first months of my PhD program I supported the collection of the last 20 subjects. In this data collection, the panel guided the execution of 10 pseudorandomized repetition of reaching towards 3 targets arranged as the three central targets in Figure 2.1.

During the second part of the data collection on healthy subject, the task was simplified to reduce both participant effort and overall experimental duration, with the aim of making the paradigm suitable for future application in post-stroke populations. To this end, reaching movements were restricted to three of the nine targets used in the original protocol. The three central targets were selected because Float provides assistance primarily in the vertical plane by supporting shoulder flexion, and thus the effects of the assistance were expected to be observable within this reduced workspace.

While this simplification limits the variability of the explored reaching motion and consequently the richness of motor behaviors that can be characterized using the muscle synergies framework (14), it represents a compromise to accommodate clinical time constraints and ensure feasibility in patient populations. Figure 2.3 shows the experimental paradigm for the two halves of the dataset collected on healthy individuals.

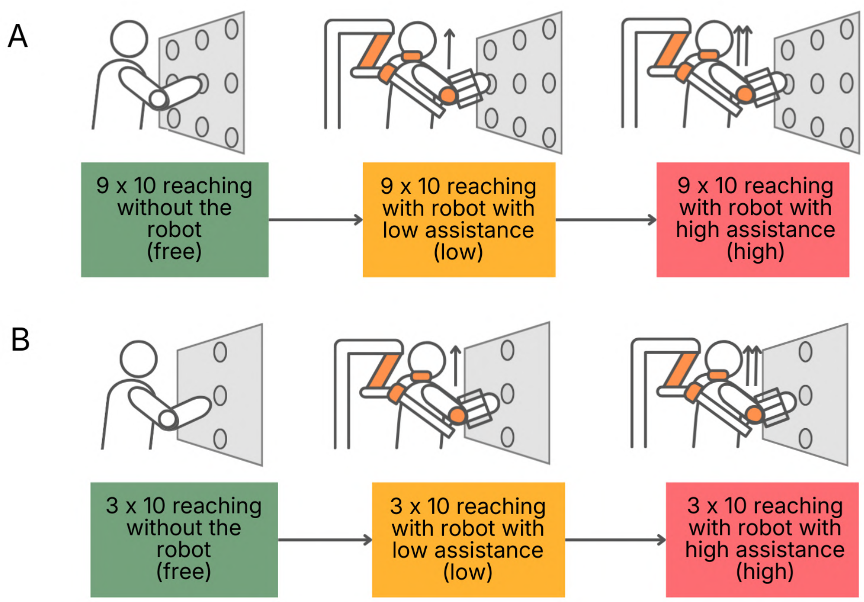

Figure 2.3 Experimental protocol for the first 20 subjects (A) and for the last 20 subjects (B) of the data collection on healthy individuals. The order of the two assistance levels was randomized across participants.

The study presented in Chapter 4 has been conducted on the entire population of 40 right-handed healthy individuals (20 males, 20 females age 44.6 $\pm$ 13.2 years old). For comparability between the two experimental protocols, data from the first 20 participants were restricted to reaching movements toward the three central targets, matching the protocol adopted for the remaining participants. The study of Chapter 4 aims to establish a reliable reference set of synergies from healthy individuals to be used as a baseline for comparison with neurological patients. It also explores the potential influence of age as a contributing factor to the observed high degree of inter-subject differences in muscle synergies structure.

In the data collection on healthy subjects, the adjustable touch panel has been synchronized with the Actichamp EEG amplifier from Brain Products, with the Cometa Waveplus EMG system and with the Float exoskeleton itself.

Figure 2.4 shows the setup used for data acquisition with healthy subjects.

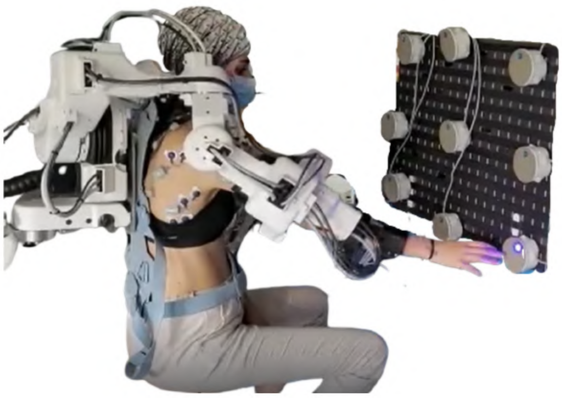

Figure 2.4 Setup for data acquisition with healthy subjects.

Post-stroke subjects

I also took part in a data collection on 36 chronic post stroke subjects (18 with right hemiparesis and 18 with left hemiparesis), that has been conducted at the Villa Beretta rehabilitation hospital in Costa Masnaga.

The data collection received the approval by the local ethics committee Comitato Etico Lombardia 5 (protocol code: IIT REHAB NeBULAS). Only post-stroke subjects who had experienced the last stroke acute event at least six months prior to the experimental session were included in the study. 36 post-stroke volunteers took part to the study (24 males and 12 females, 53.78 $\pm$ 11.37 years old, 66.86 $\pm$ 81.36 months from the last acute event)

The data collection followed the simplified paradigm involving the execution of reaching towards three central targets. The experimental protocol consisted of 10 reaching movements toward each of three targets presented in a pseudorandomized order. The reaching task was performed first without Float (Pre condition), then with Float assistance (Float condition), and finally again without Float (Post condition). This paradigm was designed to test if the assistance of Float could induce short-term modifications in the control of the affected or less-affected shoulder of chronic post-stroke subjects.

All participants received Float assistance on the right shoulder; the assistance level was set to high for subjects with right hemiparesis and low for subjects with left hemiparesis. Figure 2.5 provides a schematic representation of the experimental paradigm.

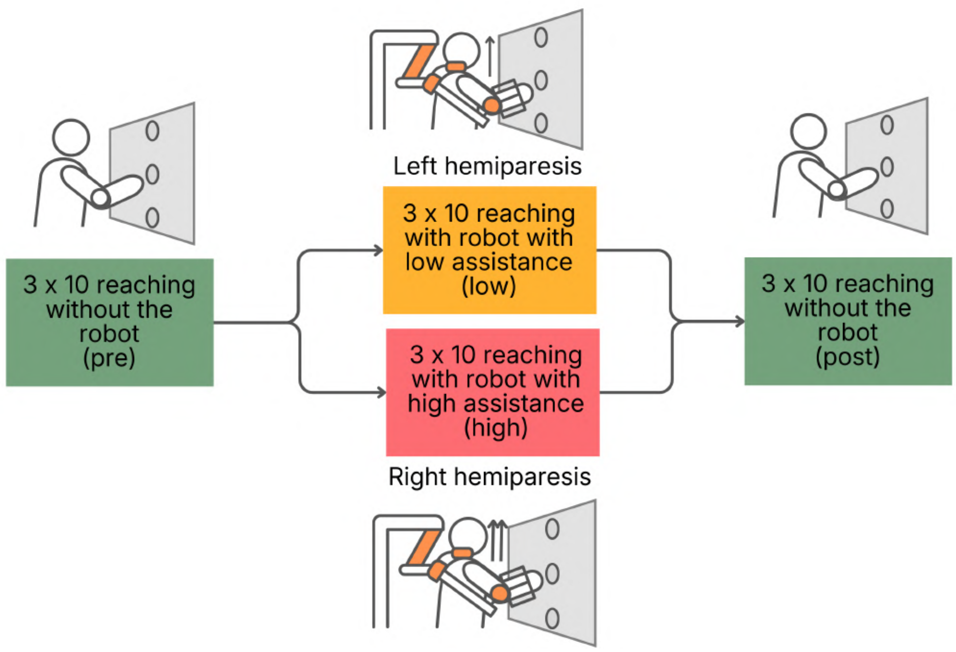

Figure 2.5 Experimental protocol for the data acquisition with post-stroke subjects.

EEG, EMG and Kinematic data were simultaneously recorded using the SynAmps RT 64 channel EEG Amplifier from Compumedics, the FreeEMG 1000 wireless system from BTS Bioengineering and the SMART DX EVO optoelectronic from BTS Bioengineering. The acquisition systems has been synchronized with the Float exoskeleton thanks to the TTL trigger provided by the panel.

Differently from previous acquisitions with healthy individuals, the data collection with post-stroke subjects involved also the use of infrared cameras and reflective markers to track the kinematic of the subject and of the exoskeleton. To minimize markers' occlusion, the panel has been substituted with a vertical support holding three targets placed at three different heights. The position of the targets was adapted to the reaching workspace of each subject. Figure 2.6 shows the experimental setup used for data acquisition with post-stroke subjects.

Figure 2.6 Setup for data acquisition with post-stroke subjects.

The study presented in Chapter 5 shows a preliminary evaluation of the impact of Float on the pattern of muscle activity in 5 post-stroke subjects with right hemiparesis.

Chapter 3

Modular characterization of unassisted and exoskeleton-assisted reaching

The study presented in this Chapter applies the muscle synergies paradigm to assess whether and how the assistance provided by the Float upper limb exoskeleton affects the modular organization of physiological reaching movement. The work is part of a use case that exploits the NeBULA framework to quantitatively assess the impact of the Float exoskeleton on the neurophysiology of reaching.

This study formed the basis for an extended abstract presented orally at the 6th International Conference on NeuroRehabilitation (ICNR 2024) and for a conference paper presented as a poster at the 9th IEEE/RAS-EMBS International Conference on Rehabilitation Robotics (ICORR 2025):

1. *I. Ceroni, F. Garro, and M. Semprini, "Modular Organization of Reaching Movement Performed With and Without the FLOAT Upper Limb Exoskeleton," in Converging Clinical and Engineering Research on Neurorehabilitation V, J. L. Pons, J. Tornero, and M. Akay, Eds., Cham: Springer Nature Switzerland, 2025, pp. 352–356.*

2. *I. Ceroni, F. Garro, and M. Semprini, "Effect of Robotic Assistance on the Synergistic Organization of Reaching Movements," IEEE International Conference on Rehabilitation Robotics, vol. 2025, pp. 796–801, May 2025.*

3.1 State of the art

Wearable robotic devices for rehabilitation own the potential to improve the outcome of rehabilitative treatments by increasing the intensity and repeatability of the performed exercises (5). However, despite advancements in mechatronic design and control, these devices can influence how motor actions are performed, making it crucial to monitor differences with unassisted movements.

In the literature, it is common practice to first evaluate robotic rehabilitative interventions in healthy populations before their application in clinical settings. These pilot studies enable the characterization of the effects of robotic assistance on motor control and muscle activation in a controlled context, providing a reference baseline for comparison with patient data. This approach facilitates the assessment of the rehabilitative potential of the technology, informing its clinical use, and supporting the identification of its areas for improvement. In this context, muscle synergies represent a valuable quantitative framework for evaluating the impact of robotic assistance on muscle coordination. Several research groups have relied on muscle synergies to explore the effects of robotic assistance on muscle activations in healthy individuals before moving to clinical populations (7; 16; 29).

3.2 Objectives

In the present study, muscle synergies are used to assess whether and how the assistance provided by the Float upper limb exoskeleton affects the modular organization of physiological reaching movement. This study aims to: (i) characterize the synergistic organization of reaching in unassisted and in exoskeleton-assisted movements; (ii) investigate modulation of level of assistance on synergy recruitment. From these findings, we will derive implications for further iterations of exoskeleton design.

3.3 Materials and methods

3.3.1 Participants

20 healthy right-handed subjects participated in this study (10 male, 10 female, age 31.6+/-6.2 years old). Subjects with any chronic inflammatory diseases, orthopedic conditions or neuro-muscular disorders were excluded from the study. All participants signed an informed

consent and the experimental procedures were approved by the local ethical committee (CER Liguria: 784/2022 - DB id 12044).

3.3.2 Experimental task

During the experiment, participants seated in an adjustable chair in front of the touch panel where 9 targets were placed according to the anthropometric measures of the subject (Figure 3.1).

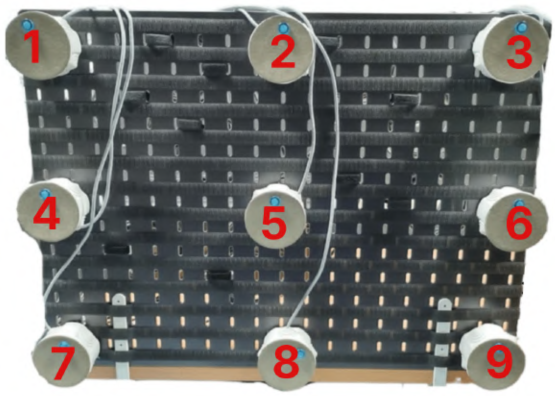

Figure 3.1 Target configuration used for the study.

The middle target was aligned with the shoulder joint of the participants and the other targets were placed to allow the participants to reach them comfortably. Participants were instructed to reach the targets with the right hand at a self-paced comfortable speed. They were instructed to start with the arm relaxed and the right hand leaning on the thigh and to reach all the targets with the elbow fully extended.

Participants were cued with LED light indicators to reach each of the nine targets ten times in a pseudo-randomized order. Each participant repeated the reaching paradigm three times: first without wearing Float, and subsequently wearing Float providing low assistance and high assistance. The order of assistance levels was randomized. Figure 3.2 depicts the entire workflow of the experiment.

We recorded bipolar surface EMG from 10 muscles of the right upper limb: biceps brachii (long head), anterior deltoid, middle deltoid, posterior deltoid, triceps brachii (long head), upper trapezius, medial trapezius, lower trapezius, pectoralis major and brachioradialis. The Cometa Waveplus System was used to acquire the EMG signals at 1 KHz. The electrode placement (shown in Figure 3.3) followed the SENIAM guidelines (30).

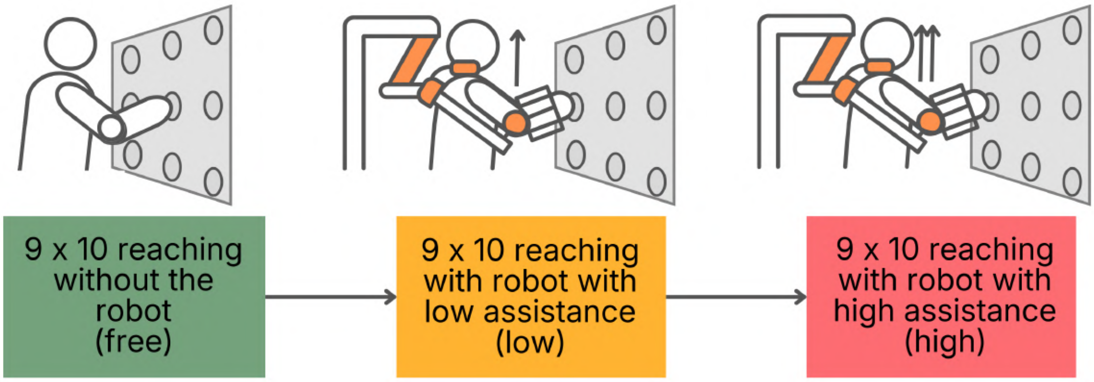

Figure 3.2 Experimental procedure.

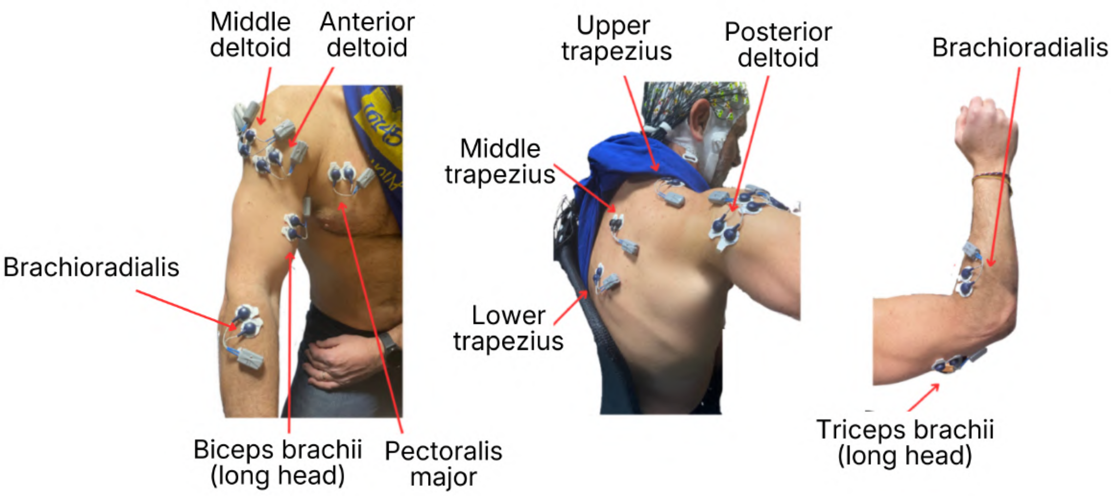

Figure 3.3 EMG electrodes positioning.

3.3.3 Data segmentation and preprocessing

We epoched the EMG recording of each subject into single trials using the logs generated by the touch panel: the reaching phase was identified as the interval between the cue light turning on and the subject touching the correct target.

For each epoch, we applied a 4th order Butterworth band-pass filter with zero-phase distortion between 20 and 350 Hz and rectified the signal. Then, we applied an ad-hoc median filter to identify values over 600 μV, which were substituted with the median value calculated over a 50-sample sliding window. Subsequently, we applied a 4th order Butterworth low-pass filter with zero-phase distortion at 5 Hz to obtain the envelope of the signal. We then normalized the EMG envelopes taking the maximum value achieved for each muscle in the complete dataset (31). Finally, since the task was self-paced, we time-scaled all epochs to the same duration of 500 samples (0.5 s) (16).

3.3.4 Muscle synergies extraction

In order to observe the motor control strategies that emerge with the use of the Float exoskeleton in the context of our standardized paradigm, we compared synergies obtained from unassisted movements with synergies derived from the entire experimental paradigm (combining both assisted and unassisted tasks).

We thus extracted the muscle synergies for each subject, grouping the experimental tasks as follows:

1. Including only the sequence executed without the assistance of Float. We named these synergies *free_synergies*; they characterize the modularity of the unassisted anterior reaching movement in the vertical plane.

2. Including all the sequences executed with and without the assistance of Float. We named these synergies *whole_synergies*; they describe the entire experimental paradigm and characterize the effect of robotic assistance.

For *free_synergies* and *whole_synergies* we concatenated the epochs to obtain a matrix of $[n_{muscles} \times (n_{samples} \cdot n_{epochs})]$. Subsequently, we used the non-negative matrix factorization algorithm (NNMF) (32) to extract the spatial synergies. The NNMF linearly separates the concatenated EMG matrix into a set of N time-invariant synergies w_i and N time-varying activation coefficients $c_i(t)$ as described in the equation:

$$EMG(t) = \sum_{i=1}^{N} c_i(t) w_i \tag{3.1}$$

Where N is the number of extracted synergies. Each spatial synergy w_i is a set of 10 weights describing how muscles synergistically couple to each other to produce movements. The coefficients of activation $c_i(t)$ describe how much each synergy is active during movement.

For each subject, we selected N as the minimum number of synergies necessary to explain the 90% of data variation. We quantified the amount of explained data variation using the Variance Accounted For (R^2 or VAF) metric, defined as 1 - SSE/SST where SSE is the sum of the squared residuals and SST is the sum of the squared differences with the mean EMG vector (31).

Thus, we performed the factorization multiple times with N increasing from 1 to the number of muscles (which represent the maximum possible dimensionality of the system). Once the computed VAF reached 0.9, we stopped the iterative factorization and retained the latest extracted synergies. During each factorization procedure, we applied the NNMF algorithm 100 times to avoid local minima.

3.3.5 Computation of reference synergies

To represent the modular structure shared across the 20 participants, we started from the *free* and *whole_synergies* extracted for each individual subject. These subject-specific synergies were then combined to obtain a set of *free* and *whole_synergies* representative of the entire cohort, hereafter referred to as reference synergies.

The reference synergies were computed using a procedure similar to that described in (16), which consisted of the following steps:

1. We computed the average number of synergies (avg_syn) across the 20 participants. This was done as subjects were expected to have a different number of synergies due to the VAF criterion used during the factorization and described in Section 3.3.4.

2. We repeated the synergies extraction procedure for each subject now setting the number of synergies apriori as avg_syn.

3. We run a clustering procedure to account for the fact that not all subjects shared the same synergies, and that the shared synergies could be extracted in different order across different subjects due to the random initialization of the NNMF algorithm. For this, we clustered the single subject synergies obtained from step 2 based on which muscle is the most expressed in the synergy (i.e., the muscle with the higher weight).

We prevented the presence of two or more synergies from the same subject in the same cluster.

4. We selected the clusters that had a number of elements equal or greater than 10 (half of the number of subjects). We averaged the synergies in such clusters to obtain a set of comparative synergies.

5. For each subject, we matched the synergies obtained from step 2 with the comparative synergies based on the value of cosine similarity (31). Cosine similarity refers to the cosine of the angle between the vectors representing the spatial synergies and can range from 1 (identical synergies) to 0. We excluded single subject synergies that did not reach a cosine similarity of at least 0.5 with any of the comparative synergies.

6. We averaged the single subject synergies that were matching the comparative synergies to obtain synergies representative of the modularity shared among the 20 subjects that participated in the experiment.

Figure 3.4 summarizes the steps detailed above.

To characterize the effect of the assistance of Float on the modular organization of anterior reaching, we computed the cosine similarity between the reference *free* and *whole_synergies*.

3.3.6 Computation of activation coefficients

To quantify the effect of robotic assistance in each assisted condition (low and high assistance) and in each of the nine movement direction, we computed the activation coefficients of the reference *free* and *whole_synergies* at the subject level for each repetition of each movement.

Specifically, we calculated the Moore-Penrose pseudoinverse (33) of the reference synergies and computed the dot product of the pseudoinverse with the matrix of concatenated EMG of each subject, as in (16). We averaged the values of each activation coefficient across repetitions of the same movement. We obtained the activation coefficients of the *free* and *whole_synergies* for each movement direction for each subject, which ranged from 0 to 1 and were distributed over 500 temporal samples.

We divided the time span of 500 samples into 3 equal segments, and we computed the integral of the activation coefficients over each segment. Wilcoxon signed rank test was performed on the estimated integrals to test for any statistical difference between the activation coefficients of each synergy in the free, low, and high assistance conditions. The results were corrected for multiple comparisons following the Bonferroni criterion.

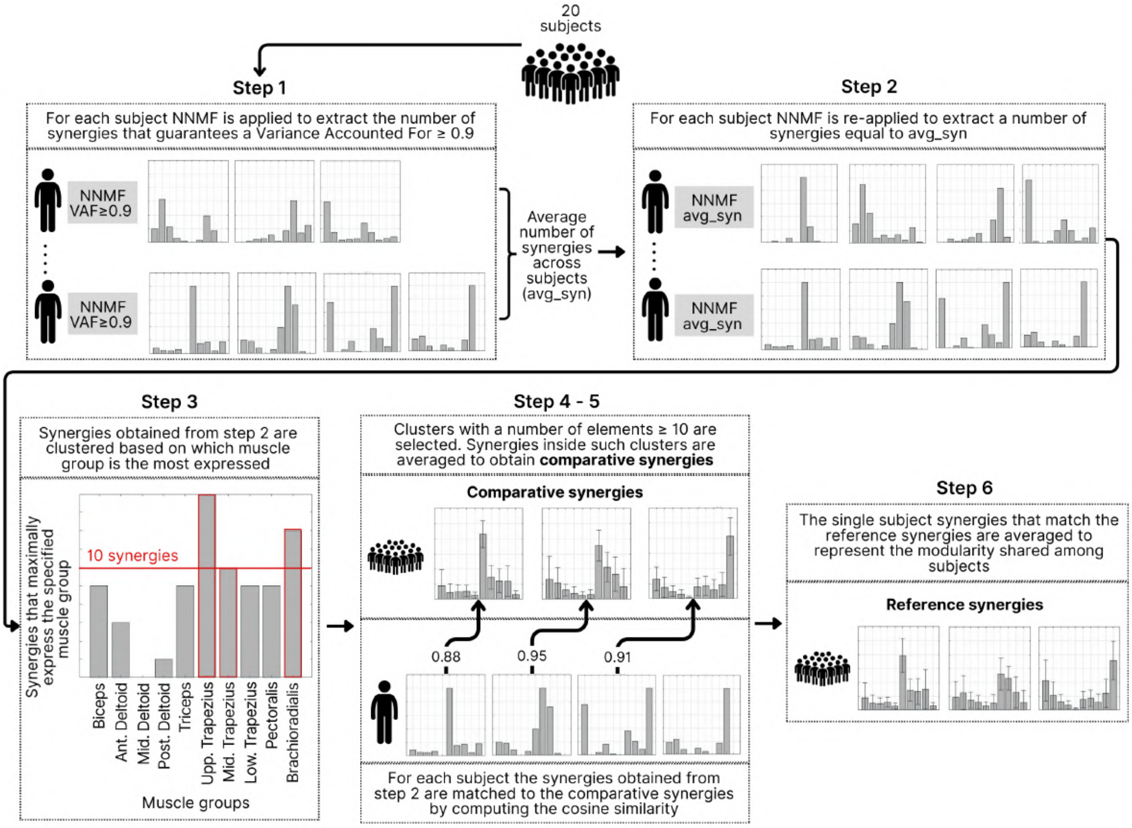

Figure 3.4 Schematic procedure for obtaining the reference synergies representing the modularity shared among the 20 subjects that participated in the study. NNMF: non-negative matrix factorization; avg_syn: average number of synergies among the subjects.

3.4 Results

3.4.1 Effect of robotic assistance on muscle synergies

Figure 3.5 describes the composition of the reference synergies and their modulation due to robotic assistance:

- The first *free_synergy* is dominated by the biceps brachii and brachioradialis, which act synergistically to generate elbow flexion. In addition, the pectoralis major shows a substantial contribution, suggesting a coordinated coupling between elbow flexion and shoulder control. Specifically, this synergy links the elbow flexor activity of the biceps and brachioradialis with pectoralis major activation, supporting shoulder horizontal adduction, flexion, and internal rotation during anterior reaching.

- The second *free_synergy* expresses mainly the deltoids, with a predominance of the anterior deltoid. Middle and lower trapezius also show relevant contribution. These muscle groups work together to enforce a smooth shoulder flexion with the scapula stabilizers (middle and lower trapezius) supporting the action of the anterior deltoid for an efficient movement production.

- The third *free_synergy* primarily expresses the trapezius with a prominence of the upper part, which acts to elevate and upwardly rotate the scapula to favor arm elevation during reaching.

The reference *whole_synergies* appear more sparse than the *free_synergies*:

- The first *whole_synergy* expresses mainly the bicep and the brachioradialis and has a high similarity with the first *free_synergy* (0.98). Differently from the first *free_synergy*, in the first *whole_synergy* the pectoralis major does not have a relevant contribution.

- The second *whole_synergy* expresses mainly the deltoids, with a predominance of the anterior deltoid. the contribution of middle and lower trapezius is lower than in the second *whole_synergy*, but the similarity is extremely high (0.99).

- The third *whole_synergy* express a significant activation of the trapezius muscle with the predominance of the upper trapezius and has a high similarity with the third *free_synergy* (0.98). The contribution of the middle and lower trapezius is lower in the *whole_synergy* with respect to the *free_synergy*.

- The fourth and fifth *whole_synergies* express mainly the middle and lower trapezius acting to medially rotate and retract the scapula.
- The fifth *whole_synergy* shows a major contribution of the pectoralis major, providing shoulder adduction, flexion, and internal rotation.

The presence of three reference *whole_synergies* closely matching the *free_synergies* indicates that the modular organization of unassisted reaching is still present during assisted movements but a higher number of synergies is needed to describe the movement. The presence of three additional *whole_synergies* exhibiting a predominance of middle trapezius, lower trapezius and pectoralis major can be explained by the absence of a relevant contribution from these muscles in the three matching synergies. The greater sparseness of *whole_synergies* suggests that the control of joint movements is more fragmented when movements are assisted by Float.

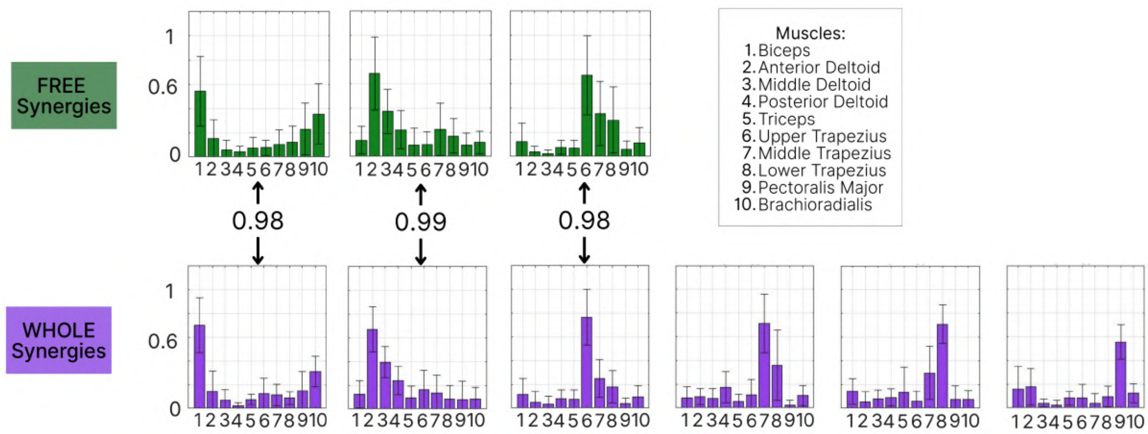

Figure 3.5 Reference *free* and *whole_synergies*. Values of cosine similarity are depicted between matching synergies.

3.4.2 Effect of robotic assistance on activation coefficients

The analysis conducted on the activation coefficients of the *free* and *whole_synergies* highlighted significant differences between the unassisted movements (free conditions) and the movements executed with Float providing high assistance (high condition) in specific phases of movements towards targets 1,2,5 and 9. Such significant differences were found for the coefficients of the third *free_synergy* and of the third *whole_synergy* which are characterized by a predominant presence of the upper trapezius. Specifically:

- In the initial phase of reaching towards target 1, the integral of the activation coefficient of the third *free_synergy* is significantly higher (p-value of 0.00039) in the high condition with respect to the free condition.
- The same difference was found in the initial phase of reaching towards target 2 (p-value of 0.00052).
- In the final phase of reaching towards target 9 the integral of the activation coefficient of the third *free_synergy* is significantly higher in the high condition with respect to the free condition (p-value of 0.00045).
- In the final phase of reaching towards target 5, the integral of the activation coefficient of the third *whole_synergy* is significantly higher in the high condition with respect to the free condition (p-value of 0.00039).

All the significant differences are summarized int Table 3.1. Figure 3.6 and Figure 3.7 depicts the activation coefficients for movements towards target 1 and target 5 respectively.

Synergy	**Target**	**Phase of movement**	**Condition**	**p-value**
free_synergy 3	1	initial	free vs high	0.00039
free_synergy 3	2	initial	free vs high	0.00052
free_synergy 3	9	final	free vs high	0.00045
whole_synergy 3	5	final	free vs high	0.00039

Table 3.1 Results of the comparison of activation coefficients among experimental conditions.

Figures 3.6 and 3.7 show also a decrease in the activation coefficients of the second *free* and *whole_synergies*. This decrease, although not significant, is relevant as the second *free* and *whole_synergies* primary express the anterior deltoid which acts to flex the shoulder. The decreased activation of anterior deltoid might therefore be a consequence to the assistance to shoulder flexion provided by Float.

3.5 Discussion

The study here described demonstrated that: (i) Float does not disrupt the modular organization of anterior reaching; (ii) the assistance provided by Float enforces increased activation of the upper trapezius.

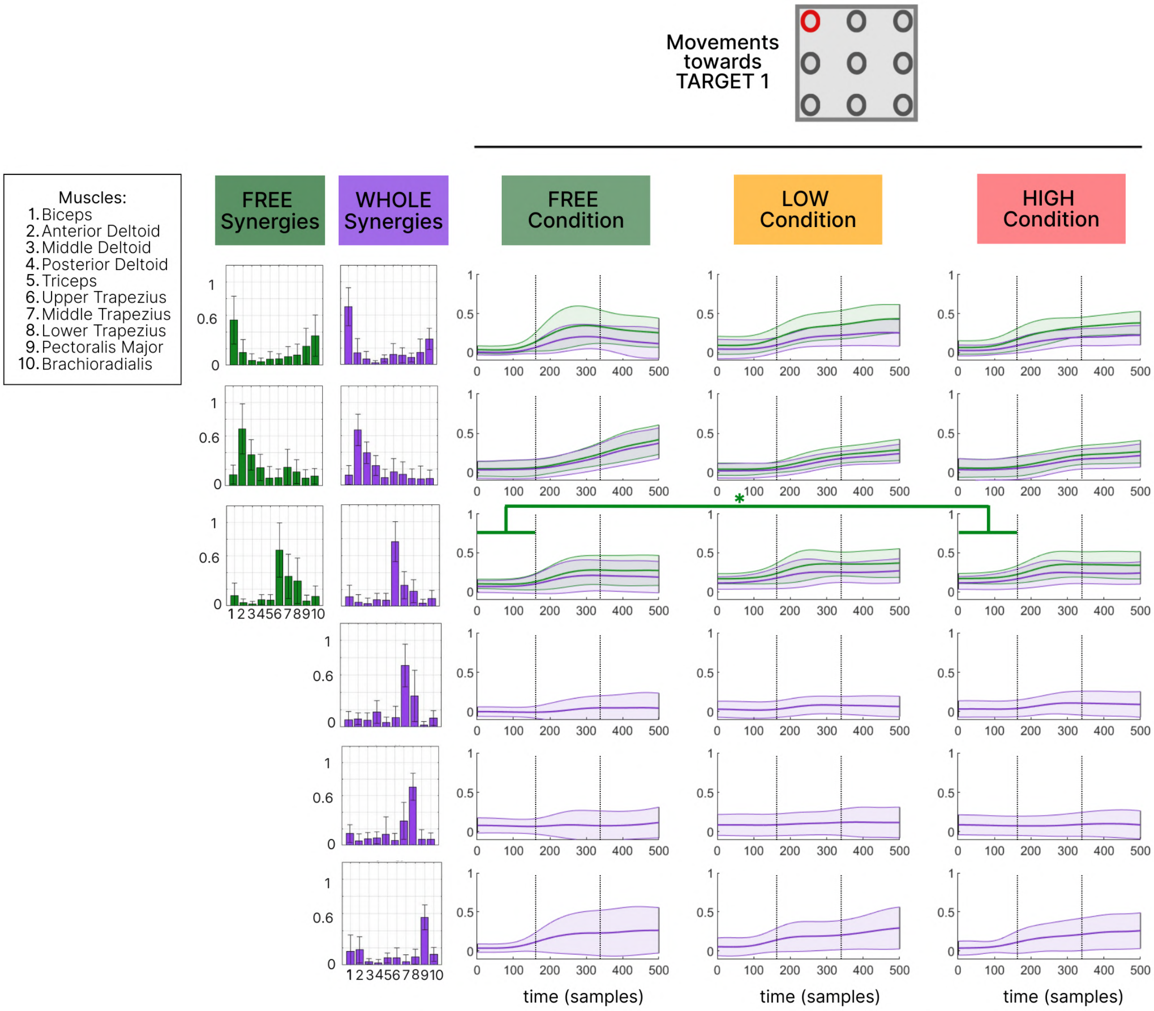

Figure 3.6 Activation coefficients for movements towards target 1. The horizontal bracket indicates the presence of a statistically significant difference.

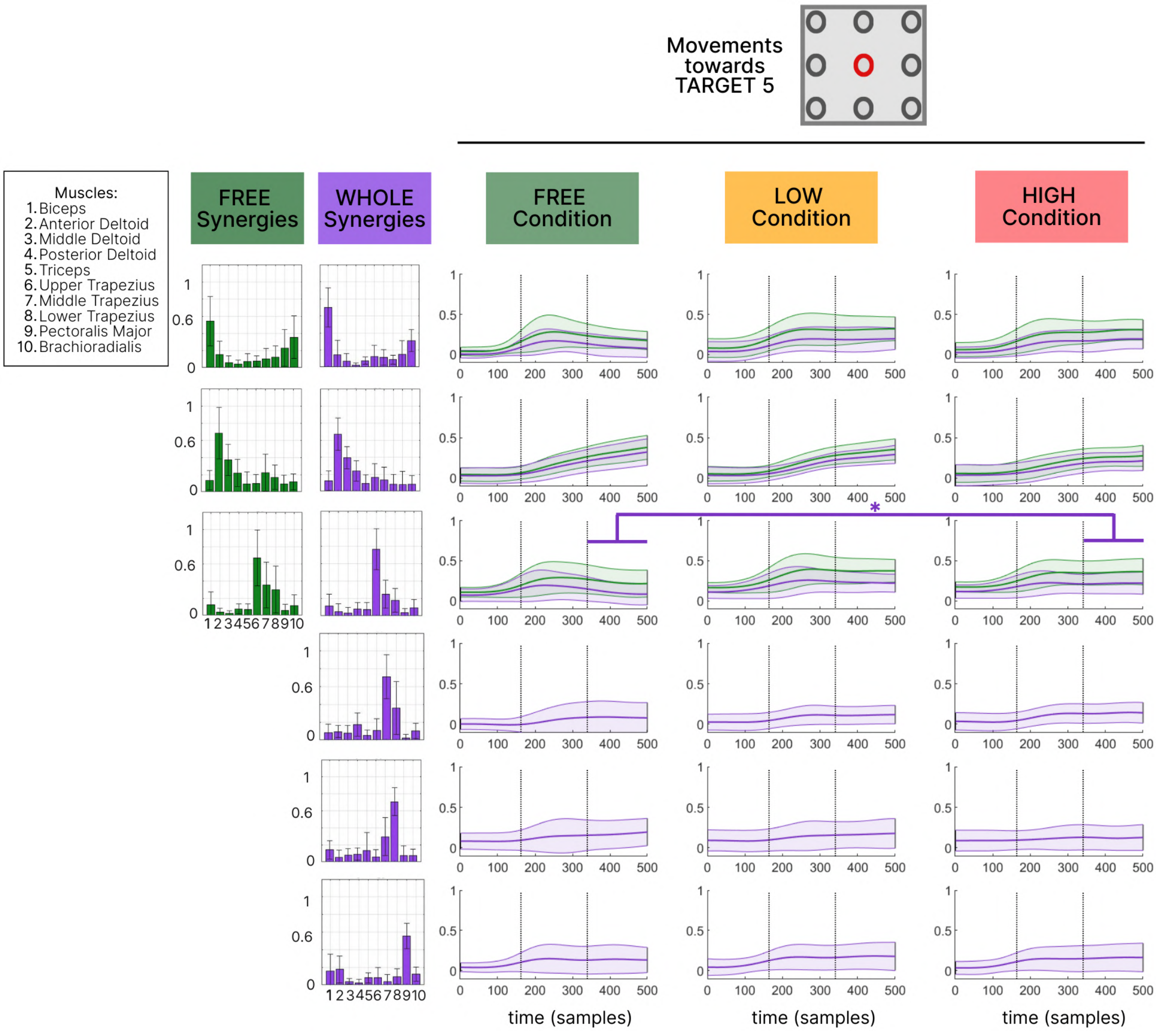

Figure 3.7 Activation coefficients for movements towards target 5. The horizontal bracket indicates the presence of a statistically significant difference.

3.5.1 Synergistic structure of reaching is modulated but not disrupted by Float's assistance

The reference synergies obtained in the present study can provide a quantitative characterization of the impact of the robotic assistance of Float on the modularity of the NeBULA standardized reaching paradigm.

The 3 *free_synergies* (Figure 3.5 upper row) are coherent with muscle synergies analyses performed by other groups on similar tasks (31; 34; 35). The first *free_synergy* mainly expresses biceps and brachioradialis and enforces elbow flexion; the second mainly expresses the deltoids with a prevalence of the anterior deltoid and enforces shoulder flexion and abduction, while the third mainly expresses the trapezius muscle with a prevalence of upper trapezius, stabilizing and rotating the scapula upwards. Differently from our work, previous studies identified an elbow extension synergy (expressing mainly the triceps), while here we identified an elbow flexion synergy (expressing mainly the biceps and the brachioradialis). This is most likely due to the fact that in previous works the 3D reaching task was executed starting with the elbow at 90 degrees, while here the movement was initiated with the hand laying on the thigh.

The high similarity between the *free_synergies* and the first three *whole_synergies* suggests that the fundamental synergistic structure of reaching is preserved when movement is assisted by Float. Moreover, 3 additional *whole_synergies* emerge (Figure 3.5 lower row), which express mainly the middle trapezius, lower trapezius, and pectoralis. These muscle groups are present with a significant activation also in the *free_synergies* (Figure 3.5 upper row): middle and lower trapezius are active in the third *free_synergy* and pectoralis in the first *free_synergy*. This suggests that a simplified yet efficient actuation of the shoulder and elbow joints is obtained in the free condition, while the control of joint movements appears fragmented into the activation of single muscles or couples of muscles when including the movement assisted by Float.

3.5.2 Modulation of synergy recruitment

We found significantly higher activation coefficients of high vs free conditions for the third *free* and *whole_synergy* (Table 3.1). This occurred in the initial phase of movement towards targets 1 and 2 and in the final phase of movement towards target 9 for the coefficients of the third *free_synergy* as well as in the final phase of movement towards target 5 in the coefficients of the third *whole_synergy*. Both the third *free* and *whole_synergy* represent trapezius activation, making the increased activity of this muscle during assisted movement appear counterintuitive.

We hypothesize that this could be attributed both to the presence of a corset to interface Float and the user as well as to the gravity and friction compensation strategy currently implemented in Float. The corset may force the user to maintain a posture more rigid and straighter with respect to the natural sitting position enforcing an increased activation of the trapezius muscle to stabilize this rigid posture. Moreover, we hypothesize that the assistance provided by Float may increase the weight and friction perceived by the user on the shoulder complex. Consequently, the higher tonic activity in the high condition with respect to the free condition observed in the initial phase of movement towards target 1 and 2 (Figure 3.6) may be generated to counterbalance the exoskeleton's perceived weight and resistance. This issue is related mainly to the action of Joint 2 of Float (Figure 2.2), which ideally should fully compensate for the weight of Float and should provide zero resistance to the action of the upper trapezius to elevate of the scapula.

3.5.3 Implications for exoskeleton design

Our analysis suggest that joint 2 of Float acts in resistance to the action of upper trapezius, in particular in the initial phase of movement. This could be due to the model-based friction compensation of the exoskeleton. This model compensates friction by providing a low-frequency sinusoidal voltage to the motors if the velocity is null. Otherwise, for non-null velocities, it models friction torque as a function of angular velocity. Such model, although sub-optimal, has proven to be effective when movements are performed slowly and continuously as it occurs during rehabilitation sessions. In our case study, the limitations of this model-based friction compensation were more evident, since we tested self-paced functional movements in healthy subjects. Especially in movements towards higher targets (i.e., 1 and 2) performed with high assistance, the friction compensation resulted ineffective. This leads to a greater tonic activation of the trapezius muscle (in particular the upper portion) to elevate the scapula and counterbalance the inertia perceived.

Currently, Float provides assistance exclusively on joint 4 (Figure 2.2, Section 2.4.1), which actuates purely shoulder flexion. This assistance is most probably responsible for the decreased activation of the second *free* and *whole_synergies* and consequently of the anterior deltoid muscle which acts specifically to flex the shoulder. We thus propose that implementing a feed forward assistance at joint 2 could be an effective strategy to reduce the described tonic activation of upper trapezius. Figure 3.8 visually describes the proposed implementation of the assistance both at the level of joint 4 and joint 2 of Float.

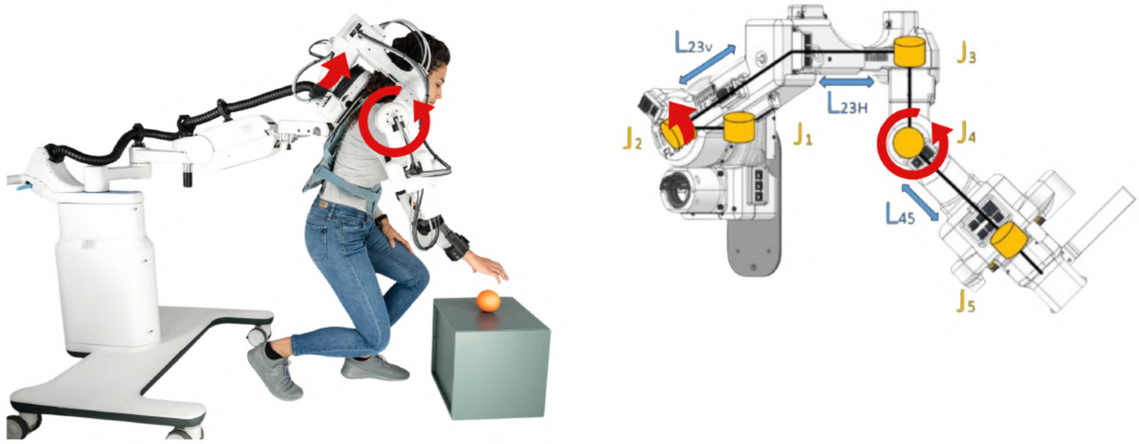

Figure 3.8 Visual representation of the actual assistance already implemented on joint J4 of Float to support shoulder flexion and of the possible assistance to be implemented on joint J2 to support scapula elevation and counterbalance the increased weight perceived on the shoulder.

The analysis of the activation coefficients (Figures 3.6 and 3.7) shows that Float reduces the activation coefficients of the second *free* and *whole_synergies*, without altering the synergy pattern. This is similar to what happens when applying arm weight support (17), which is highly promising as interventions with arm weight support have demonstrated to improve the reaching function both in healthy elderly subjects and in stroke patients (36) (37). Reducing the activation of anterior and middle deltoid could be beneficial for stroke patients, as it may counteract the abnormal coupling between shoulder abductors and elbow flexors that often affects stroke survivors (38).

3.6 Conclusion

This work exploits the NeBULA standardized framework to characterize the modularity of unassisted and exoskeleton-assisted reaching in healthy individuals before translating its use to clinical populations. We applied muscle synergy analysis to quantitatively describe the effects of the assistance of Float on the structural organization of reaching movements and found that synergistic organization of reaching is mainly preserved during assisted movements. Moreover, this study characterized the potential benefits and limitations of

Float for shoulder rehabilitation interventions, by studying its impact on the patterns of muscle activity of healthy individuals. The observed modulation of muscle synergies in healthy individuals provides a rationale for testing Float in post-stroke populations, while also providing useful insights to improve the effectiveness of Float control strategies.

Chapter 4

Exploration of age-related effects on muscle synergies during standardized exoskeleton-assisted reaching

The study presented in this Chapter, as well as the one described in Chapter 3, followed the standardized reaching framework NeBULA (4), which is described in detail in Chapter 2.

NeBULA enables the quantitative assessment of the impact of different assistive devices on motor control across populations. The work described in this Chapter is part of a use case that leverages this framework to quantitatively evaluate the impact of the Float upper limb exoskeleton (Section 2.4.1) on the neuromechanical structure of reaching movements in both healthy individuals and post-stroke subjects.

The analyses presented here are based on a dataset collected from 40 healthy individuals. As described in Section 2.4.2, the first and second halves of the dataset were acquired following slightly different experimental protocols. In this Chapter, analyses are conducted on the complete dataset after harmonizing the two parts.

This study extends the muscle synergy analysis presented in Chapter 3, which focused on the first part of the dataset and highlighted promising features of Float, suggesting its potential applicability in post-stroke rehabilitation.

Specifically, the study aims to establish a reliable set of reference muscle synergies derived from the entire dataset of healthy subjects, capturing the physiological structure of the standardized reaching task performed both with and without the Float exoskeleton. This reference set is intended to provide a robust baseline for future studies investigating how Float modulates the muscle synergy structure in post-stroke individuals.

Despite efforts to standardize the experimental reaching task, a considerable level of inter-subject variability in muscle synergy structure was observed. For this reason, the present study also focuses on characterizing such variability. In particular, we explored the potential influence of age as a contributing factor to the observed differences across subjects.

The study presented in this Chapter is also reported in the manuscript *"Age-related Effects on Muscle Synergies During a Standardized Exoskeleton-assisted Reaching Task"* by Indya Ceroni, Florencia Garro, and Marianna Semprini, currently under review.

4.1 State of the art

The use of healthy reference synergies is well established in the literature. For instance, in a clinical trial involving post-stroke patients, the similarity between patient-specific muscle synergies and average healthy synergies was employed as a metric of motor performance, with higher similarity associated with better functional outcomes (10). Similarly, recent work demonstrated that discrepancies between patient synergies and normative synergies obtained from healthy individuals can be leveraged to guide synergy-based functional electrical stimulation (FES) gait training (39). Other studies have used muscle synergies extracted from healthy participants to evaluate the effects of planar robotic therapy in sub-acute post-stroke subjects, while also reporting substantial inter-subject variability in both healthy and clinical groups (12).

These examples highlight the importance of obtaining reliable reference data from healthy participants.

However, consistent with our previous findings (40; 41) and other studies (12; 42; 43), it is noted that the computation of muscle synergies is highly sensitive to inter-subject variability. Recent literature (43) have highlighted the need to further characterize inter-subject variability in reference synergies set, suggesting that splitting large datasets into different groups based on specific factors (e.g. age or sex) may allow to better investigate their impact on muscle synergies structure and their role in inter-subject variability.

Accordingly, we focused on the quantification of inter-subject variability in a larger sample of subjects and on the exploration of age-related modulations in the synergistic structure of movement within our dataset.

We choose to focus on the possible influence of age as the NeBULA standardized reaching paradigm (Chapter 2) allows to control for factors such as task complexity and anthropometry (4; 15) . This choice was favored also by the fact that none of the previous works on the impact of age on muscle synergies was focusing on reaching (44; 45; 46; 47; 48).

The impact of aging on motor control has been well established, affecting brain structure (49), muscle couplings (50) and force outputs (51). In particular, the effect of aging on the structure of muscle synergies has been widely investigated in the lower limb (52). Several studies have explored locomotor tasks (44; 45; 46), reporting only small differences in motor modules between young and older adults.

Yet, only a few studies have focused on age-related modulations of upper-limb muscle synergies. For example, Ye and colleagues (47) investigated upper-limb muscle synergies during an object-lifting task in young and older adults, finding that while muscle recruitment is largely preserved with aging, the balance of activations is altered. Similarly, Huang and colleagues (48) explored the effect of age on upper-limb muscle synergies during a complex piano-playing task, showing that the structure of synergies can be fine-tuned by aging.
Based on previous literature, we did not expect to find major differences in the muscle synergies structure between younger and older adults in the proposed standardized task, but rather a fine tuning of muscle synergies with age.

4.2 Objectives

The objective of the present work is to assess the reference synergies obtained from a large healthy population and their potential modulation due to age in the context of our experimental paradigm. Specifically, the research questions addressed are:

1. Is the reference set of muscle synergies obtained from healthy subjects reliable for future comparisons with patient populations performing the same experimental paradigm?

2. Does age influence the synergistic structure of our standardized reaching task, and could it therefore contribute to inter-subject variability within this experimental paradigm?

4.3 Methods

4.3.1 Participants

The present study involved 40 healthy right-handed individuals (20 males, 20 females age 44.6 ± 13.2 years old). The study was conducted in accordance with the current version of the Declaration of Helsinki. All participants signed an informed consent and the experimental procedures were approved by the local ethical committee (Comitato Etico Regionale della Liguria: 784/2022 - DB id 12044).

4.3.2 Experimental task

During the experiment, participants seated in an adjustable chair in front of the touch panel where 3 targets were arranged in a vertical straight line. The middle target was aligned with the shoulder joint of the participants and the other two targets were placed to allow the participants to reach them comfortably. Participants were instructed to reach the targets with the right hand at a self-paced comfortable speed. They were instructed to start with the arm relaxed and the right hand leaning on the thigh and to reach all the targets with the elbow fully extended.

Participants were cued with the LED indicator to reach each of the three targets ten times in a pseudo-randomized order. Each participant repeated the reaching paradigm three times: first without wearing Float, and subsequently wearing Float providing low assistance and high assistance. The order of assistance levels was randomized. Figure 4.1 depicts the entire workflow of the experiment.

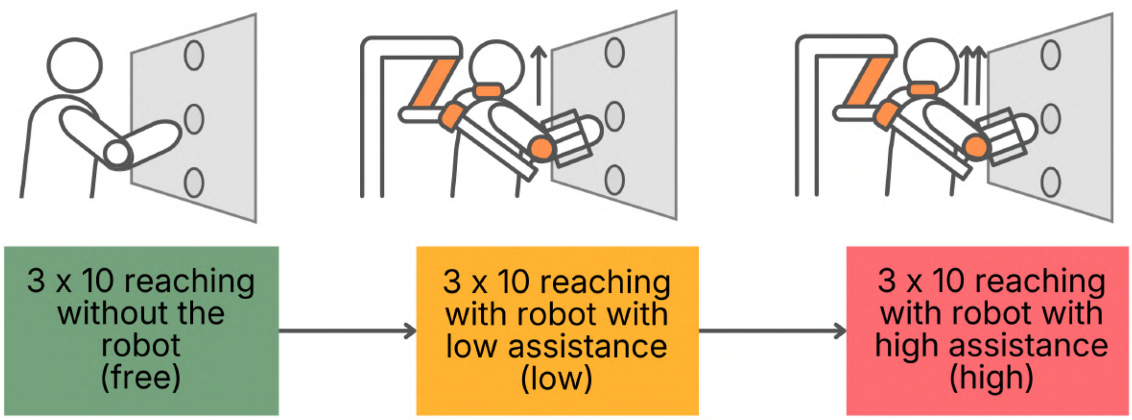

Figure 4.1 Experimental procedure.

We recorded bipolar surface EMG from 10 muscles of the right upper limb: biceps brachii (long head), anterior deltoid, middle deltoid, posterior deltoid, triceps brachii (long head), upper trapezius, medial trapezius, lower trapezius, pectoralis major and brachioradialis. The Cometa Waveplus System was used to acquire the EMG signals at 1 KHz.

4.3.3 Data segmentation and preprocessing

We epoched the EMG recording of each subject into single trials using the logs generated by the touch panel. For each epoch, we applied a 4th order Butterworth band-pass filter with zero-phase distortion between 20 and 350 Hz and rectified the signal. Then, we applied an ad-hoc median filter to identify values over 600 μV, which were substituted with the median value calculated over a 50-sample sliding window. Subsequently, we applied a 4th order Butterworth low-pass filter with zero-phase distortion at 5 Hz to obtain the envelope of the signal. We then normalized the EMG envelopes taking the maximum value achieved for each muscle in the complete dataset (31). Finally, since the task was self-paced, we time-scaled all epochs to the same duration of 500 samples (0.5 s) (16).

4.3.4 Muscle synergies extraction

The muscle synergy computation procedure adopted in this Chapter largely follows the methodology described in Section 3.3.4. For completeness, the main steps are briefly reported here. We extracted the muscle synergies for each subject, grouping the experimental tasks as follows:

1. Including only the sequence executed without the assistance of Float. We named these synergies *free_synergies*; they characterize the modularity of the unassisted anterior reaching movement in the vertical plane.

2. Including all the sequences executed with and without the assistance of Float. We named these synergies *whole_synergies*; they describe the entire experimental paradigm and characterize the effect of robotic assistance.

This was done to characterize the motor control strategies that emerge with the use of the Float exoskeleton in the context of our standardized paradigm.

For *free_synergies* and *whole_synergies* we concatenated the epochs to obtain a matrix of $[n_{muscles} \times (n_{samples} \cdot n_{epochs})]$. Subsequently, we used the non-negative matrix factorization algorithm (NNMF) (32) to extract the spatial synergies. The NNMF linearly separates the concatenated EMG matrix into a set of N time-invariant synergies w_i and N time-varying activation coefficients $c_i(t)$ as described in the equation:

$$EMG(t) = \sum_{i=1}^{N} c_i(t) w_i \tag{4.1}$$

Where N is the number of extracted synergies.

For each subject, we selected N as the minimum number of synergies necessary to explain the 90% of data variation. We quantified the amount of explained data variation using the Variance Accounted For (R^2 or VAF) metric, defined as 1 - SSE/SST where SSE is the sum of the squared residuals and SST is the sum of the squared differences with the mean EMG vector (31).

We performed the factorization multiple times with N increasing from 1 to the number of muscles (which represent the maximum possible dimensionality of the system). Once the computed VAF reached 0.9, we stopped the iterative factorization and retained the latest extracted synergies. During each factorization, we applied the NNMF algorithm 100 times to avoid local minima.

4.3.5 Age-based stratification of dataset

We grouped subjects based on their age (Figure 4.2) to compute their representative muscle synergies. We excluded 1 subject due to incomplete recording and divided the remaining 39 subjects into the following groups:

- **Group_all**: It comprises the entire dataset (N=39).
- **Group_25-50**: Includes 20 participants aged 25 to 49 years.
- **Group_50-80**: Includes 19 participants aged 50 to 79 years.

To inspect age-related effect with greater granularity, we further stratified participants in four subgroups:

- **Subgroup_25-30**: Includes 11 participants aged 25 to 29 years.
- **Subgroup_30-50**: Includes 9 participants aged 30 to 49 years.
- **Subgroup_50-60**: Includes 12 participants aged 50 to 59 years.

- **Subgroup_60-80**: Includes 7 participants aged 60 to 79 years.

As the dataset was not originally designed to examine age-related subgroup effects, these subgroups are uneven and relatively small, which was taken into account during data analysis and interpretation.

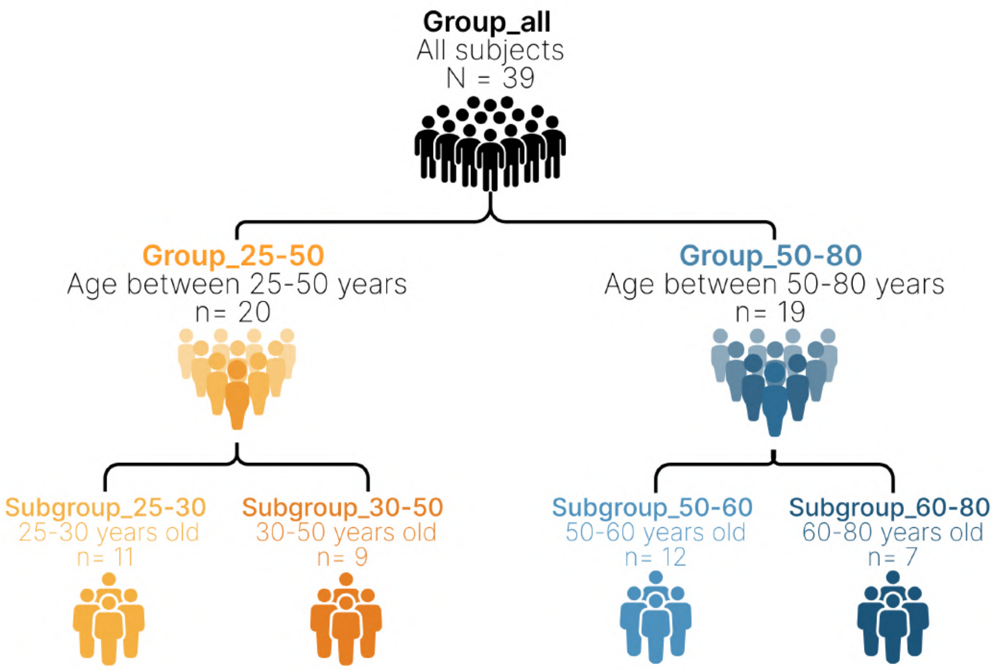

Figure 4.2 Age-based stratification of dataset.

4.3.6 Computation of reference synergies

To calculate the reference synergies of each group and subgroup, both in the *free* (unassisted) and in the *whole* (unassisted and exoskeleton-assisted) condition, we followed a procedure that is taken from (16) and is adapted from the previous study described in Chapter 3, Section 3.3.5. The starting point was the synergies extracted for each single subject, from which we performed the following steps:

1. We pooled the muscle synergies of the subjects belonging to the same group/subgroup. Subjects were expected to have a different number of synergies, due to the VAF criterion to chose the number of synergies (Section 4.3.4). We then computed the average number of synergies among the subjects of the group (avg_group).

2. We repeated the synergies extraction procedure for each subject of the group, now setting the number of synergies apriori as avg_group.

3. We run a clustering procedure to account for the fact that not all subjects shared the same synergies, and that the shared synergies could be extracted in different order across different subjects due to the random initialization of the NNMF algorithm. For this, we clustered the single subject synergies obtained from step 2 based on which muscle is the most expressed in the synergy (i.e., the muscle with the higher weight). We prevented the presence of two or more synergies from the same subject in the same cluster.

4. We selected the clusters that had a number of elements equal or greater than half of the size of the age group. We averaged the synergies in such clusters to obtain a set of comparative synergies.

5. For each subject, we matched the synergies obtained from step 2 with the comparative synergies based on the value of cosine similarity (31). We excluded single subject synergies that did not reach a cosine similarity of at least 0.5 with any of the comparative synergies.

6. We average the single subject synergies that were matching the comparative synergies to obtain the reference synergies, i.e., synergies representative of the modularity shared among the subjects of the group.

Figure 4.3 summarizes the steps detailed above.

We examined the consistency of reference synergies, i.e. how well they reflect individual synergies of single subjects, using the following metrics:

- Average percentage of single subject synergies excluded during the computation of the reference synergies;
- Coefficient of variation of the obtained reference synergies;
- Average cosine similarity of the single subject synergies with the obtained reference synergies.

We also compared the reference *free_synergies* and *whole_synergies* to characterize the effect of the assistance of Float on the modular organization of anterior reaching in the entire dataset of 39 subjects. To this end, we computed the cosine similarity between the reference *free* and *whole_synergies* of **group_all**.

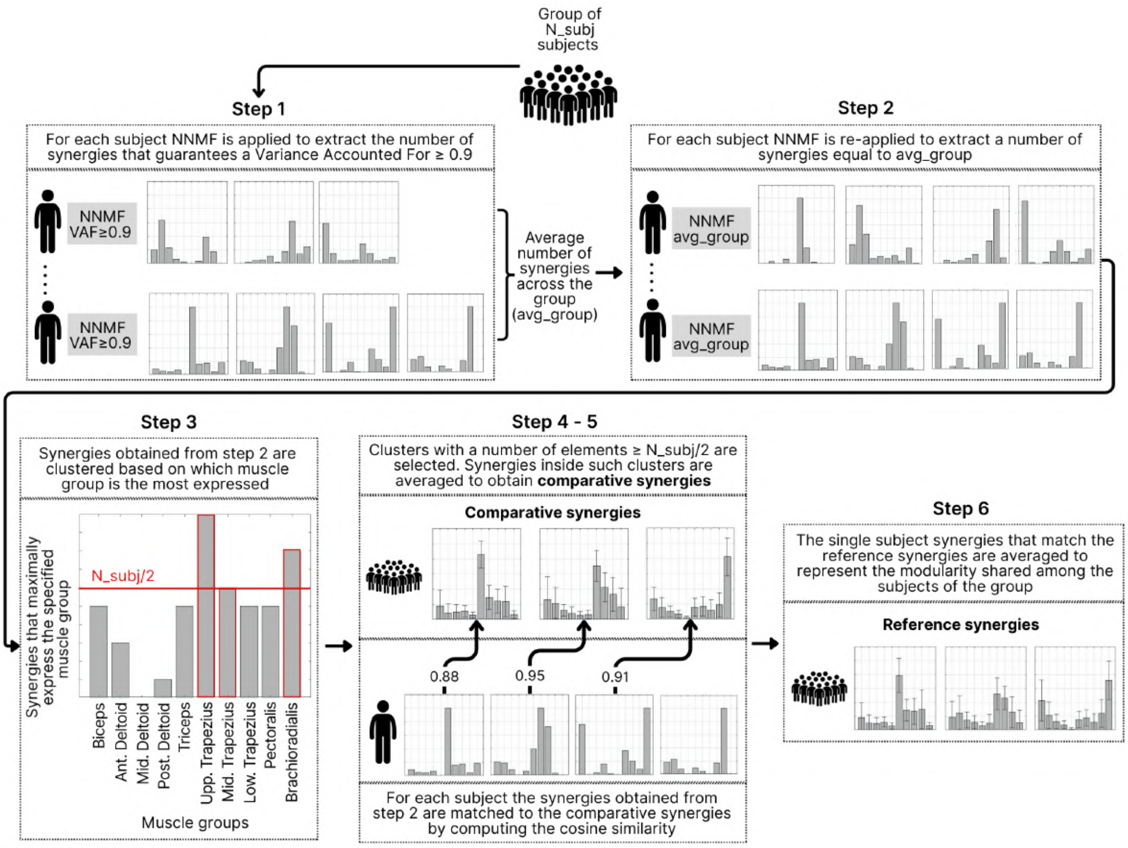

Figure 4.3 Schematic procedure for obtaining the reference synergies representing the modularity shared among the subjects of the same group or subgroup. (N_subj: number of subjects in the group; NNMF: non-negative matrix factorization; avg_group: average number of synergies among the subjects of the group).

4.3.7 Assessment of age-related modulation of muscle synergies

To investigate whether age influences the synergistic structure of the standardized reaching movement, we computed reference synergies (Section 4.3.6) for each age group and subgroup, starting from both the *free_synergies* and the *whole_synergies* of the single subjects. We thus obtained a set of *free_synergies* and a set of *whole_synergies* for each age group and subgroup, describing the impact of age on the synergistic structure of unassisted reaching movements (*free_synergies*) and of the entire experimental paradigm (*whole_synergies*).

The consistency of the reference synergies within each group was evaluated as described in Section 4.3.6, considering: (i) the average percentage of single-subject synergies excluded during the computation of the reference synergies; (ii) the coefficient of variation of the obtained reference synergies; and (iii) the average cosine similarity between single-subject synergies and the corresponding reference synergies.
For each age group and group, the quantities calculated in (i) and (iii) were compared with the same quantities obtained for **group_all** using either a paired t-test or a Wilcoxon signed-rank test, depending on data normality assessed with Kolmogorov-Smirnov test. A Bonferroni correction was applied to adjust for multiple comparisons.

In addition, we conducted a similarity analysis between individual subject synergies and reference synergies obtained from age groups and subgroups. The goal was to determine whether, and to what extent, a subject's muscle synergies more closely resembled the reference synergies derived from participants within the same age group or subgroup.

For each subject, we considered the individual *free_synergies* and *whole_synergies* and we computed their cosine similarity with respect to four different reference sets: a) own subgroup, b) own group, c) other group, d) entire dataset (Figure 4.2) for *free_synergies* and *whole_synergies* separately. For this, we: 1) computed the cosine similarity between all the possible pairs of single subject and reference synergies, 2) selected the pair with the higher similarity and excluding it from the following iteration, 3) computed again the cosine similarity to identify the next pair, 4) iterated the procedure until we identified all pairs. We then averaged the values of similarity of all pairs of single subject and reference synergies.

We hypothesized that if age-related differences exist in the modularity characterizing the proposed reaching task, then the muscle synergies of single subjects should be more similar to the reference synergies of their age subgroup. To test this hypothesis we used a linear mixed-effects model to test whether similarity values differed across the four references. Importantly,

the analysis was performed separately for the *free_synergies* (unassisted movements only) and the *whole_synergies* (both unassisted and exoskeleton-assisted movements), since the latter dataset contains the former and cannot be treated as an independent factor.
For each dataset, similarity values were arranged in a subject × condition matrix (39 subjects × 4 reference conditions: own subgroup, own group, other group, entire dataset). These values were analyzed using the model:

$$\text{Similarity} \sim \text{Age}_{\text{centered}} + \text{Reference} + (1 \mid \text{Subject}) \tag{4.2}$$

where Reference (4 levels) was treated as a fixed effect, Age was included as a centered continuous covariate, and Subject was modeled as a random intercept to account for repeated measures.
Model selection was performed by comparing additive (Age + Reference) and interaction (Age × Reference) formulations fitted with maximum likelihood. Since the interaction was not significant in either dataset, the simpler additive model was retained and refitted using restricted maximum likelihood (REML).
Post-hoc pairwise comparisons between conditions were only performed if the main effect of Reference was significant. Significance was set at $p < 0.05$.

4.4 Results

In this work, we expand the findings of Chapter 3 (40; 41), by including a greater number of subjects. After computing reference synergies from this large healthy population, we investigated their consistency, i.e. how well they reflect individual synergies of single subjects. We then further explored aging as a potential source of inter-subject variability and its specific role in our use case involving the Float exoskeleton. To this end, we stratified subjects by age in groups and subgroups and we computed reference muscle synergies for each age groups and subgroups.

4.4.1 Assessment of reference synergies

To investigate whether reference synergies obtained in our experimental paradigm could be exploited for a future comparison with patient populations performing the same task, we first calculated reference synergies of the entire dataset of 39 healthy subjects (**group_all**). To this end, as detailed in section 4.3.4, we chose to separately compute *free_synergies* that represent the modularity of unassisted reaching movements of **group_all**, and *whole_synergies* that represent the modularity of the entire experimental paradigm (including assisted and unassisted movements) of **group_all**.

The obtained reference synergies are shown in Figure 4.4.

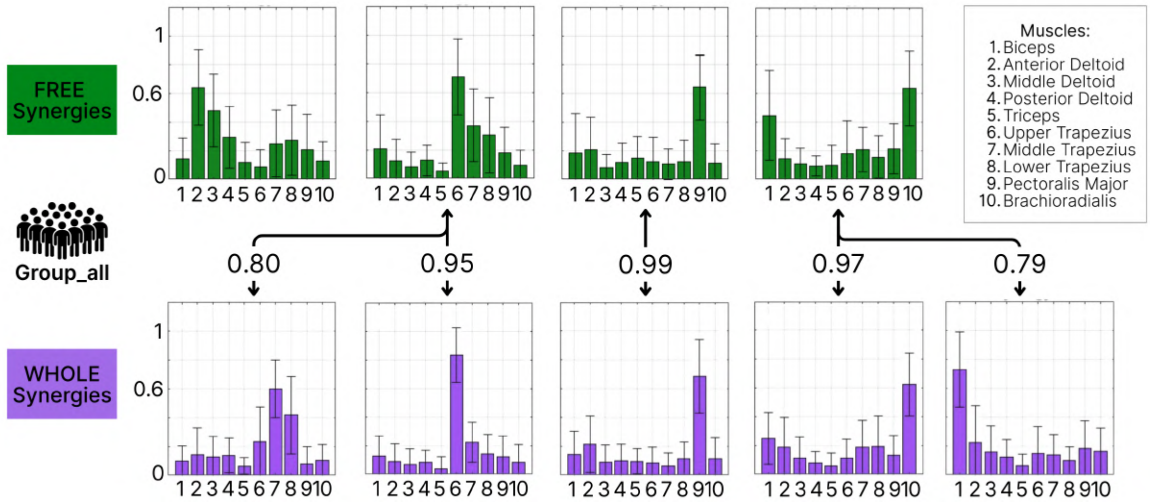

Figure 4.4 *Free_synergies* and *whole_synergies* for **group_all**, matched by cosine similarity (bold numbers).

We found that four spatial synergies were sufficient to describe unassisted reaching movements, whereas five were required when movements assisted by Float were included.

Regarding the consistency of the obtained reference synergies, we found that:

- A percentage of $13.45 \pm 13.87\%$ (mean $\pm$ standard deviation) of single subject *free_synergies* were excluded from the computation of the reference *free_synergies* (following the algorithm described in Section 4.3.6, Step 5);

- A percentage of $21.03 \pm 12.09\%$ of single subject *whole_synergies* were excluded from the computation of the reference *whole_synergies*.

This analysis indicates that although the reference synergies represent the majority of individual subject synergies, a non-negligible portion is excluded from their computation.

The coefficients of variation reported in Table 4.1 and Table 4.2 show that the composition of the individual synergies contributing to the reference synergies is highly variable. Consequently, the average cosine similarity between single-subject and reference synergies does not exceed 0.75:

- The average similarity of single subject *free_synergies* with respect to the reference *free_synergies* is 0.74 ± 0.12;

Muscles	**Coefficient of variation**			
	Syn 1	**Syn 2**	**Syn 3**	**Syn 4**
Bicep	1.02	1.12	1.49	0.70
Ant. Deltoid	0.41	1.21	1.07	1.01
Mid. Deltoid	0.52	1.19	1.10	1.06
Post. Deltoid	0.73	0.85	1.14	0.77
Triceps Lat.	1.22	1.14	1.05	1.51
Upp. Trap.	1.36	0.37	1.40	1.31
Mid. Trap	0.93	0.69	1.00	0.75
Low. Trap	0.90	0.87	1.25	0.96
Pect. Maj.	1.20	1.05	0.36	0.83
Brachiorad.	1.05	1.18	1.17	0.41
Average	0.93 ± 0.30	0.97 ± 0.27	1.10 ± 0.31	0.93 ± 0.31

Table 4.1 coefficient of variation for *free_synergies* weights.

Muscles	**Coefficient of variation**				
	Syn 1	**Syn 2**	**Syn 3**	**Syn 4**	**Syn 5**
Bicep	0.36	1.09	1.04	1.15	0.72
Ant. Deltoid	1.14	1.42	1.26	0.93	1.08
Mid. Deltoid	1.16	1.57	1.09	1.35	1.25
Post. Deltoid	0.99	0.96	0.87	1.13	1.07
Triceps Lat.	1.25	2.16	0.90	.94	1.60
Upp. Trap.	1.24	0.23	1.05	1.31	1.19
Mid. Trap.	1.01	0.62	0.34	1.42	1.00
Low. Trao.	0.96	0.97	0.65	0.98	1.07
Pect. Maj.	1.04	1.20	1.51	0.38	1.00
Brachiorad.	1.01	1.56	1.07	1.28	0.35
Average	1.01 ± 0.25	1.18 ± 0.54	0.98 ± 0.32	1.09 ± 0.30	1.03 ± 0.33

Table 4.2 coefficient of variation for *whole_synergies* weights.

- The average similarity of single subject *whole_synergies* with respect to the reference *whole_synergies* is 0.69 ± 0.10.

Overall, these results suggest that the effect of inter-subject variability is evident even when considering a robust number of individuals without any previous history of motor impairment.

Figure 4.4 (top row) describes the composition of the reference synergies and their modulation due to robotic assistance:

- The first *free_synergy* expresses mainly the deltoids, with a predominance of the anterior deltoid. Middle trapezius, lower trapezius and pectoralis major also show relevant contribution. These muscle groups works together to enforce a smooth shoulder flexion with the scapula stabilizers (middle and lower trapezius) and the pectoralis major supporting the action of the anterior deltoid for an efficient movement production.

- The second *free_synergy* primarily expresses the trapezius with a prominence of the upper trapezius, which acts to elevate and upwardly rotate the scapula to favor arm elevation during reaching.

- The third *free_synergy*, which involves mainly the pectoralis, favoring the flexion of the humerus.

- The last *free_synergy* involves mainly the biceps and the brachioradialis, acting synergistically to provide elbow flexion.

The reference *whole_synergies* are characterized by high values of similarity with the *free_synergies* (> 0.79). Nevertheless, there is no one-to-one correspondence between the two groups of synergies:

- The first and second *whole_synergies* both exhibit a high degree of similarity with the second *free_synergy* (0.80 and 0.95, respectively).

- The first *whole_synergy* expresses mainly the middle and lower trapezius, while the second *whole_synergy* expresses mainly the upper trapezius. Therefore, the second *free_synergy*, involving all the trapezius components, appears split into the first and second *whole_synergies*.

- The third *whole_synergy* has a high correspondence with the third *free_synergy* (similarity of 0.99), both involving exclusively the pectoralis major.

- The fourth and fifth *whole_synergies* exhibit high similarity with the fourth *free_synergy* (0.97 and 0.79 respectively).
- The fourth *free_synergy*, which is characterized by a significant presence of both the biceps and the brachioradialis, seems split into the fourth *whole_synergy*, expressing mainly the brachioradialis, and fifth *whole_synergy*, expressing mainly the biceps.
- None of the *whole_synergies* exhibits a high similarity with the first *free_synergy* (similarity is < 0.66 for all the *whole_synergies*).

These results indicate that in the reference *whole_synergies*, the modular organization characterizing unassisted reaching is still present but a higher number of synergies is needed to describe the movement.

4.4.2 Age-related modulation of muscle synergies

We investigated the influence of age on the structure of reference synergies to assess whether and how age contributes to inter-subject variability in our experimental paradigm.

To this end, as detailed in Sections 4.3.5 and 4.3.6, we computed reference *free_synergies* and *whole_synergies* for groups and subgroups of subjects divided by age range (Figure 4.2), to explore whether the synergistic structure of anterior reaching movements executed in our experimental framework could differ based on age.

Figures 4.5 and 4.6 show the *free* and *whole_synergies* obtained for each age group and subgroup, as well as the reference *free* and *whole_synergies* obtained from the entire dataset (**group_all**). Cosine similarity values were computed between the muscle synergies representative of each age group and the reference synergies from the entire dataset (**group_all**), revealing high similarity.

Figure 4.5 shows limited differences among age groups for *free_synergies*:

- In most age groups and subgroups, apart from **subgroup_30-50** and **subgroup_60-80**, the *free_synergies* have a one-to one correspondence with the *free_synergies* from **group_all** characterized by values of similarity above 0.92.
- In the **subgroup_30-50**, three out of four *free_synergies* have a one-to-one correspondence with the first, second and fourth *free_synergies* from **group_all** (values of similarity of 0.98, 0.92 and 0.99, respectively). One *free_synergy* from **subgroup_30-50**, expressing mainly the lower and middle trapezius, finds no correspondence in **group_all**.

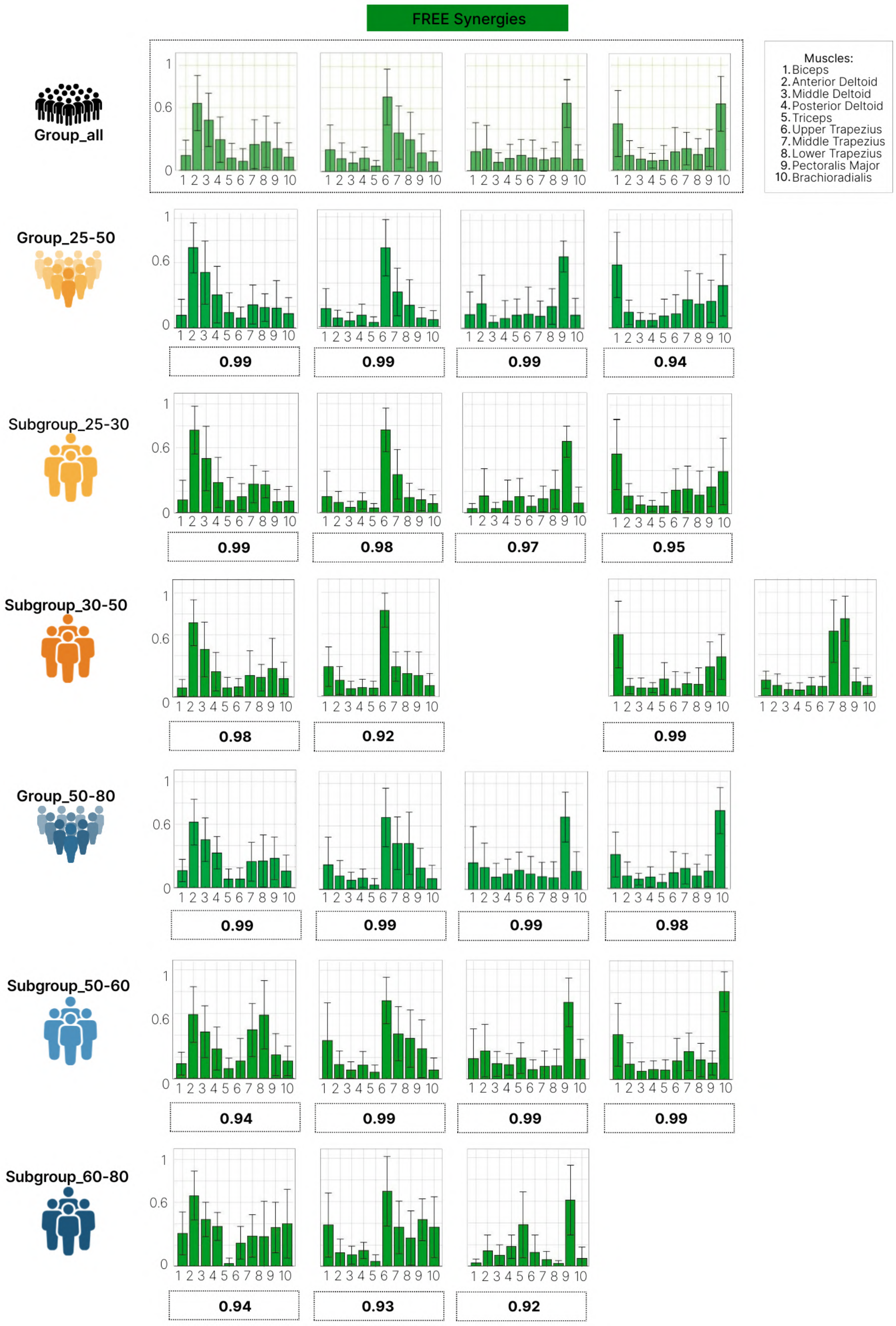

Figure 4.5 Composition of *free_synergies* for **group_all** (top row) and for all age groups and subgroups. The number shown below each synergy indicates its cosine similarity with the corresponding reference synergy from **group_all**.

Figure 4.6 Composition of *whole_synergies* for **group_all** (top row) and for all age groups and subgroups. The number shown below each synergy indicates its cosine similarity with the corresponding reference synergy from **group_all**.

- In the **subgroup_60-80** only three *free_synergies* are identified, exhibiting a high similarity with the first three *free_synergies* from **group_all** (values of 0.94, 0.93, 0.92, respectively).

In contrast, the differences among age groups for *whole_synergies* are more pronounced (Figure 4.6):

- The number of *whole_synergies* extracted from the age groups and subgroups is highly variable, ranging from 3 to 6, and rarely matching the number of *whole_synergies* extracted for **group_all**.

- None of the age groups or subgroups exhibits complete correspondence between their *whole_synergies* and those of **group_all**.

- In all the age groups and subgroups either one or more of the *whole_synergies* from **group_all** are missing or one age-specific *whole_synergy* without a corresponding *whole_synergy* of **group_all** is present.

- Age-specific *whole_synergies* not present in the **group_all** are identified across multiple age groups: a *whole_synergy* expressing the deltoids (particularly the anterior portion) is present both in **group_25-50** and **subgroup_30-50**, while a *whole_synergy* expressing mainly the triceps is identified both in **group_50-80** and **subgroup_60-80**.

- On average only 3.5 $\pm$84 *whole_synergies* per age group and subgroup match the *whole_synergies* of **group_all**.

Notably, the composition of *whole_synergies* varies more markedly across age groups and subgroups, with some age-specific patterns emerging. In particular, a synergy primarily involving the deltoid muscles is characteristic of participants younger than 50 years, whereas a synergy dominated by triceps activation is observed in participants older than 50 years.

Consistency of age-groups reference synergies

As described in Section 4.3.6, we assessed the consistency of the reference synergies obtained from each age group using the same metrics described in Section 4.4.1, to evaluate their representativeness of individual synergies. This analysis explored the consistency of the reference synergies obtained from the different age groups and subgroups, and compared them with the reference synergies obtained from **group_all**.

Table 4.3 reports the percentage of single subject synergies excluded (mean over subjects $\pm$ standard deviation) for each age group and subgroup during the computation of the reference *free* and *whole_synergies* for each age group/subgroup (Section 4.3.6). Overall, the percentage of single subject synergies excluded from the reference synergies ranges between 11% and 18%.

When comparing these values with those obtained for the **group_all** (Section 4.4.1), we observed that *free_synergies* values are comparable across age groups and subgroups. On the contrary, the percentages of *whole_synergies* excluded for the different age groups and subgroups are in most of the cases lower than for the **group_all** (21.03 ± 12.09) and are significant for **group_25-50** (p = 0.0036) and **subgroup_30-50** (p = 0.0003).

Age group	Condition	% Excluded Subject Syn
Group_25-50	free	$17.50\% \pm 11.75\%$
Group_25-50	whole	$14.00\% \pm 11.42\%$
Subgroup_25-30	free	$15.91\% \pm 12.61\%$
Subgroup_25-30	whole	$9.09\% \pm 12.61$
Subgroup_30-50	free	$13.89\% \pm 13.18$
Subgroup_30-50	whole	$6.67\% \pm 10.00$
Group_50-80	free	$11.84\% \pm 15.29\%$
Group_50-80	whole	$17.11\% \pm 14.56\%$
Subgroup_50-60	free	$14.58\% \pm 12.87\%$
Subgroup_50-60	whole	$4.17\% \pm 9.73\%$
Subgroup_60-80	free	$4.76\% \pm 12.60\%$
Subgroup_60-80	whole	$14.29\% \pm 15.12\%$

Table 4.3 Percentage (mean $\pm$ standard deviation) of single subject synergies excluded from the computation of the reference synergies for each age group and subgroup.

Moreover, coefficients of variation obtained for group and subgroup reference synergies (Table 4.4) were high, yet showed a decrease comparing to values obtained for **group_all**, with only 14/48 values greater than 1, further suggesting an increased consistency in the reference synergies derived from subjects of same age group. For the four **group_all** *free_synergies* identified in Section 4.4.1, the coefficients of variation were 0.93 ± 0.30, 0.97 ± 0.27, 1.10 ± 0.31 and 0.93 ± 0.31; while for the five **group_all** *whole_synergies*, the coefficient of variations were 1.01 ± 0.25, 1.18 ± 0.54, 0.98 ± 0.32, 1.09 ± 0.30 and 1.03 ± 0.33.

Table 4.5 reports the average similarity between individual and group and subgroup reference synergies, showing an increase with respect to the similarity obtained with **group_all**, which was 0.74 ± 0.12 for reference *free_synergies* and 0.69 ± 0.10 for *whole_synergies*

Age group	Cond	Coefficient of Variation of Muscle Synergy Weights					
		Syn 1	Syn 2	Syn 3	Syn 4	Syn 5	Syn 6
Group_25-50	free	0.95 ± 0.29	0.92 ± 0.34	0.98 ± 0.28	1.23 ± 0.48		
Group_25-50	whole	1.02 ± 0.32	0.97 ± 0.37	1.00 ± 0.43	0.99 ± 0.39	1.19 ± 0.45	1.07 ± 0.38
Subgroup_25-30	free	0.92 ± 0.30	0.94 ± 0.51	0.93 ± 0.36	1.16 ± 0.46		
Subgroup_25-30	whole	1.02 ± 0.45	1.04 ± 0.35	1.03 ± 0.40			
Subgroup_30-50	free	0.99 ± 0.48	0.83 ± 0.26	0.83 ± 0.30	0.82 ± 0.29		
Subgroup_30-50	whole	0.87 ± 0.33	0.94 ± 0.41	0.78 ± 0.32	0.90 ± 0.36		
Group_50-80	free	0.77 ± 0.31	0.90 ± 0.30	1.05 ± 0.28	0.88 ± 0.32		
Group_50-80	whole	1.12 ± 0.39	0.89 ± 0.27	1.00 ± 0.31	0.96 ± 0.34		
Subgroup_50-60	free	0.87 ± 0.28	0.75 ± 0.25	0.92 ± 0.31	0.89 ± 0.34		
Subgroup_50-60	whole	0.80 ± 0.28	0.94 ± 0.37	0.84 ± 0.27			
Subgroup_60-80	free	0.75 ± 0.44	0.75 ± 0.23	0.97 ± 0.29			
Subgroup_60-80	whole	1.17 ± 0.51	1.02 ± 0.49	0.87 ± 0.32	0.94 ± 0.58	0.88 ± 0.31	

Table 4.4 Average coefficient of variation (mean $\pm$ standard deviation) across muscle activations within the same synergy for each synergy of each age group and subgroup.

(Section 4.4.1).
For *free_synergies*, this increase was significant only for **subgroup_60-80** ($p = 0.034$).
For *whole_synergies*, this increase was significant for **subgroup_25-30** ($p = 0.004$), **subgroup_30-50** ($p < 10^{-4}$), **subgroup_50-60** ($p < 10^{-4}$), **group_50-80** ($p = 0.006$).

Age group	Condition	Similarity with Subject Syn
Group_25-50	free	0.76 ± 0.11
Group_25-50	whole	0.64 ± 0.08
Subgroup_25-30	free	0.76 ± 0.14
Subgroup_25-30	whole	0.82 ± 0.12
Subgroup_30-50	free	0.78 ± 0.11
Subgroup_30-50	whole	0.85 ± 0.07
Group_50-80	free	0.73 ± 0.14
Group_50-80	whole	0.79 ± 0.12
Subgroup_50-60	free	0.73 ± 0.12
Subgroup_50-60	whole	0.85 ± 0.07
Subgroup_60-80	free	0.83 ± 0.11
Subgroup_60-80	whole	0.76 ± 0.20

Table 4.5 Average similarity (mean $\pm$ standard deviation) of single subject synergies with respect to the reference synergies for each group and subgroup.

Overall, these results indicate that computing reference synergies within age-homogeneous groups may reduce the number of subject-level synergies excluded from the computation, slightly decreasing the high variability in muscle recruitment, and increasing similarity between individual and reference synergies, particularly when exoskeleton use is included in the analysis. This approach therefore appears to enhance the consistency of the reference synergies.

Similarity between individual and reference synergies across age groups

The similarity analysis detailed in Section 4.3.7 quantified the impact of age on muscle synergies across age groups and subgroups.

The highest similarity for both the *free_synergies* and the *whole_synergies* was observed between subjects and their own age subgroup, followed by their age group, **group_all**, and lastly the other age group, which consistently showed the lowest similarity (Figure 4.7).

However, similarity scores did not show significant differences across the four reference sets groups (own subgroup, own group, other group, entire dataset; all $p > 0.5$). Yet, in *whole_synergies*, age showed a significant negative association with similarity ($\beta = -0.0027$ per year, 95% CI [–0.0045, –0.0009], p = 0.004), suggesting reduced similarity in older participants. No age effect was observed for *free_synergies* (p = 0.22).
We observed an overall high variability of similarity values between subjects (Figure 4.7).

4.5 Discussion

This study explored the consistency of a "reference set of muscular synergies" obtained from healthy individuals to assess its reliability for future comparisons with patient populations performing the same experimental paradigm. Overall, results showed a substantial inter-individual variability in synergy structure, suggesting that "reference sets" should be applied with caution in rehabilitation scenarios, as individual differences affect how well a given participant's synergies align with the reference ones.

Moreover, we investigated whether age influences the synergistic structure within this experimental paradigm, and if it could therefore contribute to inter-subject variability. Results showed that age had only a small effect on the similarity between individual and reference synergies. However, when reference synergies were computed within homogeneous age groups, the number of excluded single-subject synergies decreased and their similarity to the reference increased.

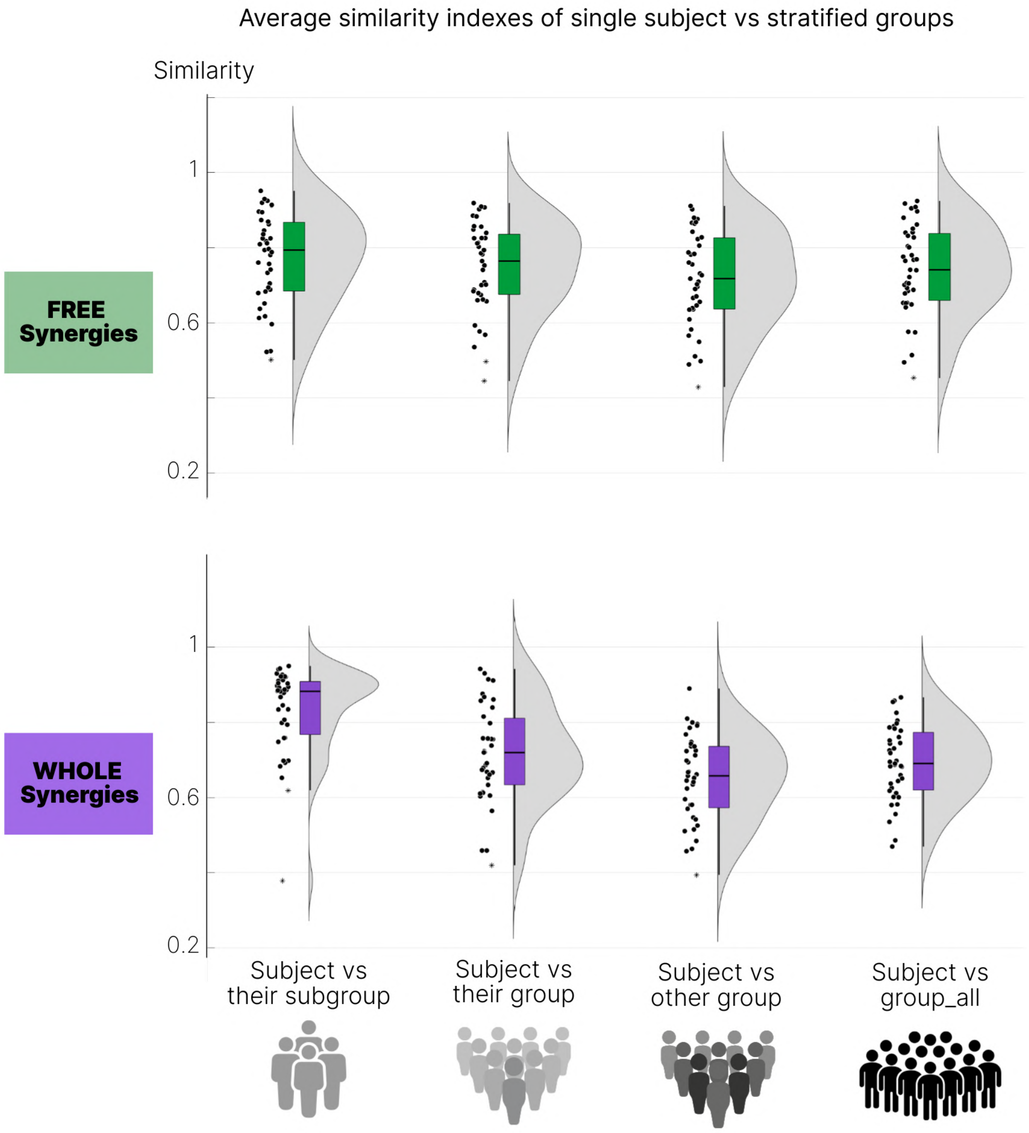

Figure 4.7 Average of cosine similarity across synergies for single subject vs. stratified groups and subgroups in the *free* (i.e., unassisted) and *whole* (i.e., unassisted and exoskeleton-assisted) conditions. The boxplots represent the median value of distribution (middle line) and 25th and 75th percentile (top and bottom of rectangle). The boxplot's whiskers represent the entire data range. Dots represent single subjects values of similarity and asterisks depict outliers. A violin plot (shaded gray area) describing the distribution of data points is superimposed on each boxplot.

These findings argue for age-stratified reference sets and, by extension, for careful consideration of key demographic factors when designing and interpreting synergy-based assessments intended for broad clinical comparison.

4.5.1 Reference synergies consistency aligns with previous literature, yet shows high variability

Overall, the reference *free* and *whole_synergies* are representative of the majority of single subject synergies, even though they dismiss a non-negligible amount of single subject motor modules (section 4.4.1). This is more notable in the reference *whole_synergies*, with $21.03\% \pm 12.09\%$ of single subject synergies excluded from its computation, compared with $13.45\% \pm 13.87\%$ excluded when computing the reference *free_synergies* (Section 4.3.6). This is directly reflected also in the values of similarity between the single subject synergies and the obtained reference synergies, where the average value for the *whole_synergies* (0.69 $\pm$ 0.10) is lower than for the *free_synergies* (0.74 $\pm$0.12).

Although a higher number of single subject synergies are included into the computation of the *free_synergies*, the composition of both *free_synergies* and *whole_synergies* still appears extremely variable across single individuals (Table 4.1 and 4.2).

We hypothesize that the higher number of single subject excluded and the lower similarity found in the reference *whole_synergies* may result from Float triggering a variable set of motor control responses in the healthy population, where multiple subjective parameters may come into play, such as for example the impact of age that we further explore in this study.

Similar previous studies have found comparable levels of variability. For example, Tropea and colleagues (12) assessed a robotic manipulator for the rehabilitation of acute post-stroke patients by building a reference set of synergies with 10 healthy subjects. The consistency of the reference synergies was tested by evaluating the cosine similarity between the single subject synergies grouped and averaged to obtain the reference synergies. They highlighted that for two out of the four identified reference synergies the median values of similarity was below 0.4. Interestingly, they found such low values both in the patient and non-patient population. Moreover, in the work by Coscia and colleagues (17), a set of reference synergies from 9 healthy subjects was used to test the effect of different levels of body weight support on the modular structure of upper limb movements. Similarly to our work, they used a set of comparative synergies to group single subject synergies accordingly to their similarity to the comparative set (section 4.3.6). Notably, for 3 out of 8 comparative synergies they found lower values of similarity (close to 0.5).

This literature indicates a relevant degree of inter-subject variability in the synergies obtained from healthy subjects across different tasks (i.e. planar or 3D movement) and different robotic platforms (i. e. manipulator or body weight support). Therefore, the high level of inter-subject variability found in the present study is not surprising. In a recent work assessing inter-subject variability during a 3D reaching task (43), the similarity of matched single subject synergies was comparable to the ones obtained in the present study. The authors raised concerns about the reliability of such reference sets, especially for future comparisons with patients population. They suggested that future investigation should focus on factors such as age or sex modulating muscle synergies reference sets. The present work can therefore be regarded as a continuation of the work by Zaho and colleagues (43) with a larger cohort of healthy individuals, while further examining the influence of age.

4.5.2 Reference synergies are modulated but not disrupted by robotic assistance

The reference synergies obtained in the present study can provide a quantitative characterization of the impact of the robotic assistance of Float on the modularity of our standardized reaching paradigm.

The 4 *free_synergies* are coherent with muscle synergies analyses performed by other groups on similar tasks (31; 34; 35), indicating the presence of anterior deltoid in combination with the upper trapezius and the pectoralis muscles.

Comparing these *free_synergies* with the *whole_synergies*, we notice a modulating effect of Float:

- The first *free_synergy* that mainly expresses the anterior deltoid and enforces shoulder flexion, is not present in the *whole_synergies* (Figure 4.4). In addition, neither the anterior deltoid shows a significant weight in any of the *whole_synergies*, suggesting a reduced activity of the anterior deltoid in assisted movements. This indicates that the feed-forward assistance to flex the shoulder provided by Float allow a reduced muscular effort at the level of the anterior deltoid;

- The second *free_synergy* expressing the trapezius muscle with a predominance of the upper trapezius, seems split into two *whole_synergies*: one expressing mainly the middle and lower trapezius and one expressing almost uniquely the upper trapezius.

Such behavior was identified also in previous work (41) and was attributed to two main features of Float: the use of a corset to interface the user and Float, which forces a straight back and a greater activation of the middle and lower trapezius; the model-based gravity compensation of Float, which does not prevent the user from perceiving the weigh of the exoskeleton on the shoulder, leading to an increased activation of the upper trapezius. These effects are explored more in detail in Chapter 3, Section 3.5.2;

- The fourth *free_synergy*, which enforces elbow flexion thanks to the synergistic action of brachioradialis and biceps is split into two *whole_synergies*: one expressing mostly the brachioradialis, and one expressing mostly the biceps. This suggests that the control of the elbow joint is fragmented into the activation of single muscles.

These results indicate that the assistance of Float modifies the underlying synergistic structure of our standardized reaching paradigm, but does not fundamentally disrupt it. Coherently with our previous study (41), which is detailed in Chapter 3, the assistance provided by Float appears to reduce the activation of anterior deltoid, which could be promising for the design of post-stroke interventions to address the often-observed abnormal coupling between deltoids and elbow flexors (38). Moreover, we observed a greater involvement of lower, middle and upper trapezius, possibly due to the coupling between the user and the exoskeleton through the corset and to the model-based friction compensation implemented at the robotic joints. In general, the control of movement appears fragmented into a greater number of motor modules, involving few muscle groups and indicating a less-optimized synergistic structure. These findings are coherent with our previous studies (40; 41) conducted in a subset of 20 participants and described in Chapter 3.

4.5.3 Age slightly modulates the synergistic structure of the standardized reaching task

When computing a set of reference *free_synergies* and a set of reference *whole_synergies* for each age group and subgroup, the reference *free_synergies* obtained from the age groups closely matched those obtained from the complete dataset (Figure 4.5). On the contrary, *whole_synergies* appeared more variable across age groups and subgroups, with no age group or subgroup having a complete match with the entire dataset (Figure 4.6). We observed that when healthy subjects perform the task with the assistance of Float, their synergistic patterns of muscular activity is altered, which may be due to age.

Moreover, the presence of age-specific motor modules in certain age groups and subgroups not present in the general reference synergies (Figure 4.6) may indicate that while the reference *whole_synergies* do reflect the overall effect of Float across the entire population considered in the study, yet they may overlook age-specific variations.

Reference synergies of age-matched subjects show higher consistency

Table 4.4 shows high variability in the composition of reference synergies: the coefficients of variation of the reference synergies obtained from the age groups and subgroups are lower than those of the general reference synergies from **group_all**, but still close to 1. Nevertheless, the average similarity of single subjects with their age-groups reference synergies is mostly higher than with those from **group_all** (Table 4.5).

This trend is statistically significant for *whole_synergies* of **subgroup_25-30**, **subgroup_30-50**, **subgroup_50-60** and **group_50-80**, as well as for the reference *free_synergies* of **subgroup_60-80**. Similarly, for age groups, the number of single subjects synergies excluded from the computation of the reference *whole_synergies* decreases (Table 4.3), which reaches statistical significance for **subgroup_25-30** and **group_25-50**. A similar trend is not observed for the *free_synergies*.

These findings suggest that dividing the participants based on age may lead to a small, yet significant improvement in the consistency of the reference synergies. This is particularly true for the *whole_synergies*, which is coherent with the greater impact that age appears to have on the *whole_synergies* with respect to the *free_synergies*.

These findings support the idea that building reference synergies with age-matched subjects could lead to more reliable baselines for rehabilitation assessments.

Older subjects show greater variability

Overall, single-subject synergies show greater similarity to the average synergies of their age-matched subgroup and group than those of other groups or **group_all** (Figure 4.7). This trend is observed for both *free_synergies* and *whole_synergies* and seems more pronounced for *whole_synergies*, but does not exhibit statistical significance.

Nevertheless, we observed a small, yet significant negative association between age and similarity, meaning that the average similarity between a subject's muscle synergies and the reference synergies decreases with age.

Notably, a significant effect of age is observed when considering movements executed with the assistance of Float (*whole_synergies*). This may indicate that older subjects develop a more personalized motor control response to perceived external disturbances. This is aligned with a recent study investigating muscle synergies in a walking task, reporting a higher inter-subject variability in the older population (44). Such effect was attributed both to different age-dependent changes in gait biomechanics and different sensorimotor experience of the subjects through the years.

These findings suggest that capturing the modularity shared among older subjects performing a reaching task with Float is more challenging than representing the modularity of younger subjects performing the same task, due to a greater level of inter-subject variability. This is particularly relevant because the incidence of many neurological conditions increases with age. Reliable reference data from an older healthy population are therefore essential to enable meaningful assessments, especially when using rehabilitative devices.

4.5.4 Study limitations and future work

The *whole_synergies* set was computed with muscle synergies grouped across all experimental conditions, including both unassisted and assisted movements performed with two different assistance levels. This methodological choice aimed to obtain an ecologically valid set of reference synergies representative of the entire standardized experimental paradigm.
This approach enables to focus on activation levels independently of specific task conditions and to characterize the overall modularity of the task, rather than compare exoskeleton-assisted versus unassisted movements. Accordingly, the activation coefficients can be derived from a common set of synergies, since comparing coefficients extracted from different synergy sets would not be methodologically sound. For this reason, all conditions were analyzed together, even though this choice precluded a direct quantification of the impact of different assistance levels on spatial modules.
Such a comparison was already addressed in our previous work (41), where the temporal coefficients of the *free* and *whole_synergies* were computed. Therefore, this analysis was beyond the scope of the present study.
This methodological choice also precluded direct comparison between the *free* and *whole_synergies*, as the latter includes the data used to compute the former. We acknowledge this limitation and, in future work, we plan to integrate reference sets of synergies describing assisted-only movements.

Another important methodological choice is the procedure for selecting the number of synergies that impacts both synergies composition and sparseness (14). We selected the number of synergies explaining at least 0.9 of data variance (quantified by VAF or R^2 (31)), as this is the most widely applied criterion (14), favoring comparison with available literature. At the same time, the robustness of our results would benefit from future comparison with other VAF thresholds or different criteria not relying on arbitrary thresholds (53).

Moreover, the subgroup analyses included a limited number of participants per group (approximately 10 subjects), even though the overall sample size of the study was relatively large compared to other muscle synergy studies. This limitation may have influenced the composition of motor modules, preventing us from drawing robust conclusions. Nevertheless, the analysis of single-subject synergies similarity with group-averaged synergies was conducted on the full dataset, enhancing the robustness and supporting the reliability of this finding.
In addition, the age groups and subgroups were not homogeneous in terms of the number of subjects and the spanned age range. This limitation arose because the dataset analyzed in this study was not originally designed to investigate age-related differences in muscle synergies. Future studies with larger cohorts, or specifically tailored to investigate age-related effects, may to further validate the consistency of the motor modules, and explore other potentially relevant factors, such as sex (54) or training level (55).

Another implication of this limitation is the reliance on self-paced movements (15). We acknowledge that movement speed is known to influence the structure and modulation of muscle synergies (34; 56). Unfortunately, the implementation of visual or auditory cues (e.g. a metronome) to directly control movements speed would be impractical within this experimental protocol, as we aimed to concurrently record electroencephalography (EEG) signals, which could be influenced by such external stimuli.
Future data collection will integrate the recording of upper-limb kinematics into the experimental protocol. This will allow to better account for potential differences related to movement speed and to more comprehensively characterize the impact of exoskeleton assistance and age on movement production. Future analysis will also directly examine single muscle activations to gain a more granular understanding on the impact of Float, thereby supporting the interpretation of the the identified synergies and their functional implications.

Lastly, the use of cosine similarity as a metric for comparing the structure of muscle synergies may be sensitive to the number of dimensions (57). However, this metric is the gold standard for evaluating similarity between muscle synergies and we adopted it to be able to compare our results with similar works (12; 17; 43). Furthermore, for the present analysis this limitation has a minimal impact, as the dimensionality of spatial modules is small and statistical significance was achieved for the similarity values, supporting the validity of our conclusions. Future work will adopt dimension-insensitive metrics such as the euclidean metric (57), or normalize cosine similarity with respect to similarity at chance level (31).

4.6 Conclusion

This study investigated muscle synergy structure and age-related inter-subject variability across healthy subjects performing a standardized reaching with and without the assistance of the Float exoskeleton. Our results suggest that the introduction of the robotic device, while maintaining fundamental synergy structure, increases both the overall complexity of the movement (evidenced by a higher number of extracted synergies) and the inter-subject variability of the resulting reference synergy set.
Our results highlights how dividing the participants in age groups allows to identify relevant age-specific adaptations to the robotic assistance while potentially improving the consistency of the reference synergy sets. This suggests that relying on age-matched reference synergies could improve the robustness of synergy-based assessment in rehabilitative applications.
Furthermore, there was an increased variability in older individuals, which could be due to more personalized adaptation strategies when interacting with the exoskeleton. This poses a significant challenge for constructing robust, age-matched healthy reference models, emphasizing that age and device context are critical considerations for the application of muscle synergies in rehabilitation technology.

Overall, this work supports the utility of muscle synergy analysis in characterizing motor control and provides useful insights into the effects that both robotic assistance and age have on muscle coordination patterns during upper-limb reaching in robot-assisted tasks. These findings could be used to inform and refine the design of personalized assistive technologies and rehabilitation protocols.

Chapter 5

Impact of Float on the modularity of anterior reaching in post-stroke subjects

The assessment of the impact of Float was carried out first with a population of 40 healthy individuals (15). In this context I explored the impact of Float on the synergistic structure of reaching, developing the studies presented in Chapter 3 and Chapter 4. Subsequently, a data collection to study the impact of Float has been conducted with 36 post-stroke subjects (18 with right hemiparesis and 18 with left hemiparesis) at the Villa Beretta Rehabilitation Center, Valduce Hospital, Lecco, Italy.

Data collection was carried out during the final year of this PhD project, and I directly contributed to the acquisition of a substantial portion of the dataset (20 out of 36 enrolled participants). Given the timing of the data acquisition, a complete analysis of the entire cohort was beyond the time frame of the present thesis. Therefore, this Chapter reports a preliminary analysis conducted on a subset of five post-stroke subjects with right hemiparesis.

The preliminary analysis here described formed the basis for an extended abstract submitted at the 7th International Conference on NeuroRehabilitation (ICNR 2026): *I. Ceroni, E. Guanziroli, F. Molteni and M. Semprini, "Impact of Float Exoskeleton on the Modularity of Anterior Reaching in Chronic Post-Stroke Subjects".*

5.1 State of the art

Stroke is one of the major causes of physical impairment, leading to hemiplegia, paraplegia, paresis, impaired speech, restricted physical abilities, and difficulty gripping or holding things (58). Based on the data from 1990 to 2019, stroke is the second-leading cause of death and the third-leading cause of death and disability globally (59). Residual chronic hemiparesis occurs in over 40% of those individuals with an acute hemiparesis following stroke (60; 61). Chronic deficits are especially prevalent in the distal upper extremities (62).

Substantial evidence indicates that motor recovery after stroke is enhanced by intensive, repetitive, and task-oriented training (5). This evidence has supported the integration of robotic devices into neurorehabilitation practice. Robot-assisted arm training has demonstrated promising effects in improving ADLs, upper limb motor function, and muscle strength in individuals post-stroke (8; 9; 10).

In this context, EMG recordings offer a valuable tool for characterizing motor control and its reorganization following neurological injury. In particular, muscle synergy analysis (1) has gained increasing attention for the characterization of muscle pattern alteration after stroke (13). Growing evidence suggests that muscle synergies provide clinically relevant information that may not be captured by conventional clinical scales or kinematic analyses (14).
The muscle synergies paradigm have been used to assess the impact of stroke on the structure of motor control (13), as well as to characterize the possible benefits of robotic rehabilitative devices on the recovery of a more physiological-like pattern of muscle activation (10; 18).

5.2 Objective

The aim of the present study is to preliminarily assess the impact of the Float upper limb exoskeleton (2) on the muscle synergies characterizing anterior reaching in chronic post-stroke subjects.

5.3 Materials and methods

5.3.1 Participants

The population included in this preliminary analysis consists of five post-stroke subjects (3 male, 2 female, age 62+/-8. years old), who experienced the last acute event from 6 to 96 months prior to the study. Table 5.1 reports the demographics of the population considered for this study and the score in the Box and Block test (BBT) (63).

Subject	Age	Gender	Months from lesion	BBT
S1	49	male	12	13
S2	69	male	6	30
S3	64	male	96	18
S4	58	female	24	13
S5	70	female	6	24

Table 5.1 Participants.

5.3.2 Experimental task

The experimental protocol of the study involved the execution of a pseudorandomized sequence of 30 reachings towards 3 targets and was repeated first without Float (condition Pre), then with Float (condition Float) and finally without Float (condition Post). During the Float condition, the five post-stroke subjects included in this study received a high level of assistance on the right shoulder (which is the most affected one for these subjects). Bipolar EMG was recorded at 1000 Hz in the following muscles: 1) biceps brachii (long head), 2) anterior deltoid, 3) middle deltoid, 4) posterior deltoid, 5) triceps brachii (long head), 6) upper trapezius, 7) medial trapezius, 8) lower trapezius, 9) pectoralis major, 10) brachioradialis.

5.3.3 EMG preprocessing

We epoched the EMG recording of each subject into single reaching trials. The EMG signal was band-pass filtered between 20 and 350 Hz using a 4th order Butterworth filter and then rectified. Subsequently, an ad-hoc median filter was applied and values over 600 μV were substituted with the median over a sliding window of 50 samples. Lastly, a low pass filter with cutoff at 5 Hz (4th order Butterworth) was applied to obtain the envelope of the signal, which was normalized in amplitude as in (31) and in time as in (16).

5.3.4 Synergies extraction

Normalized EMG envelopes were concatenated for each of the three conditions (Pre, Float, Post) and muscle synergies were extracted using the non-negative matrix factorization algorithm (32) applied 100 times with random initialization. The number of synergies was selected as the one guaranteeing a variance accounted for (VAF) of at least 0.9, similarly to (31).

5.3.5 Comparison with reference synergies

Muscle synergies were extracted for each subject and for each experimental condition. These synergies were then compared with reference synergies derived from a cohort of 39 healthy individuals performing the same standardized reaching task under a slightly different experimental paradigm.

In the healthy cohort, participants performed the reaching task first without Float (free condition), and subsequently with Float providing low assistance (low condition) and high assistance (high condition). The order of the two assisted conditions was randomized across participants.

The reference synergies representative of the modular organization shared across the 39 healthy individuals are described in detail in Chapter 4. Briefly, two sets of reference synergies were obtained: (i) the reference *free_synergies*, extracted from unassisted reaching movements only, and (ii) the reference *whole_synergies*, derived from the entire experimental paradigm, including both unassisted and assisted conditions, thus providing an ecological characterization of motor modularity across a rehabilitation-like session.

However, the experimental protocol performed by the post-stroke participants differed slightly from that of the healthy cohort, particularly with respect to the assistance configuration. The five post-stroke subjects considered in this study received high assistance during the Float condition. Therefore, to ensure condition-specific comparability, an additional set of reference synergies was computed from the healthy cohort considering exclusively the high-assistance condition (hereafter referred to as *high_synergies*). This strategy enabled comparisons between post-stroke and healthy subjects under matched assistance levels, thereby avoiding potential confounding effects associated with pooling conditions characterized by different mechanical demands.

Accordingly, condition-specific comparisons were performed as follows: (i) synergies extracted from the Pre condition were compared with the reference *free_synergies*; (ii) synergies extracted from the Float condition were compared with the reference *high_synergies*; (iii) synergies extracted from the Post condition were compared with the reference *free_synergies*. A schematic representation of the comparison framework is provided in Figure 5.1.

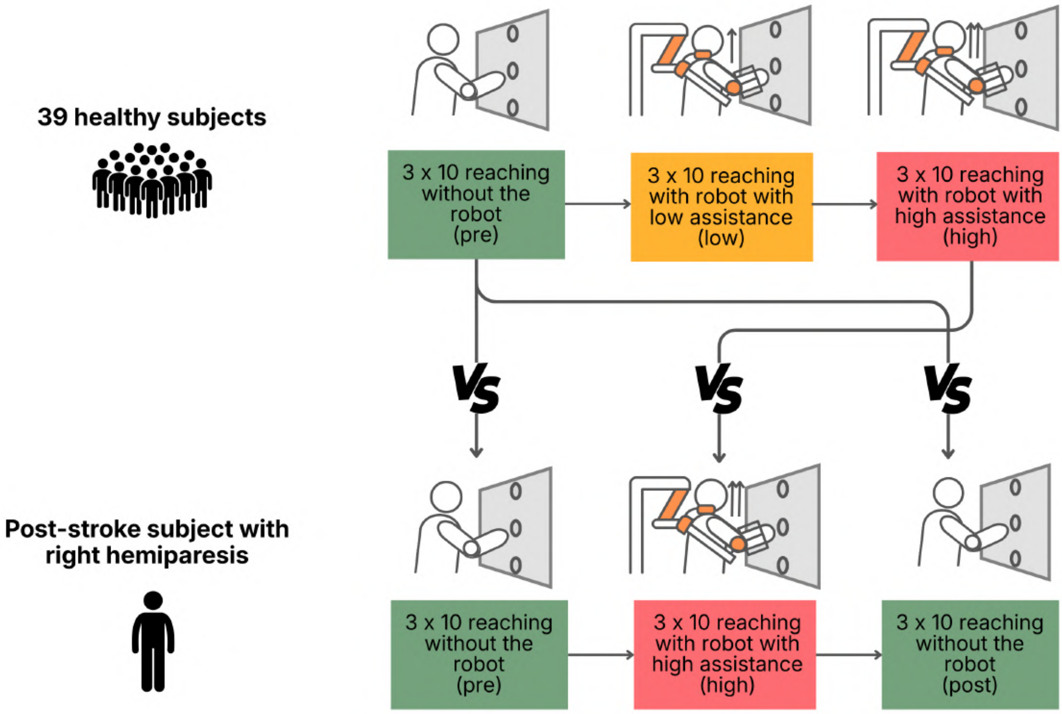

Figure 5.1 Schematic diagram of the comparisons between the synergies of single post-stroke subjects and reference synergies obtained from 39 healthy individuals.

Muscle synergies extracted from post-stroke subjects were classified as matching a reference synergy if the cosine similarity (31) exceeded 0.7, and as partially matching if the similarity was between 0.5 and 0.7.

The presence of post-stroke synergies arising from fractionation and/or merging of reference synergies was evaluated according to the linear combination model described in (13). Only one fractionation event was identified. In that case, cosine similarity was computed between the reference synergy and the linear combination of the two post-stroke synergies identified as originating from its fractionation.

To quantify the similarity between post-stroke and healthy modular organization, three metrics were computed: (i) the percentage of reference synergies that were matched or partially matched; (ii) the number of post-stroke synergies relative to the number of reference synergies; (iii) the average cosine similarity of matching synergies, normalized by the total number of reference synergies, computed as in:

$$Sim = 1/N_{reference} \sum_{(i,j)\varepsilon matching} cs_{ij} \tag{5.1}$$

where cs_{ij} denotes the cosine similarity between the i-th reference synergy and the j-th post-stroke synergy, and $N\_reference$ is the total number of reference synergies.

5.4 Results

5.4.1 Reference synergies from healthy subjects

To enable condition-specific comparisons, a set of reference synergies representative of reaching movements performed by healthy controls under high assistance was extracted and defined as *high_synergies*.

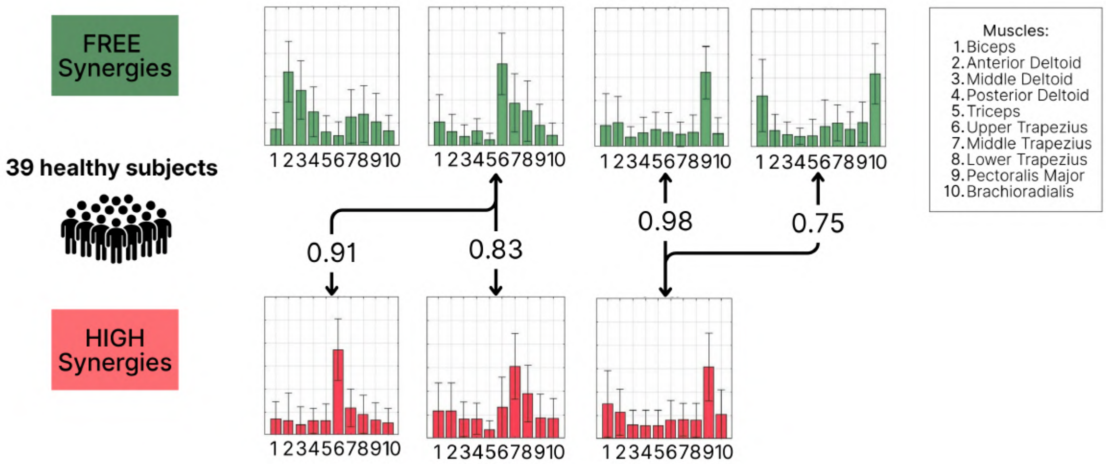

Figure 5.2 Reference muscle synergies representative of 39 healthy individuals extracted from the unassisted reaching movements (*free_synergies*, upper row) and from the reaching movements executed wearing Float providing high assistance (*high_synergies*, lower row).

Figure 5.2 reports the composition of the reference *free_synergies* (upper row) and *high_synergies* (lower row), along with the cosine similarity values between corresponding modules.

Figure 5.2 reveals the following differences between the two conditions:

- The first *free_synergy* expressing mainly the deltoids with a prevalence of anterior deltoid finds no correspondence in the *high_synergies*. In the high-assistance condition, the contribution of the anterior deltoid is reduced across modules, indicating a reduced recruitment of this muscle group and suggesting that the assistance of Float is effective in supporting shoulder flexion.

- The second *free_synergy* appears split into the first and second *high_synergy* expressing mainly the upper trapezius and the middle and lower trapezius respectively. This redistribution suggests a relative increase in the involvement of middle and lower trapezius muscles, which may be due to the posture imposed by Float, as discussed in Chapter 3 Section 3.5.2 and Chapter 4 Section 4.5.2.

- The third *free_synergy* expressing mainly the pectoralis shows a clear correspondence with the third *high_synergy*.

- The fourth *free_synergy* primarily involving the elbow flexors (biceps brachii and brachioradialis), exhibits only modest similarity with the third *high_synergy*, in which these muscles display a limited contribution.

5.4.2 Similarity analysis between post-stroke synergies and reference synergies

Figures from 5.3 to 5.7 show the comparison of the muscle synergies patterns of the 5 post-stroke subjects included in the study with the reference *free* and *high_synergies* obtained from the healthy individuals. The results of the comparison are reported in Table 7.1.

Subject	Condition	% Matched	N_{syn}	Sim
S1	Pre	100	$=$	0.82
	Float	100	> 2	0.87
	Post	100	> 2	0.86
S2	Pre	100	> 1	0.88
	Float	100	> 2	0.85
	Post	100	> 2	0.90
S3	Pre	75	$=$	0.61
	Float	100	> 1	0.76
	Post	100	> 1	0.81
S4	Pre	100	> 2	0.87
	Float	66	> 1	0.60
	Post	75	> 1	0.79
S5	Pre	75	> 1	0.63
	Float	66	> 1	0.55
	Post	100	> 1	0.80

Table 5.2 Results of muscle synergies analysis.

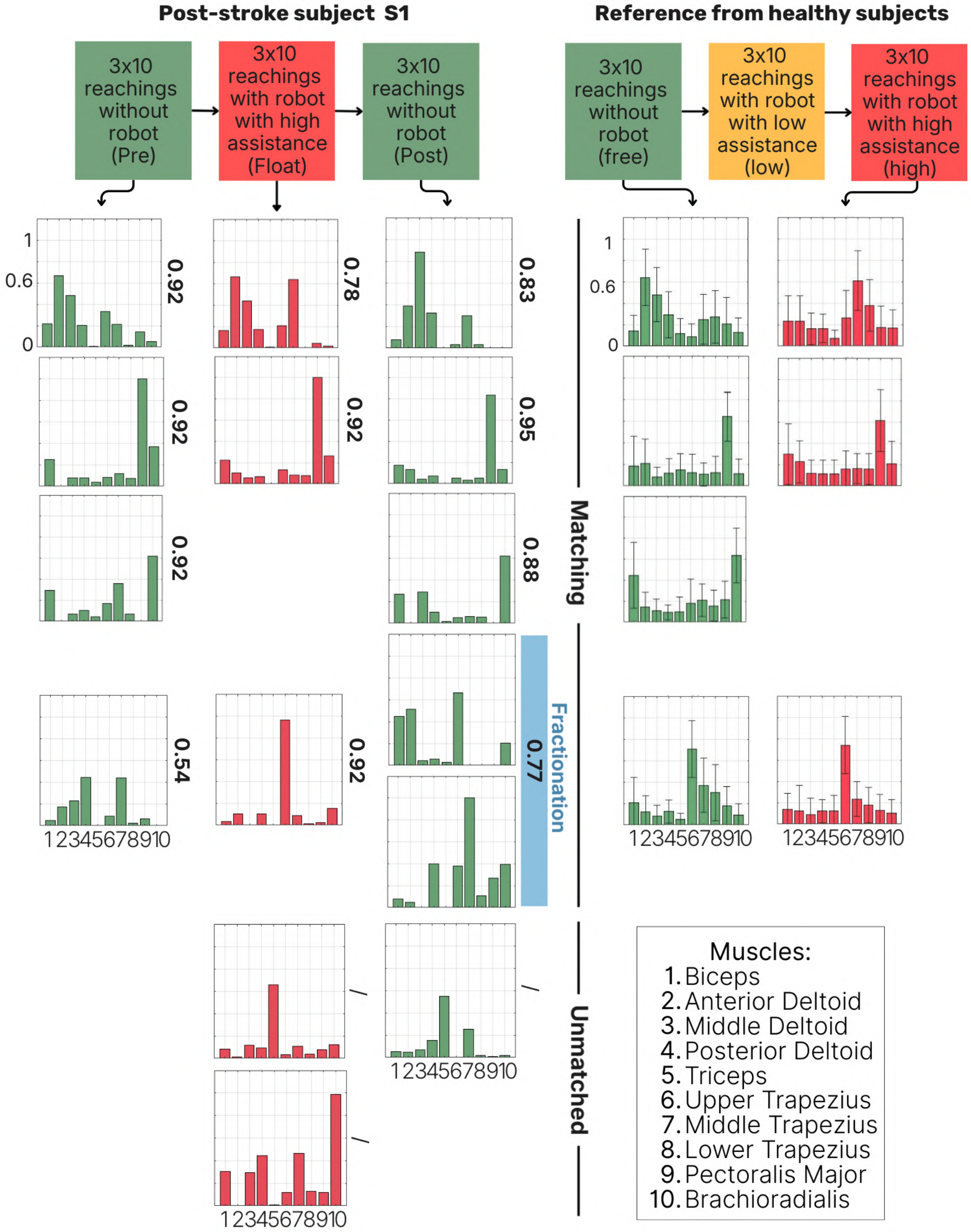

Figure 5.3 On the left side, the experimental paradigm (top) and muscle synergies for post stroke subject S1. On the right side the experimental paradigm (top) and reference muscle synergies obtained from 39 healthy individuals. Bold numbers close to synergy patterns represent cosine similarity with the corresponding reference synergies. Fractionation of one reference synergies into two S1 synergies is indicated by light blue bar.

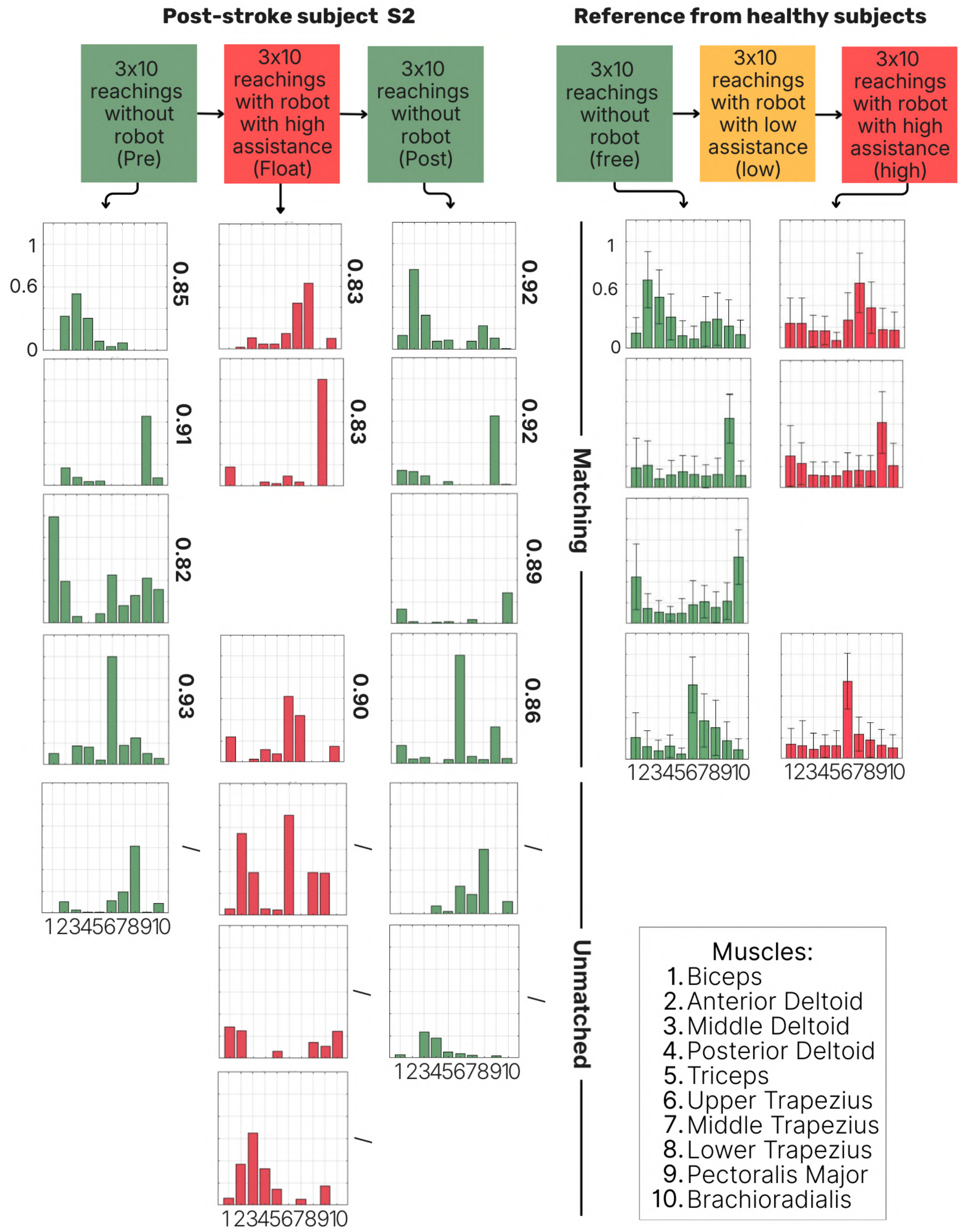

Figure 5.4 On the left side, the experimental paradigm (top) and muscle synergies for post stroke subject S2. On the right side the experimental paradigm (top) and reference muscle synergies obtained from 39 healthy individuals. Bold numbers close to synergy patterns represent cosine similarity with the corresponding reference synergies.

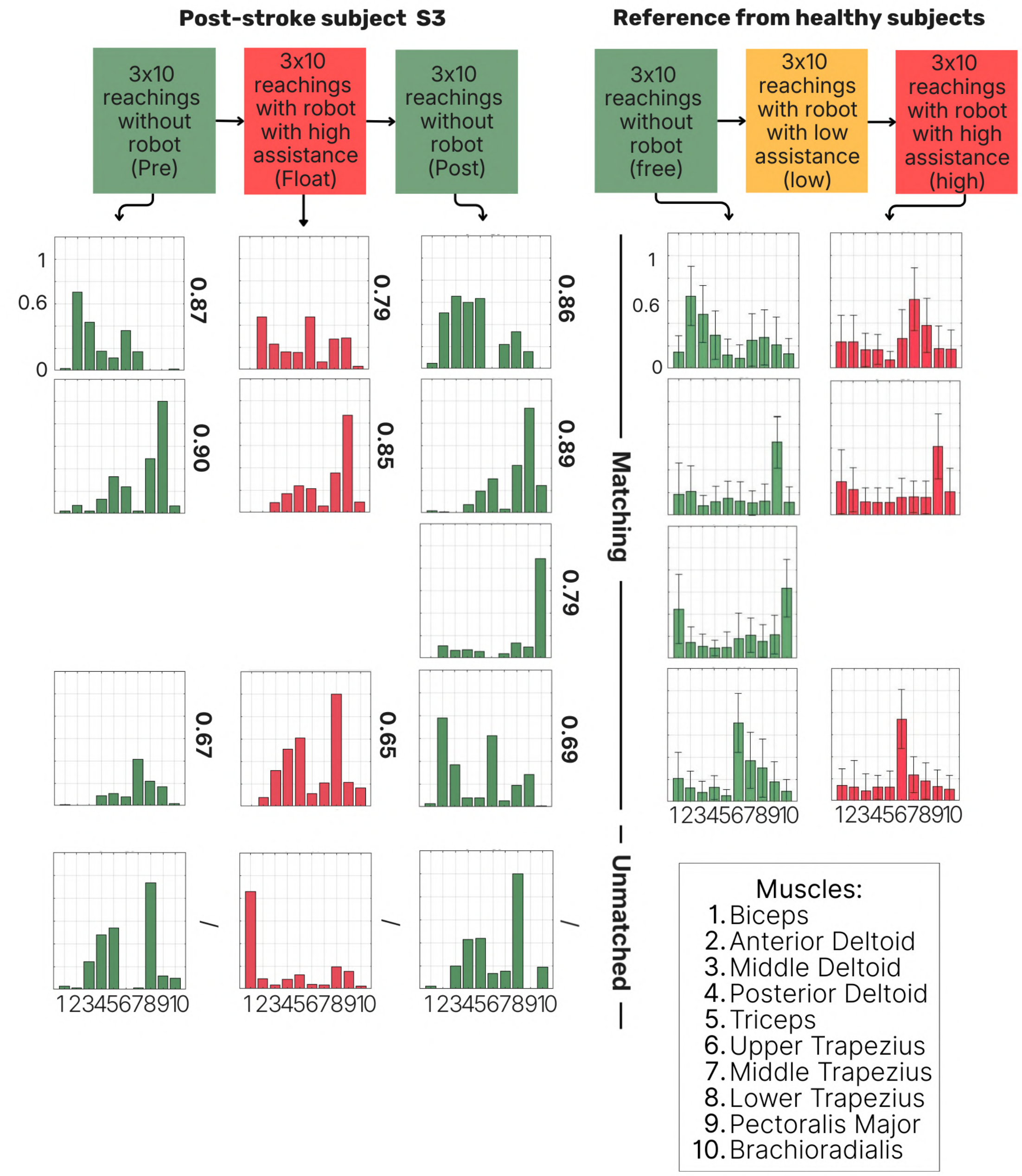

Figure 5.5 On the left side, the experimental paradigm (top) and muscle synergies for post stroke subject S3. On the right side the experimental paradigm (top) and reference muscle synergies obtained from 39 healthy individuals. Bold numbers close to synergy patterns represent cosine similarity with the corresponding reference synergies.

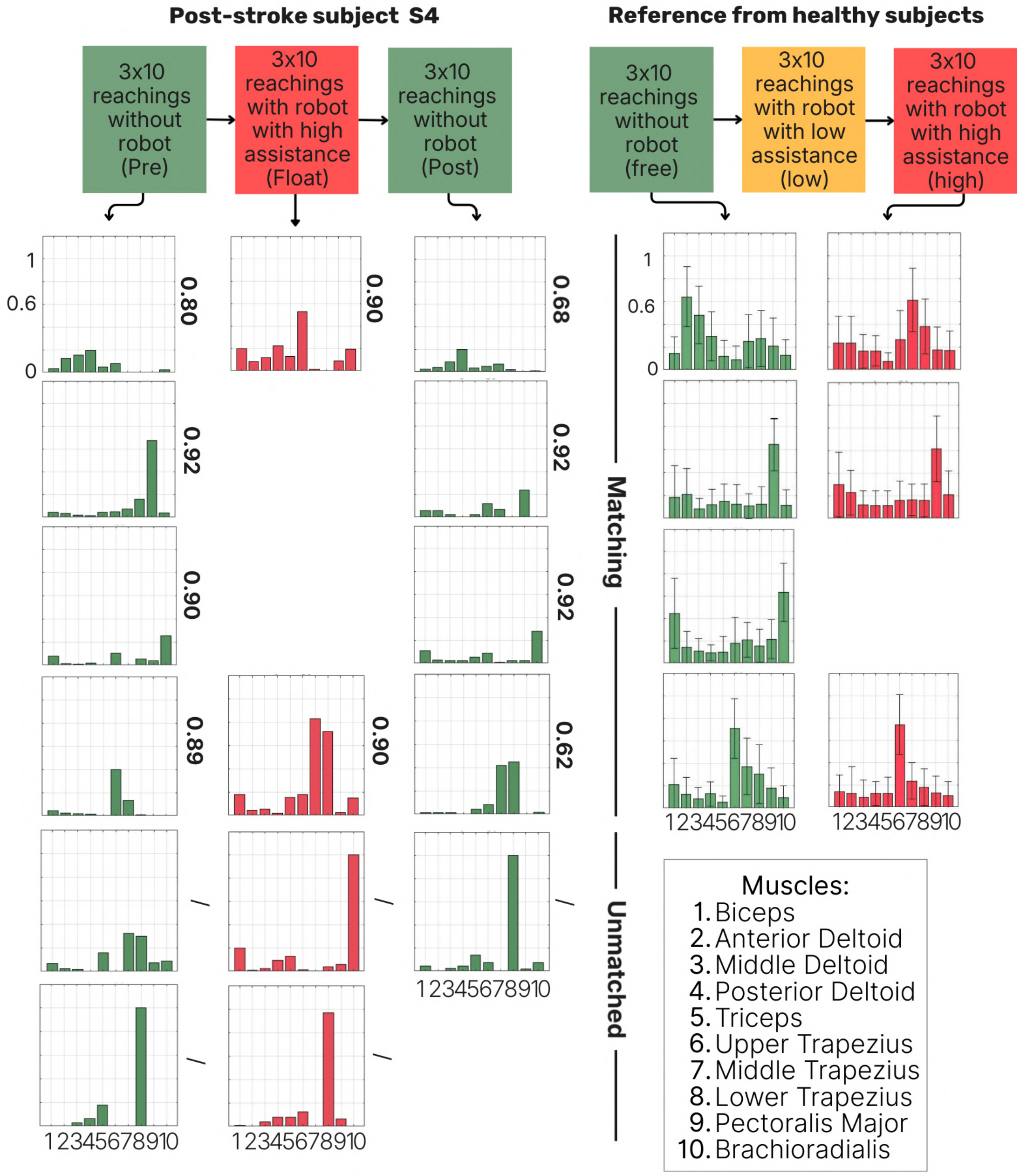

Figure 5.6 On the left side, the experimental paradigm (top) and muscle synergies for post stroke subject S4. On the right side the experimental paradigm (top) and reference muscle synergies obtained from 39 healthy individuals. Bold numbers close to synergy patterns represent cosine similarity with the corresponding reference synergies.

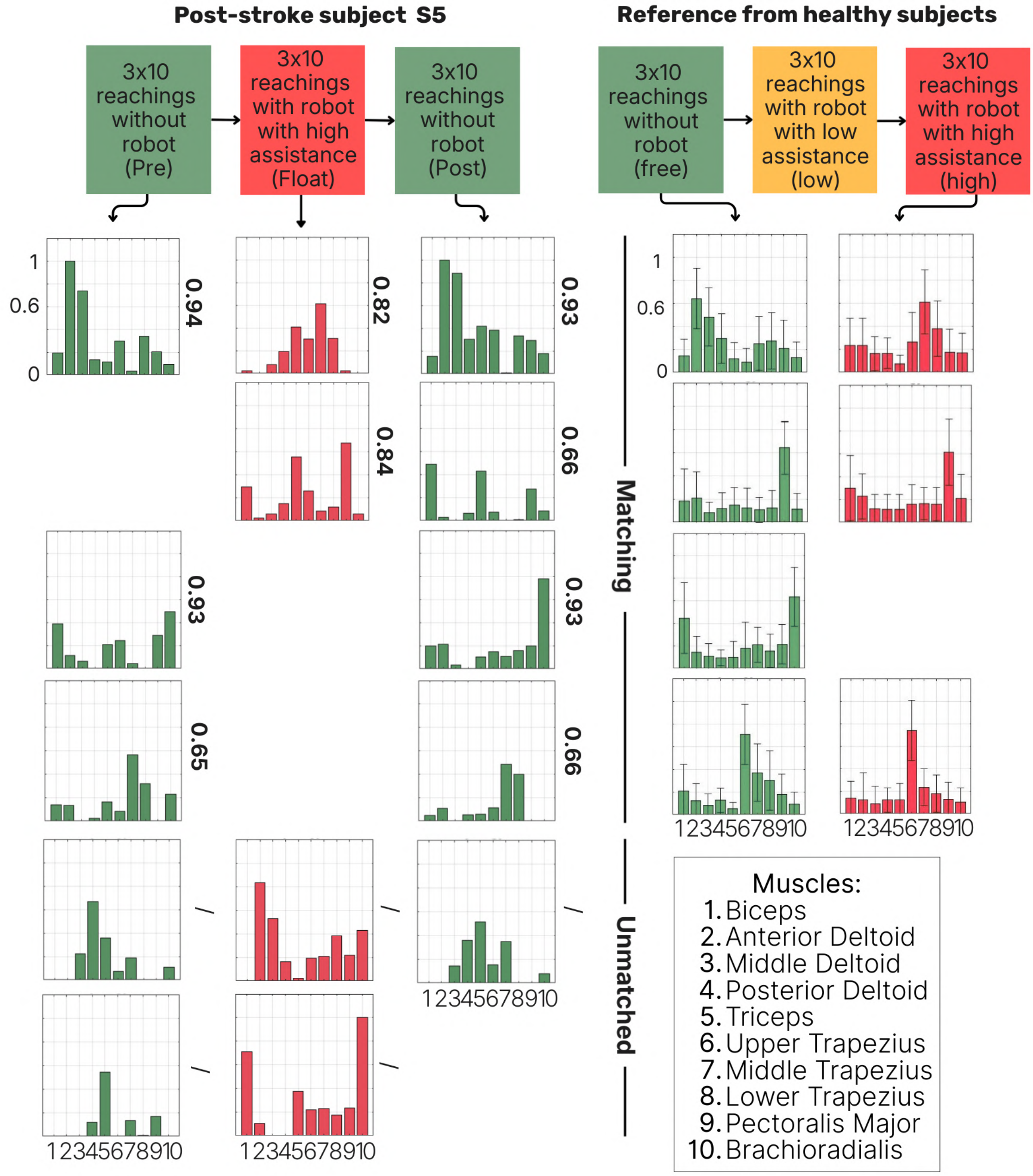

Figure 5.7 On the left side, the experimental paradigm (top) and muscle synergies for post stroke subject S5. On the right side the experimental paradigm (top) and reference muscle synergies obtained from 39 healthy individuals. Bold numbers close to synergy patterns represent cosine similarity with the corresponding reference synergies.

For 4 out of 5 subjects (S1, S2, S3 and S5), the similarity of the muscle synergies with the reference synergies from healthy individuals improved from Pre to Post condition. For these subjects, the number of synergies in the Post condition and the percentage of synergies matching with the reference synergies were equal to or higher than Pre condition.

5.5 Discussion

After a single session of reaching exercise assisted by the Float exoskeleton, four out of five chronic post-stroke participants showed an increased similarity between their muscle synergies and reference synergies derived from healthy individuals. For these subjects, the number of extracted synergies in the Post condition was equal to or greater than in the Pre condition, and the proportion of synergies matching the reference set also increased. These findings suggest that even a brief exposure to exoskeleton-assisted reaching may acutely promote a reorganization of muscle coordination patterns toward a more physiological modular structure.

Interestingly, similar changes have been reported in a longitudinal study by Pierella and colleagues (18), who investigated the effects of four weeks of intensive upper limb training using the Alex exoskeleton (7) in six subacute post-stroke individuals. In that study, the number of muscle synergies significantly increased over the training period, and their structure progressively became more similar to that of healthy controls. These neuromuscular changes were accompanied by improvements in kinematic performance and clinical scales, consistent with the spontaneous recovery processes expected in the subacute phase (64).

In contrast, the present study focused exclusively on chronic post-stroke individuals, a population in which muscle synergy structure is generally considered relatively stable. Despite the absence of spontaneous recovery mechanisms, we observed modifications in synergy number and structure after only a single, brief (around 10 minutes) session of exoskeleton-assisted reaching. This suggests that the modular organization fo reaching in chronic stroke may show a degree of short-term adaptation to robotic assistance.

While the changes observed cannot be directly interpreted as functional recovery, the direction of the modifications toward increased similarity with healthy reference synergies is promising as it has been associated with motor improvement in previous work (18). These preliminary findings therefore raise the possibility that even a short intervention with Float may temporally promote more physiological coordination strategies, potentially stimulating motor relearning. However, given the limited sample size, these results should be interpreted cautiously and further investigations including a greater number of subjects are needed to consolidate them.

Moreover, future analysis should combine muscle synergy analysis with kinematic and EEG-based metrics to establish whether changes in modular organization translate into improved task execution and to identify possible neurophysiological correlates of motor learning.

5.6 Conclusion

This preliminary study suggests that even a single, brief session of Float-assisted reaching may induce short-term modifications in the modular organization of muscle activity in chronic post-stroke individuals, promoting patterns that more closely resemble those of healthy subjects. Although these findings cannot be directly interpreted as functional recovery and must be considered in light of the small sample size, they provide initial evidence that the robotic assistance of Float may favor the emergence of more physiological muscle patterns during standardized reaching. Future studies considering a greater population and integrating kinematic and neurophysiological measures are needed to determine whether these modular changes translate into meaningful motor improvements and reflect underlying learning-related neural processes.

Part II

Motor units based characterization of grasping

Chapter 6

ReGULA experimental paradigm

Part II of this thesis presents two preliminary studies that explore the use of surface EMG decomposition algorithms (3) to characterize the activity of the motor units of relevant upper limb muscles during the execution of different types of grasps and hand gestures derived from activities of daily living.

The activation of the motor units reflects that of spinal motor neurons, which constitutes the ultimate neural representation of voluntary motor command before it is transformed into muscle forces and motion (19). For this reason, motor unit discharge patterns theoretically represent a neural-level control signal for rehabilitative devices, an approach that has recently been explored with promising results (19).

The studies presented in this part aim to leverage the neural information encoded in motor unit activity to derive insights that may inform the design and optimization of EMG-based control strategies, with a specific focus on upper limb prostheses.

Recent advancements in myoelectric upper-limb prosthetics have enabled users to control prostheses with multiple degrees of freedom (DoFs) (20). Particularly, pattern recognition is one of the most explored methods to allow the control of multiple DoFs and has been recently made available in commercial prostheses (e.g. Coapt 2017, Ottobock 2019, i-biomed 2021) (21). Nevertheless, despite technological advancements, current control algorithms often fail to reach satisfactory levels of robustness and intuitiveness, leading to high rates of upper limb prostheses abandonment (22).

The study presented in Chapter 7 focuses on the well-documented degradation of pattern recognition algorithms when tested across different arm configurations (23). Specifically, this study investigates the neural mechanisms underlying the decline in classification performance observed under varying limb postures. While previous research has characterized these effects at the level of global EMG features (24), it remains unclear how changes in arm configuration influence the action potentials of individual motor units, which constitute the fundamental building blocks of the surface EMG signal.

The study described in Chapter 8 extends this line of investigation by evaluating whether features derived from motor unit activation patterns can enhance traditional pattern recognition approaches. Rather than relying exclusively on amplitude- or frequency-based EMG descriptors, this work examines whether neural-level features provide improved performance and physiological interpretability for prosthetic control.

To enable a systematic investigation of motor control during functional behaviors relevant to prosthesis users, a standardized experimental framework was developed to characterize goal-directed upper-limb movements, including reaching, object grasping, and object transport tasks. Inspired by the NeBULA framework (developed by our research group for the standardized assessment of anterior reaching and described in Chapter 2) , this new protocol named ReGULA (Reach and Grasp for Upper Limb Assessment) integrates structured grasp and transport tasks within a scalable and reproducible assessment platform. ReGULA was leveraged for the study presented in Chapter 7 and provides a foundation for future investigations into both prosthetic control strategies and neurophysiological mechanisms of motor impairment.

The development of ReGULA was carried out in collaboration with two other PhD researchers, reflecting the interdisciplinary nature of this work.

6.1 ReGULA: Reach and Grasp for Upper Limb Assessment

While NeBULA was specifically designed to assess reaching, we were interested to extend this framework to encompass more complex, goal-directed movements that closely resemble activities of daily living (ADLs). In particular, we aimed to incorporate the assessment of grasping function, a fundamental component of upper-limb motor behavior. Grasping is essential for a wide range of ADLs and represents one of the most clinically relevant upper-limb functions for both rehabilitation and functional evaluation (11).

Impairments in grasping are among the most common and disabling consequences of neurological lesions such as stroke, and recovery of hand function remains particularly challenging (60; 62). Beyond the clinical domain, grasping is also a central function in the design of active hand prostheses. In 1989, Cutkosky (65) identified the autonomous selection and execution of appropriate grasp strategies for object manipulation as a major objective in robotics. Despite substantial advances in mechatronic design, even state-of-the-art upper-limb prostheses continue to exhibit high abandonment rates (22), highlighting persistent limitations in functionality and usability.

Another key objective was to span a large three-dimensional workspace encompassing multiple arm configurations. Sampling motor behavior across diverse limb postures enables the derivation of motor-control-related metrics that capture a broader repertoire of upper-limb configurations, thereby contributing to a more ecologically valid understanding of complex movement control. Moreover, extracting these metrics across varying limb configurations may support the development of more robust control algorithms for assistive robotic devices. It is well established, for example, that the performance of upper-limb prosthesis control algorithms often deteriorates when users modify arm posture (23), highlighting the importance of investigating motor behavior metrics across a wide workspace.

To enhance ecological validity, we opted to employ real objects rather than virtual targets. Furthermore, we incorporated an object transport phase following the grasping phase, thereby enriching the movement repertoire and enabling the assessment of sequential motor primitives within a single task.

Building upon these considerations, we developed a novel framework designed to facilitate the standardized assessment of complex upper-limb actions integrating reaching, grasping, and object transport. Referring to the movement taxonomy proposed by Schambra and colleagues (66), and subsequently adopted by Longatelli and colleagues (11), we specifically targeted the movement primitives reach for grasp and transport. We named this framework ReGULA (Reach and Grasp for Upper Limb Assessment).

Following the same development process of NeBULA, we first designed an adjustable and programmable experimental platform to standardize the reach-grasp-transport task across participants and experimental conditions. Subsequently, we leveraged this platform to implement a data collection tailored to a targeted rehabilitative device. The adjustable experimental platform is described in Section 6.2, while the data collection is described in Section 6.3.

6.2 Sensorized setup

We designed and built a sensorized setup to support the execution of the standardized reach-grasp-transport task. We called it Guided Reaching and Repositioning Adjustable Assessment Platform (GRRAASP). The GRAASP device features 10 sensorized platforms that can hold differently shaped objects. The platforms are arranged in couples in 5 different spatial position. Each couple can be shifted vertically and horizontally thanks to a structural frame constructed from PVC tubing, standard enclosures, and custom 3D-printed joints. Each platform is endowed with an infra-red sensor of proximity to detect object presence and a LED to guide the participants during task execution. The device also features a push button that is used as a trigger to synchronize different acquisition systems. The system is managed by a dedicated Data Acquisition (DAQ) unit that controls the LED timing sequences and generates logs capturing the subject-device interactions thanks to the proximity sensors. We developed the control software in LabVIEW (v. 2023 Q3), enabling the definition of complex experimental protocols by specifying the sequences and timings of visual cues. Figure 6.2 shows the main features of the GRRAASP device.

6.3 Data collection

We designed a data collection based on the GRAASP device and tailored to the grasp types that are most commonly executed in everyday life and reproducible with hand prostheses (Section 6.3.2). Specifically we focused on the grasps enabled by the Hannes hand prosthesis developed by Rehab Technologies of IIT (67). We aimed to obtain a comprehensive, clinically meaningful characterization of task execution from central neural activity to peripheral execution and biomechanical output. Therefore, we synchronized the GRRASSP setup with different recording devices, to enable the concurrent acquisition of EEG, EMG and kinematic data (Section 6.3.3). We customized the planning, execution and rest phases of the task and leveraged the adaptability of the GRAASP device to define 5 limb positions for the execution of the task standardized across participants (Section 6.3.4).

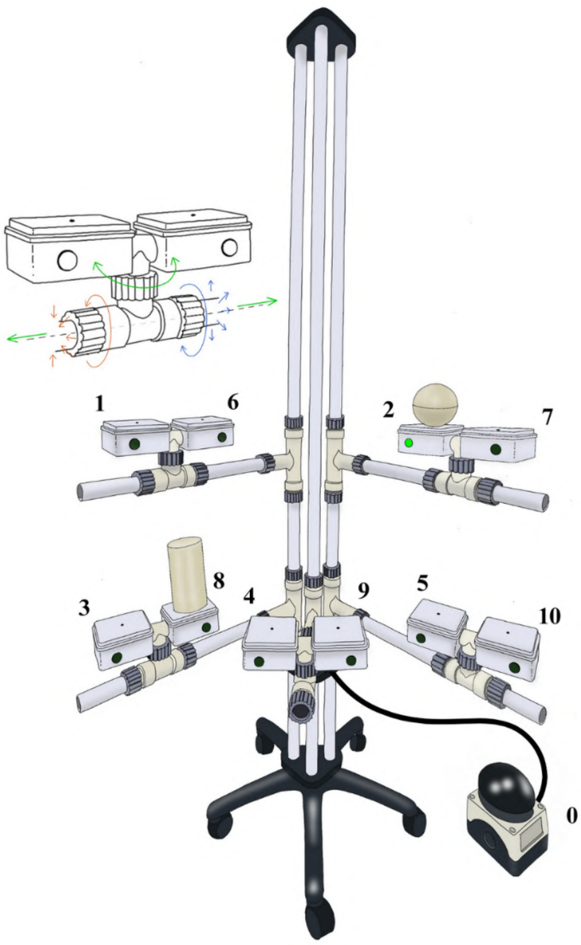

Figure 6.1 GRRAASP Assessment Platform, featuring 10 sensorized platforms mounted on an adjustable frame. The upper left side of the picture shows one of the custom 3D-printed joints that allow to vertically and horizontally adjust the position of the platforms.

6.3.1 Participants

30 healthy subjects were recruited (15 male, 15 female, age 27.3 ± 3.41 years old) with no chronic inflammatory diseases, orthopedic conditions, or neuro-muscular disorders. All subjects signed informed consent, and the experimental procedures were approved by the local ethics committee (CER Liguria: 784/2022 - DB id 12044).

6.3.2 Grasp selection

The ReGULA framework allows to assess virtually any type of grasps, but our data acquisition protocol was based on 4 types of grasps: power grasp, cylindrical grasp, tripod grasp and key grasp. The choice of these grasps was based on the quantitative grasp taxonomy defined by Stival and colleagues (68) and on the grasp configurations that can be reproduced with the Hannes hand developed by the Rehab Technologies Lab of IIT (67). We designed 3 different lightweight object for the execution of power, cylindrical and tripod grasp, while for the key grasp we used one of the objects featured in the SHAP (Southampton Hand Assessment Procedure) standardized tool for hand prosthesis assessment (69).

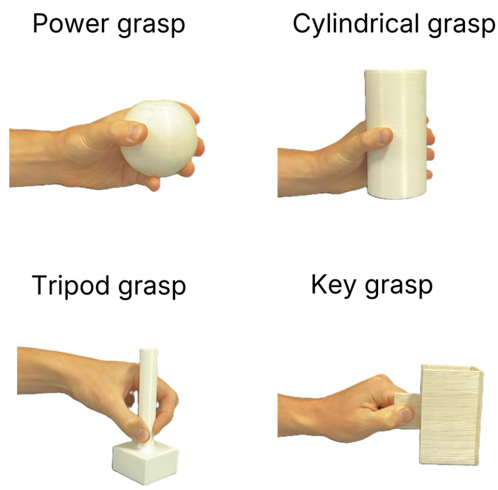

Figure 6.2 Types of grasps included in the acquisition protocol.

6.3.3 Device Synchronization

The ReGULA framework as well as the NeBULA framework are intended for multimodal assessment integrating central and peripheral measures to capture the tightly coupled perceptual, cognitive, and motor processes that underlie the execution of reaching and grasping movements. We therefore synchronized different acquisition systems to enable the concurrent recording of neural, muscular, and kinematic data during task execution. Specifically we synchronized the following equipment:

- The 64 channel wireless high-density EEG (hdEEG) cap Smarting Pro X from mBrain-Train;
- The wireless Cometa Waveplus EMG system: 5 bipolar EMG probes were positioned on upper trapezius, middle trapezius, lower trapezius, latissimus dorsi and posterior deltoid;
- The Quattrocento amplifier from OTBioelettronica: We used 6 matrices of 64 electrodes arranged in a 5x13 configuration with inter-electrode distance of 8 mm (GR08MM1305) for a total of 384 monopolar EMG channels. The matrices has been placed over the flexor carpi ulnaris (FCU), extensor carpi radialis (ECR), biceps brachii (long head), triceps brachii (long head), anteriror and middle deltoid (covered by the same matrix) and pectoralis major;
- The MTw Awinda markerless motion capture system from XSENS;
- The Quantum Metaglove motion capture glove from MANUS.

Figure 6.3 shows the complete setup.

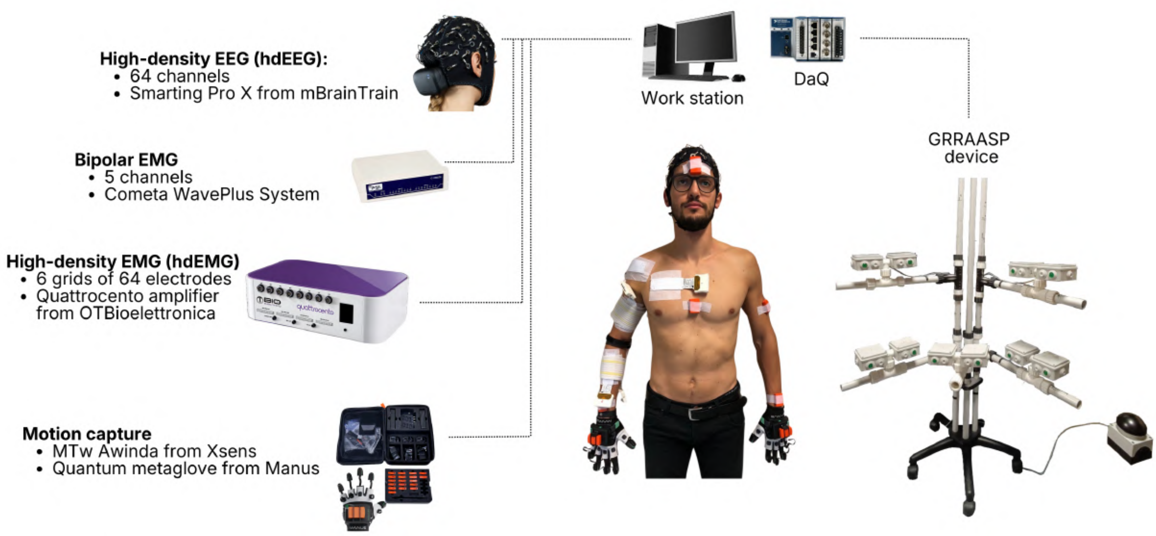

Figure 6.3 Scheme of setup synchronization.

6.3.4 Experimental procedure

In the first phase of the experiment, all sensors were applied to the participant as illustrated in Figure 6.4 A. Subsequently, participants sat on an adjustable chair and the right shoulder was used as the anatomical reference point for centering the setup. The reaching distance was individually adjusted by instructing participants to naturally extend the right arm, ensuring a comfortable near-maximal reaching amplitude.

Five target locations were standardized relative to the shoulder reference point. Two upper targets were positioned approximately 10 cm above shoulder height and oriented at $\pm 30^{\circ}$ relative to the sagittal plane passing through the right shoulder. This configuration allowed comfortable grasping with near-full elbow extension.

The three remaining targets were positioned at a lower height. The central lower target was aligned along the sagittal plane passing through the shoulder, while the two lateral lower targets were symmetrically oriented, matching the $\pm 30^{\circ}$ angular configuration of the upper targets. The vertical position of the lower targets was individually adjusted to allow grasping of the object located on the central lower platform with approximately 90° of elbow flexion.

The experimental protocol consisted of 30 reach–grasp–transport trials for each of four object types (total: 120 trials). Trials were equally distributed across space, such that each object was reached six times at each of the five target locations. The experiment lasted approximately 25–30 minutes and was divided into four blocks of 6–7 minutes to minimize fatigue. During the execution of the task 2 objects were simultaneously present on the GRRASPP setup and the system guided a pseudo-randomized sequence of reach-grasp-transport involving both objects to prevent anticipatory strategies.

Each trial was structured as follows:

- **Rest phase**: The trial started with the participant resting the right hand on a push-button positioned near the right thigh at a comfortable height. The rest phase lasted 3 seconds.
- **Reach cues**: A first LED turned on to indicate which object should be grasped. Participants were instructed to wait until the LED turned off to initiate the reaching movement.

- **Reach-to-grasp phase**: Upon LED offset, participants performed a self-paced reach-to-grasp movement toward the indicated object.
- **Holding phase**: After grasping, the object was lifted approximately 2–3 cm above the platform and held in position for 7 seconds.
- **Transport cues**: A second LED turned on to indicate the target platform for object transport. Again, participants waited until LED turned off before initiating movement.
- **Transport phase**: Participants transported the object to the indicated platform at a comfortable, self-selected speed.
- **Return phase**: After releasing the object, the hand returned to the initial resting position.

Figure 6.4 B details the structure of each trial.

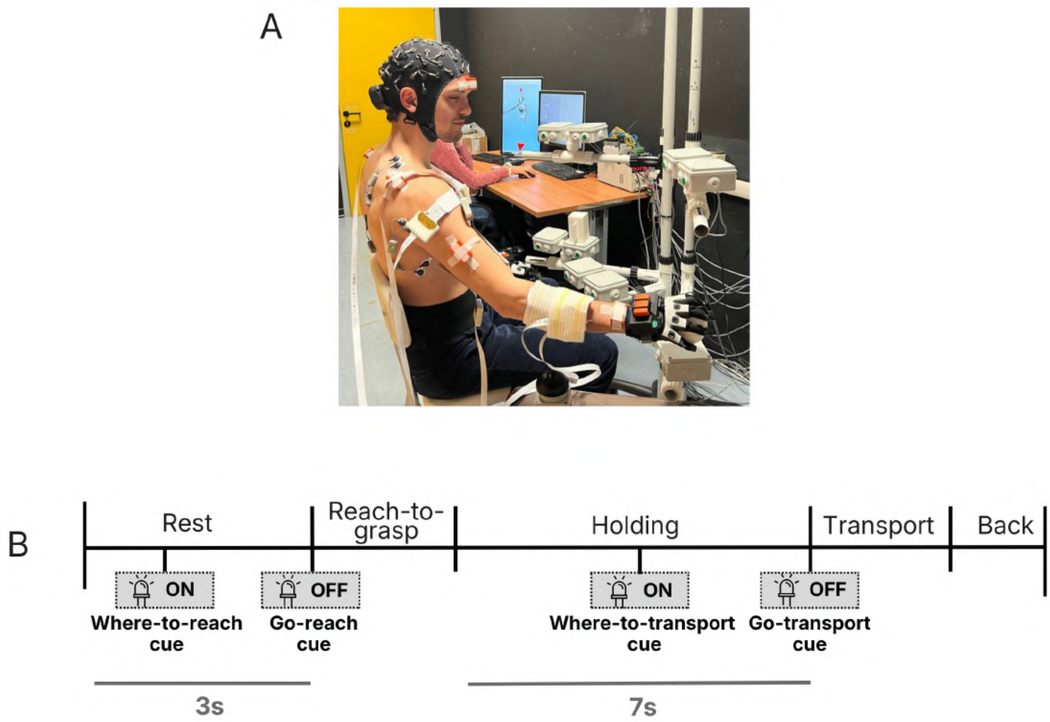

Figure 6.4 Overview of experimental protocol. A) Data acquisition setup. B) Trial composition.

Chapter 7

Influence of arm posture on motor unit action potential waveforms during grasping

7.1 Motivation

Recent advances in myoelectric upper-limb prosthetics have enabled multi–degree-of-freedom control through pattern recognition–based approaches (20; 21).

Pattern recognition approaches relies on machine learning classifiers that are trained with input EMG signals provided together with the label of the corresponding movement. Once trained, the model should be able to predict the correct movement class when it receives similar signal patterns to those seen during training.

These methods assume that surface EMG activation patterns are consistent across repetitions of the same gesture. However, previous studies have shown that muscle activation depends on the arm position and not only on the joint primarily actuated by the muscle but also on adjacent joint configurations (70; 71). Variations in arm position modify muscle properties and alter the relative position between muscle fibers and electrodes, affecting the amplitude and spatial distribution of surface EMG signals and reducing classification performance.

While previous work has characterized these effects at the global EMG signal level (24), it is still unclear how changes in arm configuration affect the action potentials of individual motor units, which constitute the fundamental building blocks of the surface EMG signal.

The present study employs state-of-the-art methods to decompose the EMG signal into the activity of single motor units with the aim to quantify how arm configuration alters motor units action potential during a three-dimensional grasping task.

The present study formed the basis for an abstract submitted at the 26th International Society of Electrophysiology & Kinesiology Congress (ISEK 2026): *I. Ceroni, H.V. Cabral, F. Negro and M. Semprini, "Influence of Arm Posture on Motor Unit Action Potential Waveforms During Grasping".*

7.2 Background

The study presented in this Chapter leverages the standardized reach–grasp–transport framework ReGULA, described in detail in Chapter 6. The experimental paradigm (Section 6.3.4) required participants to perform 120 reach–grasp–transport trials, equally distributed across four objects (corresponding to four grasp types) and five arm configurations, resulting in six repetitions for each grasp–position combination. Each trial included a 7-second holding phase during which the object was lifted approximately 2–3 cm above the support surface. The present analysis focuses specifically on this holding phase.

This choice is motivated by methodological constraints inherent to current hdEMG decomposition algorithms (3; 72), which require several seconds of isometric EMG at a relatively stable contraction level to reliably identify motor unit discharge patterns. The holding phase represents the segment of the task that most closely satisfies these requirements.

The study here presented is based on the dataset that was collected from 30 healthy individuals within the ReGULA paradigm (Section 6.3). Specifically, hdEMG signals were recorded from six upper-limb muscles using six 64-channel electrode grids. To facilitate motor unit identification, the six 7-second holding segments corresponding to each grasp–position combination were concatenated prior to decomposition. This resulted, for each participant, in 20 EMG segments (4 grasps × 5 positions), each lasting 42 seconds. The decomposition algorithm was applied separately for each of the six EMG matrix for each of the 20 EMG segment.

Preliminary analyses revealed substantial variability in motor unit decomposition efficacy across muscles and participants. In several cases, no reliable motor units could be identified.

This is likely due to the behavioral nature of the ReGULA task which make it only partially constrained: although the holding phase is theoretically isometric, there is no mechanical constraints on joint configuration or control of force output, differently from experimental protocols designed specifically for EMG decomposition.

Furthermore, preliminary analyses indicated a markedly lower number of identifiable motor units in female participants compared to male participants, a phenomenon that has recently been reported in the literature (73). Across subjects and muscles, the forearm muscles (flexor carpi radialis and extensor carpi ulnaris) yielded the highest number of reliably identified motor units, likely due to more stable contraction levels during object holding. Among the recorded muscles, the extensor carpi radialis exhibited the most consistent activation across repetitions and conditions, allowing the identification of at least four to five motor units per grasp–position combination in a subset of participants.

Based on these methodological and practical considerations, the present preliminary study focuses on the extensor carpi radialis muscle in a subset of five male participants for whom a sufficient number of reliable motor units could be consistently identified across conditions. This selection ensured the feasibility of the analysis and the robustness of the motor unit–level comparisons across arm configurations.

7.3 Materials and methods

7.3.1 Participants

The population included in the preliminary analysis here presented consist of 5 healthy subjects (all males, age 26.2 ± 2.05 years old) with no chronic inflammatory diseases, orthopedic conditions, or neuro-muscular disorders. All subjects signed informed consent, and the experimental procedures were approved by the local ethics committee (CER Liguria: 784/2022 - DB id 12044).

7.3.2 Experimental task

The subjects were seated on an adjustable chair in front of a custom-made setup (GRRAASP, described in Section 6.2) that guided the execution of reach-grasp-reposition movements across a 3D workspace defined by 5 platforms symmetrically oriented with respect to the subject and corresponding to 5 different arm configurations. The experimental paradigm (described in Section 6.3.4) involved the execution of 120 trials of reach-grasp-transport movements equally distributed over 4 objects (corresponding to 4 different grasp types) and 5 arm configurations, for a total of 6 repetitions for each combination of grasp type and arm position. Each trial involved an object holding phase of the duration of 7 seconds.

The five arm configurations were defined as follows:

1. Position 1: The subject has the elbow fully extended and is lifting the object 2/3 cm upon a platform that is located around 10 cm higher than the shoulders of the participant and at 30° left with respect to the sagittal plane passing through the right shoulder.

2. Position 2: The position is symmetrical to position 1 but the arm is oriented at 30° right with respect to the sagittal plane passing through the right shoulder.

3. Position 3: The subject has the elbow fully extended and is lifting the object 2/3 cm upon a platform that is aligned vertically with respect to position 1 but at a lower height.

4. Position 4: The subject has the elbow flexed at 90° with the upper arm resting alongside the trunk and the forearm perpendicular to the ground.

5. Position 5: The subject has the elbow fully extended and is lifting the object 2/3 cm upon a platform that is vertically aligned with respect to position 2 but at a lower height.

Overall the positions considered in the study cover different ranges of elbow flexion, shoulder flexion and shoulder adduction, and they are reported in the lower left part of Figure 7.1.

During the execution of the task hdEMG was recorded from the extensor carpi radialis (ECR) muscle using a grid of 64 electrodes distributed in 13 rows and 5 columns with 8 mm inter-electrode distance (GR08MM1305 from OTBioelettronica). The signal has been acquired at 2048 Hz using the Quattrocento amplifier by OTBioelettronica.

7.3.3 Data segmentation and preprocessing

The EMG signal of each holding phase has been epoched using the timing information registered by the sensorized GRRAASP setup. For each of the 4 grasp type and 5 positions (20 combination) we concatenated the 6 segments of 7 seconds holding to obtain a segment

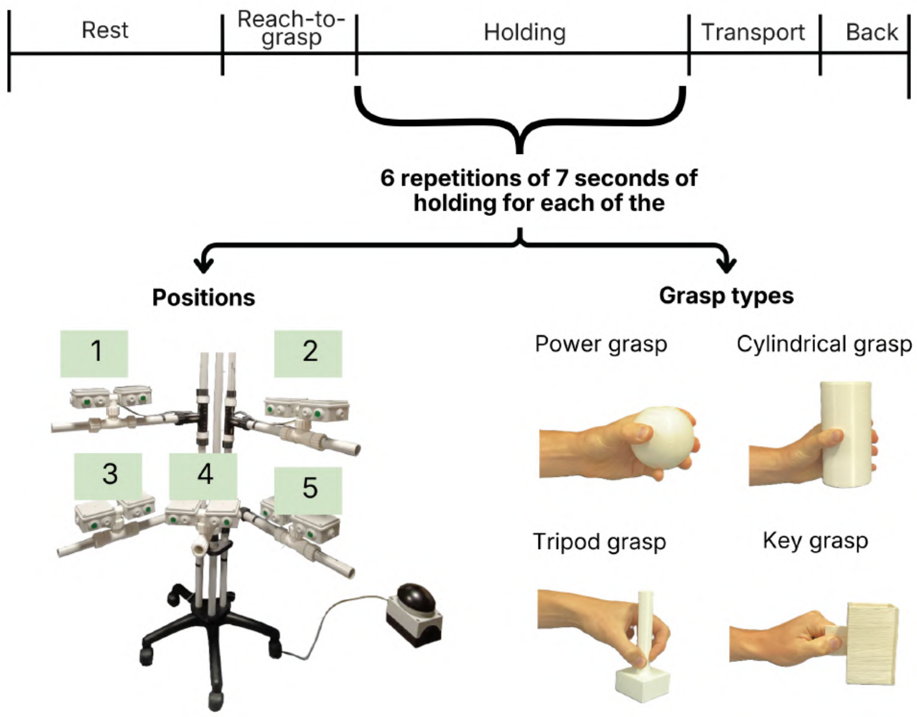

Figure 7.1 Schematic representation of trial composition (top), object positions (bottom left) and grasp types (bottom right) involved in the experimental paradigm.

of isometric quasi-steady contraction of 42 seconds. All channels were visually inspected and the ones exhibiting abnormal EMG fluctuations or peaks were discarded. Power-line interference was removed using an adaptive frequency-domain notch filtering approach implemented in the open-source HD-EMG processing tool for motor units activity reconstruction "MUedit" (74). Subsequently we applied a 3rd order Butterworth band-pass filter between 20 and 900 Hz.

7.3.4 HdEMG decompostition

High-density surface EMG signals were decomposed into their constituent motor unit spike trains using the open-source MATLAB library described in (74). The library uses the convolutive blind source separation algorithm described in (3). The algorithm relies on the identification of a set of separation vectors, that once applied to the signal allow to separate the single sources, i.e. the firing patterns of the single motor units. This is achieved through multiple steps:

1. HdEMG is extended (we used an extension factor of 16 as in (3)) and whitened.

2. The blind source separation procedure is run iteratively (we imposed 400 cycles), for every iteration:

    (a) The separation vector is initialised selecting the time instant corresponding to the maximum of the squared sum across all whitened extended hdEMG channels.

    (b) The fixed point algorithm is run iteratively until it converges to an optimized separation vector. We imposed a maximum of 500 iterations and used the Kurtosis contrast function.

    (c) The obtained separation vector is applied to the extended whitened signal to obtain a train of peaks (innervation pulse train) that is the first estimation of the source.

    (d) A peak detection algorithm is applied and a two-class K-means clustering algorithm is used to separate the high peaks that correspond to the firings of the motor unit of interest from the low peaks that arise form the contribution of multiple motor units. To estimate how good the source is separated, the silhouette coefficient (SIL) is calculated. SIL is defined as the difference between the within-cluster sums of point-to-centroid distances and the same measure calculated between clusters, normalized by taking the maximum of these two values.

    (e) The final separation vector is updated based on the results of the K-means clustering.

3. Motor units that are badly separated (we imposed a threshold of SIL $>= 0.87$ (75)) are removed.

4. Duplicate motor units are removed: motor units that shares more than 30% of spikes are considered duplicates and only the motor unit with lowest discharge rate variability was retained.

Separation vectors were manually refined by visually inspecting the innervation pulse train and the discharge rate of the identified motor units and by adding or removing spikes that were misclassified by the algorithm (76). The multi-channel motor unit action potential (MUAP) waveform of each motor unit was obtained by spike-triggered averaging (77): for each hdEMG channel, a segment of signal is isolated for every spike instant of the motor unit, using a window of 21 ms centered in the spike instant. All the segments are then averaged across the channels to obtain a multichannel estimation of the MUAP. Figure 7.2 displays the main processing steps to identify the MUAPs.

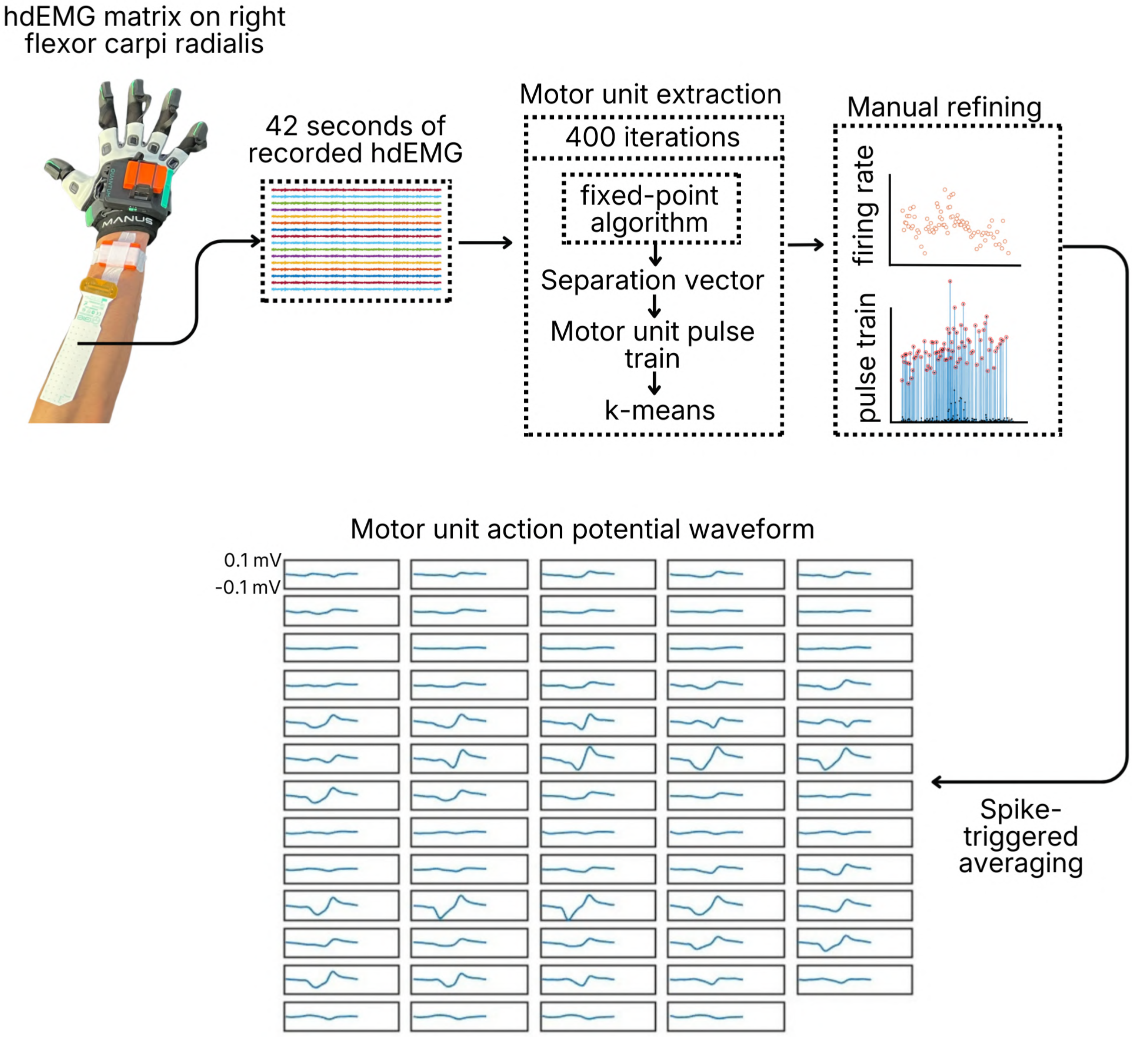

Figure 7.2 Schematic representation of the hdEMG processing pipeline to identify the motor unit action potential (MUAP) waveforms.

7.3.5 Motor unit tracking across positions

To track the motor units characterizing each grasp type across different arm configurations, we computed the cross-correlation between multichannel MUAPs extracted from the same grasp in different configurations. The MUAPs have been considered to belong to the same motor unit if the cross correlation exceeded 0.8 (78). To quantify the modulations of grasp-specific MUAPs across positions, we computed the sum of squared differences (ssd) between multichannel MUAPs of different positions and normalized it with respect to the sum of squared values of the first MUAP:

$$ssd = \frac{\sum_{i=1}^{n\_ch}\sum_{j=1}^{n\_samp}[MUAP1(i,j) - MUAP2(i,j)]^2}{\sum_{i=1}^{n\_ch}\sum_{j=1}^{n\_samp} MUAP1(i,j)^2} \tag{7.1}$$

Where MUAP1 and MUAP2 are the motor unit action potential matrices of two different motor units in which the rows represent the channels and the columns the samples of the waveform. *n_ch* is the number of channels that is 64 and *n_samp* is the number of samples of the waveform that is 42.

7.4 Results

Positions	**Correlation**	**ssd**
Pos1 vs. Pos2	0.8900 ± 0.0562	0.2412 ± 0.1792
Pos1 vs. Pos3	0.8792 ± 0.0177	1.0739 ± 1.3363
Pos1 vs. Pos4	0.8826 ± 0.0235	0.2574 ± 0.0612
Pos1 vs. Pos5	0.8538 ± 0.0390	0.3718 ± 0.2083
Pos2 vs. Pos3	0.8914 ± 0.0315	0.1302 ± 0.0417
Pos2 vs. Pos4	0.8696 ± 0.0252	0.2734 ± 0.1006
Pos2 vs. Pos5	0.8618 ± 0.0496	0.3906 ± 0.1338
Pos3 vs. Pos4	0.8437 ± 0.0306	0.2967 ± 0.1355
Pos3 vs. Pos5	0.8917 ± 0.0401	0.0853 ± 0.0510
Pos4 vs. Pos5	0.8492 ± 0.0362	0.3522 ± 0.159

Table 7.1 Results of motor unit tracking across positions.

Preliminary results on 5 subjects indicate an average correlation of 0.87 ± 0.04 and an average sum of squared residuals of 0.33 ± 0.31, suggesting that MUAP spatial structure is largely preserved, although noticeable amplitude modulations occur across configurations. Maximum preservation of MUAP shapes was found when moving from the lower left fully

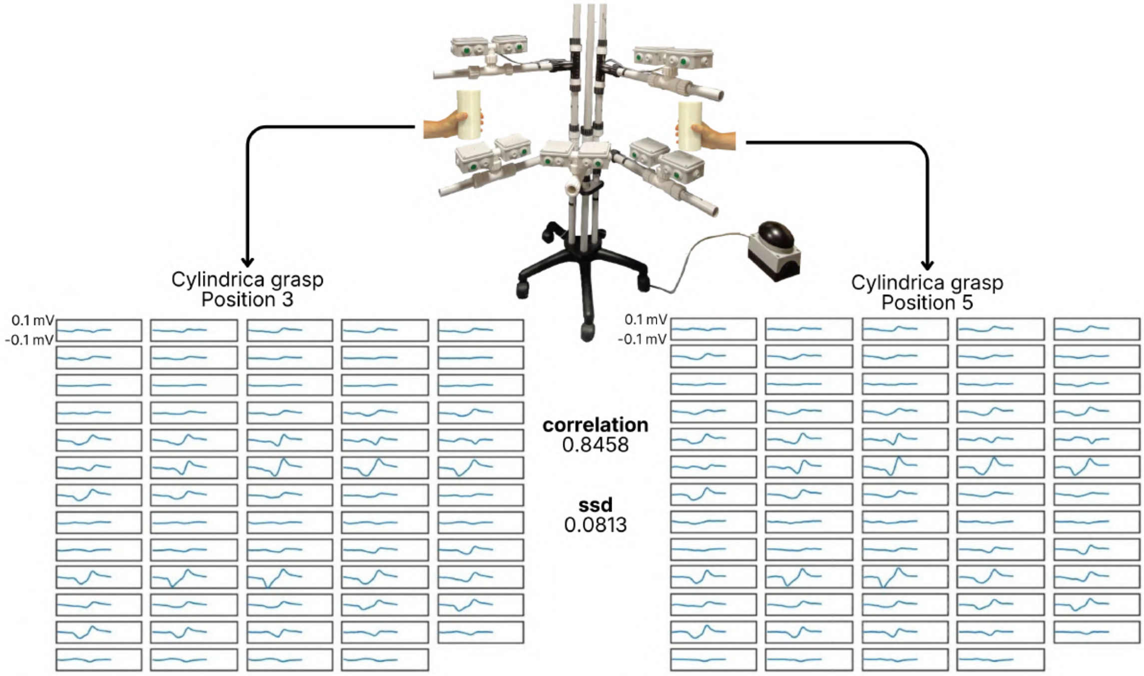

Figure 7.3 Example of tracking of one motor unit obtained from subject 4 between cylindrical grasp performed in position 3 and cylindrical grasp performed in position 5.

extended arm position to the lower right fully extended arm position. This is reflected both in the highest correlation values (0.8917 ± 0.04) and in the lowest sse values (0.09 ± 0.07) meaning that the higher preservation is observed when only shoulder adduction/abduction is involved. The lowest values of correlation (0.85) were found when moving the configuration with 90° elbow flexion to the lower left fully extended arm position and to the fully extended arm position, indicating that elbow flexion has the higher impact on MUAPs correlation. The highest values of sse were found when changing the degree of elbow flexion, moving from higher left to lower left fully extended arm position (1.07 ± 1.34) and from higher right to lower right arm position (0.39 ± 0.13).

7.5 Discussion

The relatively high correlation values (0.87 ± 0.04) found across upper-limb positions indicate that the spatial-temporal structure of MUAPs is largely preserved across arm configurations, supporting the successful tracking of motor units across positions. However, the larger variability observed in the normalized SSE (0.33 ± 0.31) suggests that significant amplitude modulations occur despite the preservation of waveform shape. These amplitude variations are likely caused by changes in the electrode–muscle geometry and volume conduction properties resulting from limb repositioning. In particular, while shoulder adduction/abduction is associated to the lowest degree of change in MUAP shape and ampitude, elbow flexion produced the largest increases in sse and the lowest correlation values, indicating that this joint movement induces greater distortions of MUAP spatial distributions compared with shoulder abduction/adduction.

The observed modulation of MUAP amplitude and spatial distribution across arm configurations provides a potential physiological explanation for the limb position effect reported in previous EMG pattern recognition studies. In particular, the study from Fougner and colleagues (24) showed that classification error increased substantially when training and testing were performed in different arm positions and that this is particularly significant when variations in elbow angle are involved. Our results indicate that elbow flexion induces the largest changes in MUAP similarity, reflected by both lower correlation values and higher normalized SSE. These findings suggest that changes in elbow angle alter the electrode–muscle geometry and volume conduction properties, leading to modifications in MUAP amplitude distributions. Such changes can shift the statistical distribution of EMG time-domain features, thereby explaining the degradation in classifier performance observed when limb posture varies.

Overall, the results of this preliminary study highlight a potential neural basis for the observed degradation in pattern recognition performance under different limb postures.

Chapter 8

Evaluation of hand gesture classification based on motor units activation for prosthetic application

This chapter extends the motor unit–based characterization of grasping actions developed in Chapter 7. While the previous Chapter focused specifically on grasps, the study presented here includes a wider range of fundamental movements and addresses a research question more directly related to intention detection.

Specifically, the study investigates whether features derived from motor unit activation patterns can enhance traditional pattern recognition approaches for movement classification. The work is motivated by previous research (79), which demonstrated promising results using neural-level features to discriminate among hand gestures relevant for prosthetic control. Building on this concept, the present study examines whether a similar approach can provide improvements in classification performance while also offering greater physiological interpretability.

The work presented in this chapter formed the basis of a conference paper that was presented orally at the Annual International Conference of the IEEE Engineering in Medicine and Biology Society (EMBC 2025): *D. Enrico, I. Ceroni, H. V. Cabral, F. Negro, and M. Semprini, "Evaluation of Hand Gesture Classification Based on Motor Units Activation for Prosthetic Application," Annu Int Conf IEEE Eng Med Biol Soc, vol. 2025, pp. 1–7, Jul. 2025 (80).*

8.1 Motivation

Recent advancements in myoelectric upper-limb prosthetics have enabled users to control prostheses with multiple degrees of freedom (DoFs) (20). Particularly, pattern recognition is one of the most explored methods to allow the control of multiple DoFs and has been recently made available in commercial prostheses (e.g. Coapt 2017, Ottobock 2019, i-biomed 2021) (21). In these approaches, the electromyographic (EMG) signal of the residual muscles is recorded non-invasively, simplified into time or frequency-domain features (81), (82), and used to train machine learning models able to identify the movement class corresponding to the user intent.

Although effective, the use of simple EMG features neglects the biological origin of the EMG signal (83). Moreover, the obtained performance can be equaled or overtaken by the use of features that directly reflect the neurophysiological origin of the EMG signal (83),(79).

Since the pattern of activation of the motor units reflects that of the motor neurons innervating the muscle, it directly represents the neural drive to muscles that encodes the motor command (83). Studies have thus used features built on the activation pattern of motor units to train machine learning algorithms used for traditional pattern recognition (79; 83; 84; 85).
In their work of 2020 (79), Chen and colleagues have proposed a hand-gesture recognition approach based on the decomposition of EMG into the activity of motor units.
By decomposing the hdEMG recorded from the forearm of able-bodied individuals into the activity of the motor units, they have classified 11 hand gestures (8 fundamental movements and 3 types of grasp). The obtained classification accuracy was comparable or even superior to the one obtained with a traditional machine learning approach based on the root-mean-square (RMS) amplitude of the EMG signal.

Such results, although obtained in offline conditions, seemed extremely promising for prosthetic applications. We were thus motivated to assess the feasibility of applying this approach to control the Hannes prosthetic hand (67), to replicate the gestures it enables.

To this end, we developed a classifier based on offline motor unit decomposition as in (79), able to discriminate between 4 grasps and 10 fundamental movements.
hdEMG data were collected from the forearm muscles of 5 able-bodied individuals and decomposed into the activity of motor units. Subsequently, different state-of-the-art classifiers were optimized and trained to classify the extracted motor units. A simple time domain feature

(RMS amplitude) was also computed to allow accuracy comparison with the traditional pattern recognition approach.

The main difference with the work of Chen and colleagues (79) lies in that the hand gestures utilized here are based on the case study of the Hannes hand prosthesis (67) and are tested with multiple classifier models to inspect differences in the accuracy of the classification. Moreover, subjects here performed the hand gestures with real objects while seated in a chair with the arm relaxed and the elbow flexed at 90°, as during prosthetic training sessions, while in the work of Chen and colleagues (79), subjects were seated with the arm fully extended and pointing toward the ground.

8.2 Materials and methods

8.2.1 Participants

Five able-bodied, right-handed subjects with no neurological or psychiatric disorders participated in this study (4 males, average age $\mu = 29.00 \pm 7.97$). All subjects provided written informed consent and the study was approved by local Ethics Committee (IIT REHAB HT01 363/2022).

8.2.2 Experimental setup

Myoelectric activity was measured by recording hdEMG signals using a wireless acquisition system (Muovi+Pro, OTBioelettronica), which included two multichannel amplifiers connected to 64-channel electrode grids (GR08MM1305 grid from OTBioelettronica which distributes the 64 channels over 5 columns x 13 rows, with 8 mm inter-electrode distance). The grids were positioned longitudinally on the flexor carpi radialis (FCR) and extensor carpi ulnaris (ECU) as in the dual-site prosthetic control strategy (21). Muscle belly location was determined through palpation (Figure 8.1). EMG signals were sampled at 2000 Hz using a 24-bit A/D converter.

8.2.3 Experimental protocol

Subjects sat in front of a horizontal plane with a straight torso, positioning their right arm with a 90° elbow angle and keeping the shoulder relaxed (Figure 8.1). The chair height was adjusted so that the right forearm was positioned 1 to 3 cm above the horizontal plane in

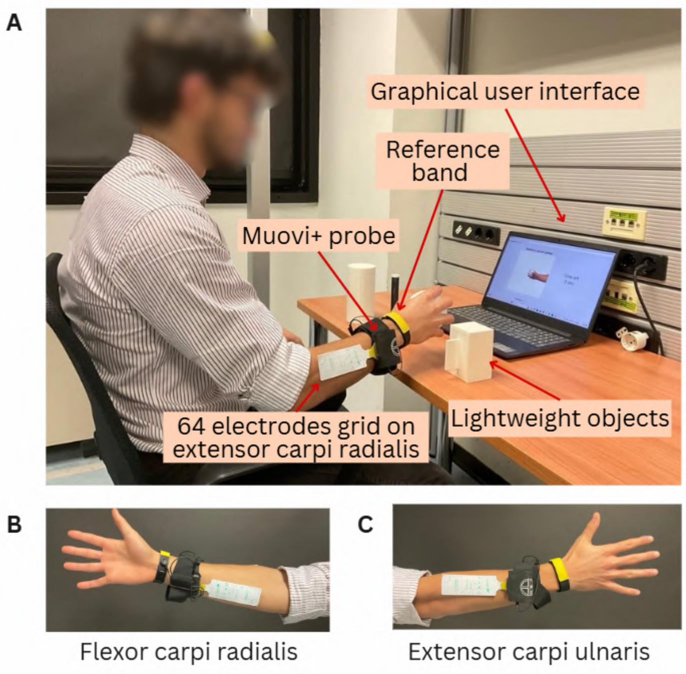

Figure 8.1 Experimental setup (A) and electrodes positioning on flexor carpi radialis (B) and extensor carpi ulnaris (C).

front of subjects.

The experimental procedure was organized in 8 trials. Each trial consisted in the execution of 14 different hand gestures (Figure 8.2). These included 10 fundamental hand gestures and 4 object grasps. In each trial, subjects performed each hand gesture for 10 seconds, followed by a 5 seconds rest interval in the same position. Subjects were instructed to maintain a consistent, not excessive contraction force across the 10 seconds duration of each hand gesture to facilitate motor unit decomposition. For the execution of the 4 object grasps, 4 differently shaped lightweight objects were positioned on the horizontal plane in front of the subject, allowing to reach them with a minimal adjustment of hand position. Task order was randomized for each trial. A graphical user interface (GUI) guided the execution, showing the hand gesture to be performed and providing timing cues. A training trial was conducted to allow subjects to familiarize with the protocol.

8.2.4 EMG preprocessing

Low-quality EMG channels were identified and removed by visual inspection. Data segmentation was performed using temporal triggers provided by the GUI. To reliably decompose the motor units involved in the recorded hand gestures, only the steady parts of the EMG signal

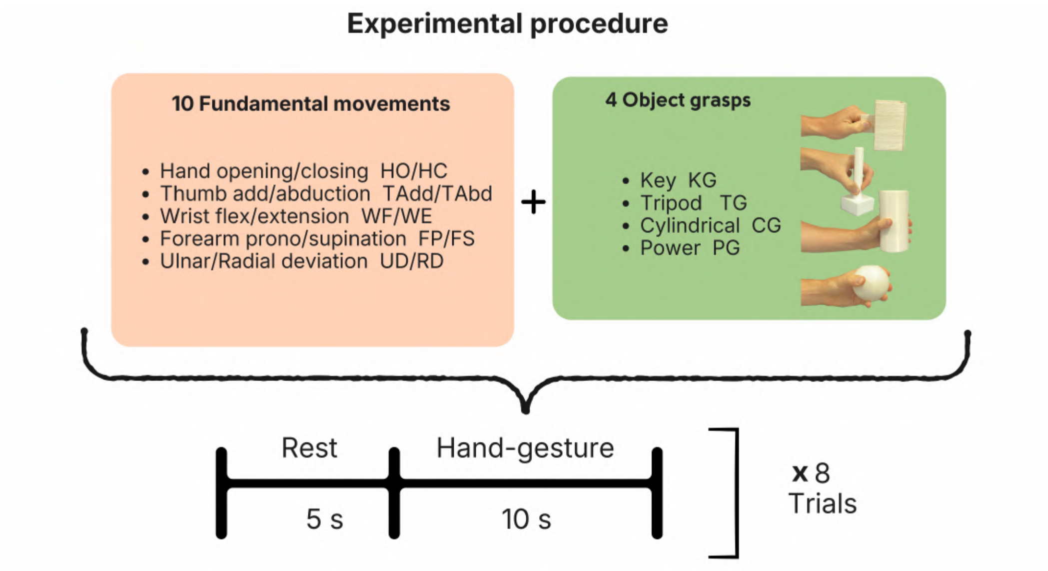

Figure 8.2 Experimental procedure.

were considered: the first second of hand gesture following the appearance of the image on the GUI was excluded to avoid non-stationary signal properties typical of transitional phases. Finally, we applied a notch filter to eliminate power line interference and a second-order Butterworth bandpass filter with a frequency range of 20-500 Hz.

8.2.5 HdEMG decomposition

HdEMG signals were decomposed into their constituent motor unit spike trains using the open-source MATLAB library described in (74). The library uses the convolutive blind source separation algorithm described in (3). Briefly, after extending the EMG signal by a factor of 16 and whitening it, a fixed-point algorithm was applied to identify the sources (i.e., motor unit spike trains) (3). We iterated the source identification procedure 100 times and used the skewness contrast function to maximize the sparseness of the sources. The decomposition procedure was applied offline and repeated independently for each segment of stationary EMG corresponding to each hand gesture (14 segments per trial). EMG channels from the two electrode grids were decomposed separately and the quality of the decomposition was assessed by computing the silhouette coefficient (SIL) (3). Extracted motor units were retained only if SIL value exceeded 0.9. After decomposition, duplicate motor units within the same grid were identified and removed. Two motor units were considered as duplicates if they shared more than 30% of their discharge times. Among duplicates, the motor unit with lowest discharge rate variability was retained.

8.2.6 Feature Extraction

Two different feature sets were used in this study. The first was based on motor unit action potential waveform, with feature extraction performed immediately after the signal decomposition process. The second one, used for comparison with standard pattern recognition methods, was based on a time-domain EMG global feature, i.e. the RMS amplitude of the pre-processed EMG signals (86). For both sets, removed channels were interpolated using the neighboring channels.

Motor unit based feature

The first step of MU-based feature extraction involved computing the multi-channel motor unit action potential (MUAP) waveforms for each motor unit extracted. This was achieved using a spike-triggered averaging technique (77), with all discharge times of a motor unit used as triggers across the 128 EMG channels. An averaging interval of 50 ms centered in the discharge times was used. For each channel, the peak-to-peak (P2P) MUAP amplitude was calculated, resulting in a feature vector of 128 P2P values associated with each motor unit.

RMS

RMS was calculated for all 128 channels of pre-processed EMG signals using a sliding window of 200 ms with 50 ms overlap. To enable comparison across different movements, RMS values were normalized to a range between 0 and 1 by subtracting the minimum value of each EMG channel and dividing by the difference between the maximum range. As a result, each sliding window was associated with a feature vector consisting of 128 RMS values.

8.2.7 Classification

The same dataset partitioning approach was applied to both feature sets. Features from one of 8 trials were designated as the test set, while the remaining formed the training set. With this partitioning strategy, each test set contained feature data for all hand gestures once, while each training set included feature data for all hand gestures 7 times. To avoid potential bias deriving from the trial selected for the test, 8 distinct dataset partitions were created.
The classifier training was repeated for each partition, and the final accuracy was calculated as the average accuracy across all 8 test sets. Four classifier models were employed: linear

discriminant analysis (LDA) (87), support vector machine (SVM) (88), artificial neural network (ANN) (89), and logistic regression (LR) (90). For each model, hyperparameters were optimized leveraging the data of the training set using five-fold cross-validation with a Bayesian optimization (91). For this, the training set was randomly split into 5 equal-sized folds while maintaining class distribution across them. To prevent overfitting, L2 regularization (92) was applied to the ANN and LR models, shrinkage regularization (93) was used for LDA, and SVM regularization was controlled through the BoxConstraint hyperparameter (88).

Motor unit based classification

The classification process for the MU-based feature is illustrated in Figure 8.3. First, the MU-based features computed on the training set are used to optimize the hyperparameters and train the 4 classifiers. Subsequently, the 4 classifiers are applied on the MU-based features computed on the test set to associate each motor unit with a label corresponding to a hand gesture (Figure 8.3 A). After this procedure, each motor unit of the test set is classified and associated with a specific gesture, but the classification of the gestures themselves is not performed yet. A last step is necessary to associate the corresponding gesture to all the time segments of the trial considered as test. For this, a sliding window of 200 ms with 50 ms overlap was applied to the test trial (Figure 8.3 B). Within each sliding window, motor unit spike trains (MUSTs) were grouped based on assigned labels and a voting mechanism assigned the hand gesture with the highest number of spikes (Figure 8.3 C).
Furthermore, we implemented an abstention criterion such that if the total number of discharges across all classes within a window was fewer than 5, no output was assigned, and the interval was directly marked as misclassified. The accuracy of the gesture classification was computed as the percentage of correctly assigned labels across the entire trial. Classifiers performance was thus evaluated both in terms of accuracy and of percentage of abstention.

RMS-based classification

The RMS-based classification followed the same dataset partitioning as the MU-based classification. The classifier models were optimized, trained and tested on the RMS values (Sec. 8.2.6). Thus, the temporal intervals were directly classified without any intermediate step.

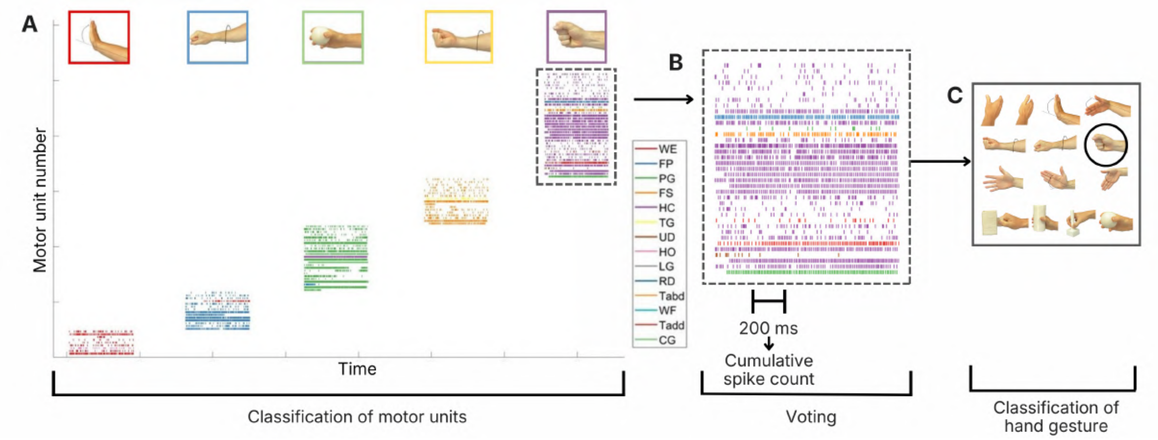

Figure 8.3 MU-based classification procedure. A) The motor units spike trains of each hand gesture are classified. Here, the process is depicted for 5 illustrative hand gestures and the different colors represent the labels assigned to the motor units. B) The motor units are grouped based on the assigned label. The cumulative number of spikes is computed for each group in a sliding window of 200 ms. C) The final label assigned to the window is the one with the highest number of spikes.

8.2.8 Statistical analysis

The hand gesture classification was conducted using 8 combinations of two key variables: 4 classifier models and two feature sets. Two separate statistical analyses were performed to evaluate the impact of these variables on classification performance. First, a normality test was conducted on the accuracy data for all combinations using a one-sample Kolmogorov-Smirnov test. As expected, given the small number of subjects, none of the combinations exhibited a normal distribution. Consequently, only non-parametric analyses were applied. To assess the effect of the classifier model, a Friedman test was performed separately on the accuracy results obtained from each feature set, comparing the 4 models within each feature set. Post-hoc pairwise comparisons were conducted using the Tukey-Kramer test. As a second analysis, a two-sample Kolmogorov-Smirnov test was applied to compare the performance of the two feature sets for each classifier model individually. The significance level was set at 0.05 and we used Bonferroni correction for multiple comparisons.

8.3 Results

8.3.1 Decomposition results

The decomposition results are summarized in Table 8.1, which reports the average number of motor units extracted for each hand gesture. The contribution from grid 1 (FCR) and from grid 2 (ECU) are separated. The values represent the mean number of motor units extracted across all trials for all subjects. The average SIL coefficient is also provided. Across all hand gestures, an average of 18.9 ± 3.2 motor units were extracted, with an average SIL of 0.937 ± 0.002, indicating high level of decomposition accuracy.

Hand Gesture	**Number of Motor Units**			**SIL**
	Grid 1	Grid 2	Total	
Wrist extension	6 ± 1	7 ± 1	13 ± 3	0.935 ± 0.002
Wrist pronation	5 ± 1	11 ± 1	16 ± 3	0.939 ± 0.002
Power grasp	8 ± 2	8 ± 2	16 ± 3	0.936 ± 0.002
Thumb adduction	12 ± 4	12 ± 4	24 ± 5	0.937 ± 0.002
Lateral grasp	6 ± 1	13 ± 1	19 ± 4	0.937 ± 0.002
Thumb abduction	11 ± 2	12 ± 2	23 ± 4	0.935 ± 0.002
Wrist flexion	11 ± 1	7 ± 1	18 ± 2	0.936 ± 0.003
Hand closing	11 ± 2	10 ± 2	22 ± 4	0.937 ± 0.003
Hand opening	10 ± 1	11 ± 1	21 ± 4	0.937 ± 0.002
Wrist supination	8 ± 2	7 ± 2	15 ± 4	0.939 ± 0.003
Cylindrical grasp	8 ± 2	10 ± 2	18 ± 4	0.935 ± 0.003
Wrist adduction	10 ± 1	8 ± 1	18 ± 2	0.940 ± 0.003
Wrist abduction	8 ± 3	11 ± 3	19 ± 6	0.934 ± 0.001
Tripod grasp	7 ± 1	15 ± 1	22 ± 4	0.937 ± 0.002

Table 8.1 Decomposition results.

8.3.2 Classification results

Accuracy of motor units classification

Table 8.2 presents the classification results of MUST extracted from the decomposition. This classification represents only the first step of the overall motor unit based approach and serves as a basis for the subsequent hand gesture classification (Figure 8.3 A). The LDA model exhibited lower accuracy compared to other classifiers, with the SVM, ANN, and LR models achieving accuracy levels of approximately 80%. The degree of misclassification can be explained by the recruitment of the same motor units during different movements.

Subject	**Model accuracy (%)**			
	LDA	**SVM**	**NN**	**LR**
Subj. 1	61.7 ± 3.1	83.9 ± 4.2	83.2 ± 5.9	84.6 ± 3.6
Subj. 2	64.8 ± 6.1	77.3 ± 7.1	75.7 ± 16.2	79.4 ± 6.1
Subj. 3	66.5 ± 8.2	78.4 ± 10.1	74.7 ± 9.5	79.6 ± 10.3
Subj. 4	74.5 ± 4.3	88.2 ± 5.9	90.1 ± 3.6	97.0 ± 5.4
Subj. 5	57.9 ± 5.2	73.9 ± 4.2	75.6 ± 7.7	75.3 ± 4.5
Average	65.1 ± 6.2	80.4 ± 5.7	79.9 ± 6.7	82.0 ± 6.0

Table 8.2 Accuracy of motor unit classification.

Accuracy of hand gesture classification

Table 8.3 reports the results of the hand gesture classification for the MU-based classification, while and Table 8.4 lists the results of the hand gesture classification for the RMS-based classification. Overall LDA model demonstrated the lowest performance for both MU-based and RMS-based classification. This trend is more emphasized for the MU-based classification. Average accuracy shows that overall, the RMS-based classification achieves higher accuracies than the MU-based classification approach, indicating the global superiority of the standard pattern recognition approach. Single subjects' accuracies highlight that lower performance in the MU-based classification is influenced by considerable subject variability. For instance, while Subject 1 achieves a maximum accuracy of 98.5% with the LR classifier, Subject 2 achieves only 80% with the same model. This variability is likely due to the sensitivity of the MU-based classification method to decomposition quality, which can vary significantly across subjects. Table 8.5 reports the average abstention rate across all trials, representing the percentage of temporal intervals where no hand gesture label was assigned due to an insufficient number of motor unit spikes within those intervals.

Comparison of classification models

Figure 8.4 depicts performance of the different classifier models. Green box-plots report accuracy median and inter-quartile range for the MU-based classification, while the blue ones display values for the RMS-based classification. For MU-based classification, LDA model showed lowest performance and the statistical analysis confirmed significant differences

Subject	**Model accuracy (%)**			
	LDA	**SVM**	**NN**	**LR**
Subj. 1	90.0 ± 6.7	98.3 ± 1.4	96.8 ± 4.4	98.5 ± 1.4
Subj. 2	70.2 ± 6.9	78.8 ± 5.9	81.3 ± 5.7	80.0 ± 5.5
Subj. 3	81.8 ± 14.2	91.3 ± 9.6	89.6 ± 10.3	91.9 ± 9.1
Subj. 4	88.1 ± 7.6	94.1 ± 4.3	95.3 ± 2.4	94.5 ± 3.6
Subj. 5	73.7 ± 10.9	84.5 ± 3.3	88.7 ± 4.5	86.5 ± 3.5
Average	80.6 ± 8.7	88.4 ± 7.7	90.4 ± 6.2	90.3 ± 7.2

Table 8.3 Accuracy of MU-based classification.

Subject	**Model accuracy (%)**			
	LDA	**SVM**	**NN**	**LR**
Subj. 1	96.1 ± 2.6	96.1 ± 3.4	95.4 ± 3.2	96.2 ± 3.3
Subj. 2	91.9 ± 6.6	92.7 ± 7.1	91.9 ± 7.7	92.8 ± 7.1
Subj. 3	92.1 ± 7.1	95.4 ± 4.7	94.4 ± 4.8	95.8 ± 4.2
Subj. 4	98.4 ± 2.1	98.6 ± 2.8	98.3 ± 2.3	98.8 ± 2.0
Subj. 5	89.7 ± 3.5	91.9 ± 4.2	90.1 ± 4.9	91.4 ± 0.4
Average	93.6 ± 3.5	94.9 ± 2.7	94.0 ± 3.2	95.0 ± 2.9

Table 8.4 Accuracy of RMS-based classification.

between the LDA model and both the ANN and LR models, which exhibited the best performance for the MU-based classification. RMS-based classification showed generally similar performance across the 4 models. Among these, LR model achieved highest performance, as confirmed by a statistical difference compared to both the LDA and ANN models.

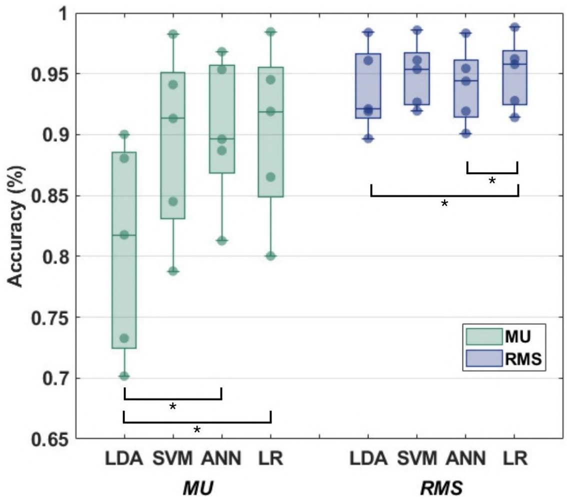

Figure 8.4 Comparison of accuracy results across the 4 classifier models. Green box-plots represent the MU-based classification results, while the blue ones represent the RMS-based classification. The dots in each boxplot represent single subjects data, the lower and upper sides of the boxes represent the 25th and 75th percentiles, respectively, while the dash in the middle represents the median value. * indicates statistically significant differences ($p < 0.05$, Bonferroni corrected).

Comparison of feature sets

Although a general trend favors the RMS-based classification (Figure 8.4), no significant difference was found between the two classification approaches in any of the classifiers. Classification results are also reported in Figure 8.5 as confusion matrices.

8.4 Discussion

This study aimed to evaluate whether motor unit features, extracted from hdEMG signals through a decomposition algorithm (3), could be used for classifying the 14 hand gestures enabled by the multi-DoF adaptation of Hannes prosthesis (67).

The decomposition process led to the extraction of more than 13 motor units per gesture, with an average SIL higher than 0.93, demonstrating the feasibility of reliably identifying at

Subject	Abstention rate (%)
Subj. 1	1.5 ± 1.4
Subj. 2	16.8 ± 6.0
Subj. 3	2.3 ± 1.9
Subj. 4	4.2 ± 2.0
Subj. 5	3.2 ± 3.2
Average	5.6 ± 6.3

Table 8.5 Abstention rates for MU-based classification.

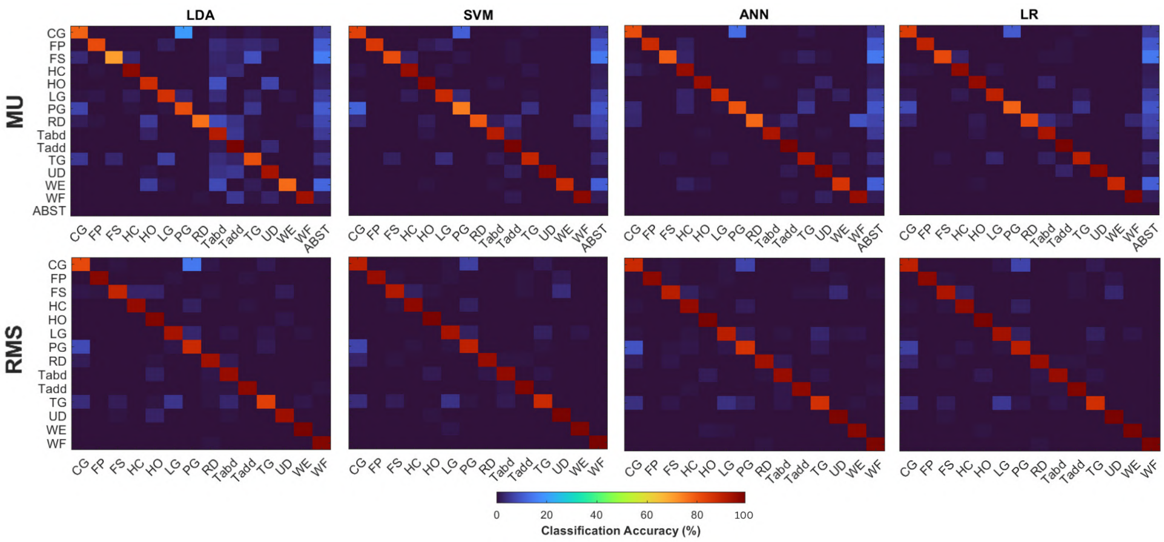

Figure 8.5 Confusion matrices for hand gesture classification. Top row shows results using motor unit based features, while bottom row shows RMS-based results. Each column depicts results for each of the 4 models (LDA, SVM, ANN, LR). True labels are on the y-axis, and predictions are on the x-axis. Labels are introduced in Figure 8.2.

least part of the motor units involved in the 14 hand gestures considered.
The motor unit spike trains extracted were then used to compute features reflecting the spatial distribution of the motor unit action potential waveform across the electrode grids. Such features were used to classify each motor unit spike train and to associate them to a specific hand gesture, while a voting mechanism led to final classification.

The classification of the motor unit spike trains was strongly influenced by the fact that a single motor unit could be activated across multiple hand gestures, thus the average accuracy values reached in this phase were moderate. On the contrary, the complete hand gesture classification procedure demonstrated a robust classification accuracy, with average values consistently above 80%. This result supports the feasibility of leveraging spatial information about the neural drive to forearm muscle to discriminate the hand gestures made possible by a multi-degrees-of-freedom prosthesis.

While this result is promising for the development of new and more effective control strategies for upper limb prosthetic devices, it must be noted that the analyses here presented were performed exclusively on the steady parts of the EMG signal and were executed completely offline. Thus, they cannot be applied to real-time applications. The main obstacle to adapt the procedure here described to real-time application lies in the fact that the algorithm used for decomposition (3) is extremely time consuming and requires long recordings of isometric EMG to reliably identify the motor units involved in the task. Nevertheless, this present work paves the way for future exploration on how to apply this motor unit based classification approach to prosthetic control.

8.4.1 Motor unit based classification reliably discriminates hand gestures

We compared the accuracies obtained with this MU-based classification approach to a more traditional pattern recognition technique based on RMS. The results reported that for all the classifier models tested, the RMS-based method reached higher accuracies with respect to the MU-based approach, although the difference was not statistically significant. It is true that the MU-based classification showed a greater inter-subject variability with subjects reaching high classification accuracies, for instance, subject 1 performs better with the MU-based classification, achieving accuracies of approximately 98% with the SVM, ANN, and LR classifiers, compared to 96% with the RMS-based method. These findings, combined with the fact that no significant differences were found across the models, emphasize that RMS-based method could be surpassed by MU-based approach.

8.4.2 Comparison with a similar study

The results of the comparison with the standard pattern recognition are in contrast with the findings reported in the study by Chen and colleagues (79), which inspired this work. In fact, in the study by Chen and colleagues, the MU-based classification achieved better performance than RMS-based classification.

This incongruence could be related to a key difference in the experimental protocols: the present study implemented a setup designed to better resemble daily living activities, with participants instructed to position their arms at a 90° elbow angle. Conversely, (79) used a setting designed to favor the decomposition, requiring participants to keep their arms fully extended toward the ground.

Additionally, this study included a higher number of classes, incorporating 4 grasp types, which increased the complexity of the classification task. In fact, as illustrated in Figure 8.5, the MU-based approach exhibits a high degree of misclassification when grasping is involved. For instance, across all 4 models, the cylindrical grasp is often misclassified as the power grasp, and vice versa. This misclassification can likely be attributed to the fact that these grasp types involve similar digit movement patterns, possibly leading to recruitment of similar group of motor units and consequently making MU-based classification more challenging.

Moreover, while this study used only two electrode grids, placed specifically on the FCR and ECU muscles, in (79) three matrices were used to completely surround the forearm circumference, facilitating the extraction of a larger number of motor units. In our case, the absence of recordings from other parts of the forearm likely impacted classification performances since motor units active in those areas could not be detected.

The differences in performance compared to (79) should not be attributed to the type of motor unit feature used, but rather to the consistency of the decomposition results. This is evident from the observed relationship between subject variability in accuracy (Table 8.3), and the degree of abstention shown in Table 8.5. Specifically, subjects with the lowest MU-based classification performance were those with the highest degree of abstention, due to an insufficient number of motor unit spikes within the analyzed temporal intervals. For instance, Subject 2 exhibited the lowest level of accuracy, having an abstention rate of 16.8%. Indeed, extracting a high number of motor units from surface EMG signals remains a challenging task: indeed, as mentioned in (94), the decomposition algorithm typically captures only a limited subset of active motor units, primarily those located close to the skin. Moreover, the presence of multiple overlapping muscles in the forearm increases MUAP summation, making motor unit extraction more difficult.

Differently from (79), in this study, 4 different classifier models were used: LDA, SVM, ANN, and LR. Across both classification approaches, LDA demonstrated the lowest performance, particularly in the MU-based classification. This difference in performance is likely due to LDA's relatively simpler structure compared to the other models, which may limit its ability to handle the high dimensionality of the feature vectors used in both approaches (128 values in each case) (95). In contrast to (79), no dimensionality reduction technique, such as Principal Component Analysis (PCA), was applied in this study, which may have impacted classification performance.

8.4.3 Study limitations

An important limitation of this study is the small sample size. This number is insufficient to draw definitive conclusions, especially since the statistical analyses performed are constrained by the limited dataset.

Further, the offline nature of the proposed procedure is clearly not suitable for prosthetic applications. However, as technology continues to evolve, particularly with advancements in computational power, data processing speeds, and machine learning techniques, it is likely that these constraints will be overcome, and in the future, it may become feasible to deploy MU-based classification in real-time.

8.5 Conclusions

This study evaluates the feasibility of using motor unit based features for hand gesture classification in the context of prosthetic applications. A realistic experimental protocol was designed to simulate daily conditions encountered by amputees. Motor unit features inherently reflect the physiological processes involved in movement coding at the spinal cord level, offering a more biologically inspired approach to control. However, our findings highlight the high sensitivity of decomposition techniques to task conditions and their lack of robustness, demonstrating that further research is needed for developing robust hand gesture classifications based on hdEMG decomposition.

Chapter 9

General Conclusion

This final chapter revisit the two main objectives that guided this doctoral research. These objectives have been addressed in the two main parts of the thesis, each focusing on a specific aspect of the research problem. The results obtained from these investigations provide a comprehensive basis for reflecting on the contributions of this work and for drawing broader conclusions.

Accordingly, the following sections summarize the main findings related to each research objective and discuss how these results connect with and contribute to existing literature in the field. This chapter also examines the significance and implications of the findings, both from a scientific and technological perspective. In addition, the limitations of the research and of the adopted methodologies are considered.

Finally, recommendations for future research directions are outlined, highlighting opportunities to further expand and build upon the work presented in this thesis.

9.1 Muscle synergy analysis is a valuable tool for technology assessment in rehabilitation

The studies presented in Part I of this thesis support the use of muscle synergy analysis as a valuable framework for evaluating how assistive technologies influence motor control. By providing a compact representation of coordinated muscle activation, muscle synergies allow the investigation of how robotic assistance interacts with the modular organization of movement during functional tasks in healthy subjects and neurological patients.

Across the studies conducted in healthy individuals, synergy-based analyses proved capable of capturing systematic modulations in muscle coordination induced by the Float exoskeleton. In particular, robotic assistance altered the relative contribution of specific muscles within the synergy structure while preserving the overall modular organization underlying anterior reaching. For example, the assistance provided by Float reduced the activation of the anterior deltoid during shoulder flexion, suggesting that the device effectively compensates part of the mechanical effort required to lift the arm. At the same time, an increased activation of the upper trapezius was observed, potentially reflecting limitations in the current gravity-compensation control strategy, which may increase the load perceived at the shoulder.

These findings indicate that the device can support task execution without disrupting the physiological coordination patterns underlying reaching, while also highlighting aspects of the control strategy that may benefit from further refinement. More broadly, they illustrate how muscle synergy analysis can provide quantitative information that is directly relevant to the design and optimization of assistive devices.

At the same time, the analyses performed on healthy participants highlighted the substantial inter-subject variability that characterizes muscle coordination. This variability appeared to become even more pronounced when robotic assistance was introduced, and preliminary observations suggested that factors such as age may influence the way individuals adapt their motor strategies in assisted conditions. These findings underline the challenges involved in establishing normative reference datasets of muscle synergies for comparison with pathological populations. Although such reference datasets are essential for interpreting alterations in motor coordination after neurological injury, the intrinsic variability of human motor control complicates the definition of a single reference synergy structure. Future efforts aimed at building normative synergy databases should therefore carefully consider potential sources of variability, including demographic factors and experimental conditions.

The exploratory study conducted in a small cohort of individuals with chronic post-stroke hemiparesis provided preliminary evidence that muscle synergy analysis can also capture changes in motor coordination induced by robotic assistance in neurological populations. Despite the limited sample size, the results suggested that the use of the Float exoskeleton may induce short-term modifications in the modular organization of muscle activity, with post-stroke participants showing an increased similarity between their synergy patterns and those observed in the healthy reference population following assisted reaching.

Although these observations should be interpreted with caution, they raise the possibility that robotic assistance may promote adaptive reorganization of motor coordination patterns even in chronic stages of stroke. Such changes could reflect mechanisms of motor learning or neuroplasticity that may support functional recovery. Future studies involving larger patient cohorts and integrating additional modalities, such as kinematic and electroencephalographic measures, will be necessary to determine whether these modifications in modular organization translate into measurable improvements in motor performance and to clarify their underlying neurophysiological mechanisms.

One factor limiting the interpretability of the muscle synergies presented in this work is the reduced variability of the reaching task. The number of targets was decreased from nine to three to improve clinical feasibility; indeed, only one post-stroke participant was unable to complete the protocol due to fatigue. However, this simplification also constrained task variability, which is crucial for extracting synergies that truly reflect the coordination strategies of the central nervous system. This limitation highlights a broader challenge in translating muscle synergy analysis to clinical settings. Motor control studies in healthy individuals typically rely on a wide range of movements to ensure the extraction of robust and representative synergies. In contrast, such variability is difficult to achieve in patients, particularly those with severe impairments. Clinical protocols tend to prioritize functional, task-specific movements that are practical and relevant but may lead to suboptimal estimation of the available synergy repertoire or to the identification of task-specific modules.

Therefore, as also noted in the literature (14), an effective clinical application of muscle synergy analysis requires a balance between experimental richness and practical feasibility. The task adopted in this PhD work represents a compromise in this sense: it is clinically relevant and reproducible in post-stroke individuals, even when performed with the most affected limb. Nevertheless, from a motor control perspective, despite involving a three-dimensional, multi-joint movement, it still lacks sufficient variability to ensure that the extracted synergies fully capture the underlying coordination strategies. Future work could explore the feasibility of introducing greater task variability in post-stroke populations, for example by increasing the number and spatial distribution of targets.

Overall, the findings presented in the first part of the thesis reinforce previous evidence that muscle synergy analysis constitutes a feasible and informative approach for the evaluation of rehabilitation technologies (7; 10; 12; 29).

One of the main factors preventing the adoption of synergy-based metrics for technology assessment in clinical practice is the heterogeneity of experimental paradigms, signal processing pipelines, and synergy extraction methods used across studies, which complicates the comparison and interpretation of results (14). The work presented in this thesis contributes to addressing this issue by relying on a standardized experimental framework based on a simplified yet functionally relevant three-dimensional reaching task that requires multi-joint coordination. This approach facilitates the extraction of meaningful synergy patterns while maintaining a level of experimental control that enables reproducibility across studies.

Furthermore, particular attention was devoted to the adoption of widely used EMG preprocessing procedures and standard methods for synergy extraction, with the aim of improving the comparability of the results with existing and future research. By combining a standardized experimental paradigm with established analysis methods, this work contributes to the broader effort of promoting muscle synergy analysis as a reliable neuromechanical biomarker for the objective assessment of assistive rehabilitation technologies.

9.2 The NeBULA framework provides a flexible structure for the multimodal assessment of technology

The studies presented in this thesis were conducted within the NeBULA (Neuromechanical Biomarkers for Upper Limb Assessment) framework, which proved to be a flexible platform for the multimodal evaluation of assistive technologies. The framework was designed to combine standardized experimental tasks with the acquisition of multiple physiological and biomechanical signals, enabling the systematic characterization of motor control during functional upper-limb movements.

One of the key advantages of the NeBULA paradigm is its ability to balance standardization and adaptability. While the framework provides a structured experimental protocol that ensures the comparability of measurements across sessions and participants, it can also be adapted to accommodate different experimental needs and populations. In this work, the paradigm was progressively refined during data collection in healthy individuals in order to reduce participant effort and overall experimental duration.

Similarly, the experimental design was adapted to address specific research questions when applied to post-stroke participants, enabling the investigation of potential short-term modifications in the control of anterior reaching induced by robotic assistance.

These adaptations demonstrate that the NeBULA framework can accommodate different experimental scenarios while preserving a common methodological structure. This balance between flexibility and standardization enables meaningful comparisons across datasets and populations, which is essential for the interpretation of neuromechanical biomarkers.

More broadly, standardized assessment frameworks such as NeBULA may contribute to improving the reproducibility and comparability of studies investigating rehabilitation technologies. By providing a structured yet adaptable platform for multimodal data collection, such frameworks can facilitate the creation of shared datasets and benchmarking protocols, ultimately supporting the development and evaluation of assistive devices across different research groups and clinical contexts.

9.3 Motor unit analysis provides a deeper knowledge on the neural control of movement

The studies presented in Part II of this thesis explored the potential of high-density EMG decomposition to characterize the neural drive to muscles during functional grasping tasks. By enabling the non-invasive identification of individual motor unit discharge patterns, hdEMG decomposition techniques provide access to the activity of spinal motor neurons, offering a more direct representation of motor commands than traditional surface EMG features.

The results of these studies demonstrate that motor unit analysis can provide valuable insight into the neural mechanisms underlying well-known limitations of myoelectric control systems. In particular, the analysis presented in Chapter 7 provide a neural-level interpretation of the variations observed in global EMG features across arm positions, which have long been recognized as a major factor contributing to the degradation of pattern recognition performance in real-life prosthetic control scenarios.

By linking posture-dependent variations in EMG signals to the behavior of individual motor units, this analysis contributes to a deeper understanding of how the neural drive to muscles is reorganized during functional movements. Such insights are important not only from a neurophysiological perspective but also for the design of more robust myoelectric interfaces capable of maintaining reliable performance across the wide range of limb configurations encountered in daily activities.

The study presented in Chapter 8 further explored the potential of motor unit–level descriptors for the decoding of motor intentions. The study demonstrated the feasibility of using motor unit–derived features to discriminate between different grasp types and different hand gesture in an offline setting. Importantly, the identification of distinct populations of motor units associated with specific gestures provides additional insight into the neural organization of hand motor control and suggests that gesture-specific patterns of motor unit activity may serve as informative signals for human–machine interfaces.

From the perspective of assistive technology, these findings highlight the potential advantages of interfacing control systems directly with motor unit activity. In principle, this could lead to more intuitive and reliable control of assistive devices such as myoelectric prostheses.

However, despite these promising results, several technical challenges currently limit the practical implementation of motor unit–based control strategies in real-time applications. The identification of motor units from high-density EMG signals relies on computationally intensive decomposition algorithms that require substantial processing time and careful validation of the extracted sources. As a consequence, the identification of reliable motor unit separation vectors is typically performed offline, which restricts the direct use of these methods for real-time control.

Some approaches have attempted to address this limitation by reapplying separation vectors obtained during an offline calibration phase to subsequent recordings (84). While this strategy may enable the online extraction of previously identified motor units, its reliability strongly depends on the stability of the recording conditions and on the accurate selection of physiologically valid separation vectors. In practice, even small changes in electrode placement, muscle geometry, or signal quality may lead to the extraction of signals that no longer exhibit the physiological characteristics of motor unit activity. These challenges highlight the need for further methodological developments before motor unit–based decoding can be robustly implemented in real-time assistive systems.

Overall, the results presented in this part of the thesis illustrate both the potential and the current limitations of motor unit analysis for the characterization and decoding of motor behavior during functional tasks. On one hand, hdEMG decomposition provides a powerful tool for investigating the neural mechanisms underlying motor control and for interpreting variations in surface EMG signals observed during natural movements. On the other hand, translating these insights into practical control strategies for assistive devices will require further advances in signal processing methods, computational efficiency, and recording stability.

Nevertheless, the ability to non-invasively access the activity of spinal motor neurons represents a significant step toward the development of human–machine interfaces that operate closer to the neural sources of motor commands. Continued research in this direction may ultimately contribute to the design of more robust and physiologically grounded control strategies for next-generation assistive technologies.

9.4 Motor unit characterization in complex motor tasks remains challenging

The analyses conducted within the ReGULA framework highlighted several methodological challenges associated with the extraction of motor unit activity during functional motor tasks. In particular, the efficacy of motor unit decomposition during the grasping phase of the protocol varied substantially across muscles and participants, and in some cases no reliable motor units could be identified.

One possible explanation for this variability lies in the behavioral nature of the ReGULA task. Although the grasp holding phase was designed to approximate an isometric contraction, the task was only partially constrained, as no mechanical restrictions were imposed on joint configuration or force output. This differs substantially from experimental paradigms specifically designed for motor unit decomposition, which typically involve tightly controlled isometric contractions with well-defined force levels. The greater freedom allowed in the execution of the task may therefore have complicated the identification of motor unit discharge patterns.

Additional factors may also have influenced the decomposition performance. Preliminary observations indicated a lower number of identifiable motor units in female participants compared with male participants, a phenomenon that has recently been reported in the literature and may be related to physiological and anatomical differences affecting the detectability of motor unit action potentials with surface recordings (73). These observations further highlight the importance of considering participant-specific factors when designing experimental protocols and interpreting motor unit analyses.

The contrast between the results obtained in Chapters 7 and 8 further illustrates the impact of experimental design on motor unit identification. In the latter study, a substantially higher number of motor units could be extracted, likely due to the more constrained experimental conditions. The protocol involved a single arm configuration that was relatively easy for participants to maintain, and transitions between hand gestures were separated by rest periods rather than dynamic arm movements. These conditions likely reduced variability in muscle activation and improved the stability of the recorded signals, facilitating motor unit decomposition. In addition, the use of a wireless recording system may have contributed to reducing the amount of environmental noise in the recording, improving overall signal quality.

Taken together, these observations highlight the inherent trade-off between ecological validity and experimental controllability in motor unit studies. While functional tasks such as those implemented in the ReGULA framework are essential for investigating motor control in contexts that resemble everyday activities, they also introduce variability that complicates the reliable extraction of motor unit activity. Careful experimental design therefore plays a crucial role in balancing these competing requirements and in enabling meaningful characterization of neural drive during complex motor behaviors.

9.5 Careful design of experimental protocol is a key point in the characterization of complex motor tasks

One important aspect addressed in this work was the development of structured experimental frameworks aimed at improving the reproducibility and comparability of measurements. The NeBULA and ReGULA paradigms were specifically designed to provide standardized tasks for the investigation of upper-limb motor behavior while enabling the synchronized acquisition of multiple physiological and biomechanical signals. Accurate synchronization between the different recording devices proved essential for the extraction of reliable neuromechanical metrics, particularly when combining information derived from EMG with kinematic or other physiological measurements.

At the same time, the experience gained throughout this research also highlighted how the questions that can be addressed by an experimental dataset are strongly constrained by the design choices made during protocol development. In some cases, additional analyses were performed to explore aspects that had not been explicitly considered during the initial design phase, which introduced methodological limitations. For example, in the study investigating potential age-related differences in muscle synergy structure, participants were stratified by age only during the analysis phase. As a consequence, the resulting age groups were relatively small and imbalanced, limiting the strength of the conclusions that could be drawn regarding the influence of age on motor coordination.

Similarly, in the design of the ReGULA framework, the primary objective was to investigate motor behavior during functional reaching and grasping tasks. Although these tasks provided valuable insights into the neural control of natural movements, the limited control over contraction levels and joint configurations reduced the efficacy of motor unit decomposition in some conditions. This complicated the identification of large populations of motor units but also enabled the exploration of neural activity during tasks that more closely resemble everyday behavior, which is rarely addressed in motor unit studies typically conducted under highly controlled laboratory conditions.

Taken together, these considerations underline the importance of carefully aligning experimental protocol design with the specific research questions being addressed. In studies of neuromuscular control, achieving a balance between experimental controllability and ecological validity remains a central challenge. Protocols that are too constrained may limit the relevance of the findings to real-world motor behavior, whereas more naturalistic tasks may introduce variability that complicates signal analysis. The development of experimental frameworks capable of navigating this balance will therefore remain a key aspect in advancing the study of motor control and in translating neurophysiological insights into practical applications for rehabilitation and assistive technologies.

9.6 Future Work

The results presented in this thesis open several directions for future research aimed at further advancing the use of EMG-derived metrics for the characterization of motor control and the development of assistive technologies.

Future directions for muscle synergy analysis

A first important direction concerns the extension of the muscle synergy analyses conducted in post-stroke participants. The exploratory results presented in this thesis were obtained from a limited subset of the available dataset, and future work will involve the analysis of the complete cohort of post-stroke subjects collected within the NeBULA framework. This larger dataset will allow a more comprehensive evaluation of how robotic assistance provided by the Float exoskeleton influences the modular organization of muscle activity during reaching movements.

Importantly, the dataset includes post-stroke participants who performed the task both with the paretic arm and with the less affected arm. This offers the opportunity to investigate whether muscle synergy analysis can detect subtle alterations in motor coordination also on the less affected side of hemiparetic individuals, a phenomenon that has been suggested in previous studies (96; 97). Such analyses may provide additional insight into the bilateral effects of stroke on motor control.

Another important aspect that emerged from the studies on healthy participants concerns the influence of age on the structure and variability of muscle synergies. Building on these findings, future analyses should aim to compare muscle synergies obtained from post-stroke subjects with reference synergies derived from age-matched healthy populations.

Constructing balanced and homogeneous reference datasets across different age ranges would improve the interpretability of synergy-based comparisons and could facilitate the identification of pathological deviations in motor coordination.

If the results of the complete analysis confirm the trends observed in the preliminary study presented in this thesis, they may motivate further investigations into the longer-term effects of robotic rehabilitation. In particular, future studies could explore whether repeated training sessions with the Float exoskeleton induce longitudinal changes in muscle synergy organization, potentially reflecting adaptive processes associated with motor recovery.

Future directions for motor unit analysis

Future work will also expand the motor unit analyses presented in this thesis. In the study reported here, the investigation focused primarily on the extensor carpi radialis muscle; however, extending the tracking of motor units to additional muscles involved in grasping, such as the flexor carpi ulnaris, may provide a more comprehensive characterization of the neural strategies underlying hand function.

Beyond the identification and tracking of motor units across conditions, further analyses will investigate additional descriptors of motor unit behavior, including discharge patterns and recruitment characteristics. These features may provide deeper insight into how the neural drive to muscles is modulated during different grasp types and across varying arm configurations.

Methodological improvements in signal acquisition may also contribute to enhancing the reliability of these analyses. In this context, future experimental campaigns may leverage newer hdEMG amplifiers, such as the Novecento system developed by OT Bioelettronica, which are expected to provide improved signal quality and stability. Higher-quality recordings may facilitate the identification of larger populations of motor units and improve the efficiency of decomposition algorithms during functional tasks.

Furthermore, the effect of limb position on myoelectric control remains an important topic for future investigation. The ReGULA dataset provides a particularly rich range of data for addressing this problem, as it includes recordings from multiple high-density EMG matrices distributed across the upper limb, as well as bipolar EMG and kinematic measurements. This comprehensive dataset could enable the exploration of strategies to mitigate the impact of limb posture on hand gesture recognition, potentially improving the robustness of pattern recognition–based control systems for prosthetic devices.

Integration of multimodal neuromechanical data

More broadly, a significant portion of the data collected within the NeBULA and ReGULA frameworks has not yet been fully explored within the scope of this thesis. Both paradigms were designed to acquire multimodal datasets combining EMG, high-density EMG, kinematics, and electroencephalography during functional upper-limb tasks. The integration of these complementary sources of information represents a promising direction for future research.

Combining neural, muscular, and biomechanical signals could enable the identification of multimodal biomarkers that capture different levels of the motor control hierarchy, from cortical activity to muscle activation and movement execution. Such integrated analyses may provide a more comprehensive understanding of the mechanisms underlying motor behavior and may support the development of more robust and physiologically grounded control strategies for rehabilitation technologies and assistive devices.

Overall, the datasets collected during this thesis provide a foundation for future investigations into the neural and neuromechanical mechanisms of upper-limb motor control. This may contribute not only to advancing fundamental knowledge in motor neuroscience but also to improving the design, assessment, and control of robotic technologies for individuals with motor impairments.

References

[1] E. Bizzi, V. C. K. Cheung, A. d'Avella, P. Saltiel, and M. Tresch, "Combining modules for movement," *Brain Research Reviews*, vol. 57, pp. 125–133, Jan. 2008.

[2] S. Buccelli, F. Tessari, F. Fanin, L. De Guglielmo, G. Capitta, C. Piezzo, A. Bruschi, F. Van Son, S. Scarpetta, A. Succi, P. Rossi, S. Maludrottu, G. Barresi, I. Creatini, E. Taglione, M. Laffranchi, and L. De Michieli, "A Gravity-Compensated Upper-Limb Exoskeleton for Functional Rehabilitation of the Shoulder Complex," *Applied Sciences*, vol. 12, p. 3364, Jan. 2022. Publisher: Multidisciplinary Digital Publishing Institute.

[3] F. Negro, S. Muceli, A. M. Castronovo, A. Holobar, and D. Farina, "Multi-channel intramuscular and surface EMG decomposition by convolutive blind source separation," *Journal of Neural Engineering*, vol. 13, p. 026027, Feb. 2016. Publisher: IOP Publishing.

[4] F. Garro, E. Fenoglio, I. Forsiuk, M. Canepa, M. Mozzon, L. De Michieli, S. Buccelli, M. Chiappalone, and M. Semprini, "NeBULA: A Standardized Protocol for the Benchmarking of Robotic-based Upper Limb Neurorehabilitation," *Annual International Conference of the IEEE Engineering in Medicine and Biology Society. IEEE Engineering in Medicine and Biology Society. Annual International Conference*, vol. 2023, pp. 1–4, July 2023.

[5] J. M. Veerbeek, E. van Wegen, R. van Peppen, P. J. van der Wees, E. Hendriks, M. Rietberg, and G. Kwakkel, "What is the evidence for physical therapy poststroke? A systematic review and meta-analysis," *PloS One*, vol. 9, no. 2, p. e87987, 2014.

[6] R. Riener, T. Nef, and G. Colombo, "Robot-aided neurorehabilitation of the upper extremities," *Medical & Biological Engineering & Computing*, vol. 43, pp. 2–10, Jan. 2005.

[7] E. Pirondini, M. Coscia, S. Marcheschi, G. Roas, F. Salsedo, A. Frisoli, M. Bergamasco, and S. Micera, "Evaluation of the effects of the Arm Light Exoskeleton on movement execution and muscle activities: a pilot study on healthy subjects," *Journal of Neuroengineering and Rehabilitation*, vol. 13, p. 9, Jan. 2016.

[8] J. Mehrholz, M. Pohl, T. Platz, J. Kugler, and B. Elsner, "Electromechanical and robot-assisted arm training for improving activities of daily living, arm function, and arm muscle strength after stroke," *The Cochrane Database of Systematic Reviews*, vol. 9, p. CD006876, Sept. 2018.

[9] J. M. Veerbeek, A. C. Langbroek-Amersfoort, E. E. H. van Wegen, C. G. M. Meskers, and G. Kwakkel, "Effects of Robot-Assisted Therapy for the Upper Limb After Stroke," *Neurorehabilitation and Neural Repair*, vol. 31, pp. 107–121, Feb. 2017.

[10] T. Lencioni, L. Fornia, T. Bowman, A. Marzegan, A. Caronni, A. Turolla, J. Jonsdottir, I. Carpinella, and M. Ferrarin, "A randomized controlled trial on the effects induced by robot-assisted and usual-care rehabilitation on upper limb muscle synergies in post-stroke subjects," *Scientific Reports*, vol. 11, p. 5323, Mar. 2021.

[11] V. Longatelli, D. Torricelli, J. Tornero, A. Pedrocchi, F. Molteni, J. L. Pons, and M. Gandolla, "A unified scheme for the benchmarking of upper limb functions in neurological disorders," *Journal of Neuroengineering and Rehabilitation*, vol. 19, p. 102, Sept. 2022.

[12] P. Tropea, V. Monaco, M. Coscia, F. Posteraro, and S. Micera, "Effects of early and intensive neuro-rehabilitative treatment on muscle synergies in acute post-stroke patients: a pilot study," *Journal of Neuroengineering and Rehabilitation*, vol. 10, p. 103, Oct. 2013.

[13] V. C. K. Cheung, A. Turolla, M. Agostini, S. Silvoni, C. Bennis, P. Kasi, S. Paganoni, P. Bonato, and E. Bizzi, "Muscle synergy patterns as physiological markers of motor cortical damage," *Proceedings of the National Academy of Sciences of the United States of America*, vol. 109, pp. 14652–14656, Sept. 2012.

[14] K. Zhao, Z. Zhang, H. Wen, B. Liu, J. Li, n. Andrea d'Avella, and A. Scano, "Muscle synergies for evaluating upper limb in clinical applications: A systematic review," *Heliyon*, vol. 9, p. e16202, May 2023.

[15] F. Garro, E. Fenoglio, I. Ceroni, I. Forsiuk, M. Canepa, M. Mozzon, A. Bruschi, F. Zippo, M. Laffranchi, L. De Michieli, S. Buccelli, M. Chiappalone, and M. Semprini, "An EEG-EMG dataset from a standardized reaching task for biomarker research in upper limb assessment," *Scientific Data*, vol. 12, p. 831, May 2025. Publisher: Nature Publishing Group.

[16] M. Semprini, A. V. Cuppone, I. Delis, V. Squeri, S. Panzeri, and J. Konczak, "Biofeedback Signals for Robotic Rehabilitation: Assessment of Wrist Muscle Activation Patterns in Healthy Humans," *IEEE transactions on neural systems and rehabilitation engineering: a publication of the IEEE Engineering in Medicine and Biology Society*, vol. 25, pp. 883–892, July 2017.

[17] M. Coscia, V. C. K. Cheung, P. Tropea, A. Koenig, V. Monaco, C. Bennis, S. Micera, and P. Bonato, "The effect of arm weight support on upper limb muscle synergies during reaching movements," *Journal of Neuroengineering and Rehabilitation*, vol. 11, p. 22, Mar. 2014.

[18] C. Pierella, E. Pirondini, N. Kinany, M. Coscia, C. Giang, J. Miehlbradt, C. Magnin, P. Nicolo, S. Dalise, G. Sgherri, C. Chisari, D. Van De Ville, A. Guggisberg, and S. Micera, "A multimodal approach to capture post-stroke temporal dynamics of recovery," *Journal of Neural Engineering*, vol. 17, p. 045002, Aug. 2020.

[19] D. Farina and A. Holobar, “Human?Machine Interfacing by Decoding the Surface Electromyogram [Life Sciences],” *IEEE Signal Processing Magazine*, vol. 32, pp. 115–120, Jan. 2015.

[20] I. Vujaklija, D. Farina, and O. C. Aszmann, “New developments in prosthetic arm systems,” *Orthopedic Research and Reviews*, vol. 8, pp. 31–39, 2016.

[21] A. Marinelli, N. Boccardo, F. Tessari, D. Di Domenico, G. Caserta, M. Canepa, G. Gini, G. Barresi, M. Laffranchi, L. De Michieli, and M. Semprini, “Active upper limb prostheses: a review on current state and upcoming breakthroughs,” *Progress in Biomedical Engineering*, vol. 5, Jan. 2023. Place: Bristol, England.

[22] S. Salminger, H. Stino, L. H. Pichler, C. Gstoettner, A. Sturma, J. A. Mayer, M. Szivak, and O. C. Aszmann, “Current rates of prosthetic usage in upper-limb amputees - have innovations had an impact on device acceptance?,” *Disability and Rehabilitation*, vol. 44, pp. 3708–3713, July 2022.

[23] R. N. Khushaba, A. Al-Timemy, S. Kodagoda, and K. Nazarpour, “Combined influence of forearm orientation and muscular contraction on EMG pattern recognition,” *Expert Systems with Applications*, vol. 61, pp. 154–161, Nov. 2016.

[24] A. Fougner, E. Scheme, A. D. C. Chan, K. Englehart, and O. Stavdahl, “Resolving the limb position effect in myoelectric pattern recognition,” *IEEE transactions on neural systems and rehabilitation engineering: a publication of the IEEE Engineering in Medicine and Biology Society*, vol. 19, pp. 644–651, Dec. 2011.

[25] F. Garro, M. Chiappalone, S. Buccelli, L. De Michieli, and M. Semprini, “Neuromechanical Biomarkers for Robotic Neurorehabilitation,” *Frontiers in Neurorobotics*, vol. 15, Oct. 2021. Publisher: Frontiers.

[26] L. Zhang, G. Jia, J. Ma, S. Wang, and L. Cheng, “Short and long-term effects of robot-assisted therapy on upper limb motor function and activity of daily living in patients post-stroke: a meta-analysis of randomized controlled trials,” *Journal of Neuroengineering and Rehabilitation*, vol. 19, p. 76, July 2022.

[27] M. A. Gull, S. Bai, and T. Bak, “A Review on Design of Upper Limb Exoskeletons,” *Robotics*, vol. 9, Mar. 2020. Company: Multidisciplinary Digital Publishing Institute Distributor: Multidisciplinary Digital Publishing Institute Institution: Multidisciplinary Digital Publishing Institute Label: Multidisciplinary Digital Publishing Institute Publisher: publisher.

[28] R. Magill, *Motor Learning and Control. Concepts and Applications*. Jan. 2007.

[29] A. Cancrini, P. Baitelli, M. L. Nicora, M. Malosio, A. Pedrocchi, and A. Scano, “The effects of robotic assistance on upper limb spatial muscle synergies in healthy people during planar upper-limb training,” *PLOS ONE*, vol. 17, p. e0272813, Aug. 2022. Publisher: Public Library of Science.

[30] H. J. Hermens, B. Freriks, C. Disselhorst-Klug, and G. Rau, “Development of recommendations for SEMG sensors and sensor placement procedures,” *Journal of Electromyography and Kinesiology: Official Journal of the International Society of Electrophysiological Kinesiology*, vol. 10, pp. 361–374, Oct. 2000.

[31] A. d'Avella, A. Portone, L. Fernandez, and F. Lacquaniti, "Control of fast-reaching movements by muscle synergy combinations," *The Journal of Neuroscience: The Official Journal of the Society for Neuroscience*, vol. 26, pp. 7791–7810, July 2006.

[32] D. D. Lee and H. S. Seung, "Learning the parts of objects by non-negative matrix factorization," *Nature*, vol. 401, pp. 788–791, Oct. 1999. Publisher: Nature Publishing Group.

[33] R. Penrose, "A generalized inverse for matrices," *Mathematical Proceedings of the Cambridge Philosophical Society*, vol. 51, pp. 406–413, July 1955.

[34] A. d'Avella, L. Fernandez, A. Portone, and F. Lacquaniti, "Modulation of phasic and tonic muscle synergies with reaching direction and speed," *Journal of Neurophysiology*, vol. 100, pp. 1433–1454, Sept. 2008.

[35] A. Scano, A. Chiavenna, M. Caimmi, M. Malosio, L. M. Tosatti, and F. Molteni, "Effect of human-robot interaction on muscular synergies on healthy people and post-stroke chronic patients," *IEEE ... International Conference on Rehabilitation Robotics: [proceedings]*, vol. 2017, pp. 527–532, July 2017.

[36] G. B. Prange, L. a. C. Kallenberg, M. J. A. Jannink, A. H. A. Stienen, H. van der Kooij, M. J. Ijzerman, and H. J. Hermens, "Influence of gravity compensation on muscle activity during reach and retrieval in healthy elderly," *Journal of Electromyography and Kinesiology: Official Journal of the International Society of Electrophysiological Kinesiology*, vol. 19, pp. e40–49, Apr. 2009.

[37] G. B. Prange, M. J. A. Jannink, A. H. A. Stienen, H. van der Kooij, M. J. Ijzerman, and H. J. Hermens, "Influence of gravity compensation on muscle activation patterns during different temporal phases of arm movements of stroke patients," *Neurorehabilitation and Neural Repair*, vol. 23, pp. 478–485, June 2009.

[38] T. M. Sukal, M. D. Ellis, and J. P. A. Dewald, "Shoulder abduction-induced reductions in reaching work area following hemiparetic stroke: neuroscientific implications," *Experimental Brain Research*, vol. 183, pp. 215–223, Nov. 2007.

[39] J. T. Levine, X. S. Yu, R. Muñoz, A. Fiorenza, T. Smith, I. Djuraskovic, J. D. Peiffer, E. Ambrosini, S. Ferrante, R. Webster, J. Sakai, J. Robison, E. J. Roth, J. Laczko, R. J. Cotton, A. Pedrocchi, and J. L. Pons, "Synergy-based functional electrical stimulation for gait rehabilitation in chronic stroke: a pilot study," Sept. 2025. ISSN: 3067-2007 Pages: 2025.05.21.25328035.

[40] I. Ceroni, F. Garro, and m. Semprini, "Modular Organization of Reaching Movement Performed With and Without the FLOAT Upper Limb Exoskeleton," in *Converging Clinical and Engineering Research on Neurorehabilitation V* (J. L. Pons, J. Tornero, and M. Akay, eds.), (Cham), pp. 352–356, Springer Nature Switzerland, 2025.

[41] I. Ceroni, F. Garro, and M. Semprini, "Effect of Robotic Assistance on the Synergistic Organization of Reaching Movements," *IEEE ... International Conference on Rehabilitation Robotics: [proceedings]*, vol. 2025, pp. 796–801, May 2025.

[42] A. Scano, L. Dardari, F. Molteni, H. Giberti, L. M. Tosatti, and A. d'Avella, "A Comprehensive Spatial Mapping of Muscle Synergies in Highly Variable Upper-Limb Movements of Healthy Subjects," *Frontiers in Physiology*, vol. 10, Sept. 2019. Publisher: Frontiers.

[43] K. Zhao, Z. Zhang, H. Wen, and A. Scano, "Intra-Subject and Inter-Subject Movement Variability Quantified with Muscle Synergies in Upper-Limb Reaching Movements," *Biomimetics*, vol. 6, Oct. 2021. Company: Multidisciplinary Digital Publishing Institute Distributor: Multidisciplinary Digital Publishing Institute Institution: Multidisciplinary Digital Publishing Institute Label: Multidisciplinary Digital Publishing Institute Publisher: publisher.

[44] X. Guo, B. He, K. Y. S. Lau, P. P. K. Chan, R. Liu, J. J. Xie, S. C. W. Ha, C.-Y. Chen, G. L. Y. Cheing, R. T. H. Cheung, R. H. M. Chan, and V. C. K. Cheung, "Age-Related Modifications of Muscle Synergies and Their Temporal Activations for Overground Walking," *IEEE transactions on neural systems and rehabilitation engineering: a publication of the IEEE Engineering in Medicine and Biology Society*, vol. 30, pp. 2700–2709, 2022.

[45] V. Monaco, A. Ghionzoli, and S. Micera, "Age-related modifications of muscle synergies and spinal cord activity during locomotion," *Journal of Neurophysiology*, vol. 104, pp. 2092–2102, Oct. 2010.

[46] R. J. Baggen, J. H. v. Dieën, E. V. Roie, S. M. Verschueren, G. Giarmatzis, C. Delecluse, and N. Dominici, "Age-Related Differences in Muscle Synergy Organization during Step Ascent at Different Heights and Directions," *Applied Sciences*, vol. 10, Mar. 2020. Company: Multidisciplinary Digital Publishing Institute Distributor: Multidisciplinary Digital Publishing Institute Institution: Multidisciplinary Digital Publishing Institute Label: Multidisciplinary Digital Publishing Institute Publisher: publisher.

[47] C. Ye, S. S. Saboksayr, W. Shaw, R. O. Coats, S. L. Astill, G. Mateos, and I. Delis, "A tensor decomposition reveals ageing-induced differences in muscle and grip-load force couplings during object lifting," *Scientific Reports*, vol. 14, p. 13937, June 2024. Publisher: Nature Publishing Group.

[48] S. Huang, X. Guo, J. J. Xie, K. Y. S. Lau, R. Liu, A. D. P. Mak, V. C. K. Cheung, and R. H. M. Chan, "Rectified Latent Variable Model-Based EMG Factorization of Inhibitory Muscle Synergy Components Related to Aging, Expertise and Force–Tempo Variations," *Sensors*, vol. 24, Apr. 2024. Company: Multidisciplinary Digital Publishing Institute Distributor: Multidisciplinary Digital Publishing Institute Institution: Multidisciplinary Digital Publishing Institute Label: Multidisciplinary Digital Publishing Institute Publisher: publisher.

[49] R. D. Seidler, J. A. Bernard, T. B. Burutolu, B. W. Fling, M. T. Gordon, J. T. Gwin, Y. Kwak, and D. B. Lipps, "Motor control and aging: links to age-related brain structural, functional, and biochemical effects," *Neuroscience and Biobehavioral Reviews*, vol. 34, pp. 721–733, Apr. 2010.

[50] W. G. Darling, J. D. Cooke, and S. H. Brown, "Control of simple arm movements in elderly humans," *Neurobiology of Aging*, vol. 10, no. 2, pp. 149–157, 1989.

[51] L. M. Shiffman, "Effects of aging on adult hand function," *The American Journal of Occupational Therapy: Official Publication of the American Occupational Therapy Association*, vol. 46, pp. 785–792, Sept. 1992.

[52] C. Dussault-Picard, S. Havashinezhadian, N. A. Turpin, F. Moissenet, K. Turcot, and Y. Cherni, "Age-related modifications of muscle synergies during daily-living tasks: A scoping review," *Clinical Biomechanics*, vol. 113, p. 106207, Mar. 2024.

[53] S. Ranaldi, C. De Marchis, G. Severini, and S. Conforto, "An Objective, Information-Based Approach for Selecting the Number of Muscle Synergies to be Extracted via Non-Negative Matrix Factorization," *IEEE transactions on neural systems and rehabilitation engineering: a publication of the IEEE Engineering in Medicine and Biology Society*, vol. 29, pp. 2676–2683, 2021.

[54] R. Macchi, A. Santuz, A. Hays, F. Vercruyssen, A. Arampatzis, A. Bar-Hen, and C. Nicol, "Sex influence on muscle synergies in a ballistic force-velocity test during the delayed recovery phase after a graded endurance run," *Heliyon*, vol. 8, p. e09573, June 2022.

[55] M. Kristiansen, A. Samani, P. Madeleine, and E. A. Hansen, "Effects of 5 Weeks of Bench Press Training on Muscle Synergies: A Randomized Controlled Study," *Journal of Strength and Conditioning Research*, vol. 30, pp. 1948–1959, July 2016.

[56] M. Flanders and U. Herrmann, "Two components of muscle activation: scaling with the speed of arm movement," *Journal of Neurophysiology*, vol. 67, pp. 931–943, Apr. 1992.

[57] F. Tessari, K. Yao, and N. Hogan, "Surpassing Cosine Similarity for Multidimensional Comparisons: Dimension Insensitive Euclidean Metric," Mar. 2025. arXiv:2407.08623 [cs].

[58] D. o. H. . H. Services, "Effects of stroke." Publisher: Department of Health & Human Services.

[59] V. L. Feigin, M. Brainin, B. Norrving, S. Martins, R. L. Sacco, W. Hacke, M. Fisher, J. Pandian, and P. Lindsay, "World Stroke Organization (WSO): Global Stroke Fact Sheet 2022," *International Journal of Stroke: Official Journal of the International Stroke Society*, vol. 17, pp. 18–29, Jan. 2022.

[60] H. Nakayama, H. S. Jørgensen, H. O. Raaschou, and T. S. Olsen, "Recovery of upper extremity function in stroke patients: the Copenhagen Stroke Study," *Archives of Physical Medicine and Rehabilitation*, vol. 75, pp. 394–398, Apr. 1994.

[61] V. M. Parker, D. T. Wade, and R. Langton Hewer, "Loss of arm function after stroke: measurement, frequency, and recovery," *International Rehabilitation Medicine*, vol. 8, no. 2, pp. 69–73, 1986.

[62] C. A. Trombly, *Occupational Therapy for Physical Dysfunction*. Lippincott Williams & Wilkins, 1989. Google-Books-ID: v6lzrgEACAAJ.

[63] V. Mathiowetz, G. Volland, N. Kashman, and K. Weber, "Adult norms for the Box and Block Test of manual dexterity," *The American Journal of Occupational Therapy: Official Publication of the American Occupational Therapy Association*, vol. 39, pp. 386–391, June 1985.

[64] G. Kwakkel, B. Kollen, and E. Lindeman, "Understanding the pattern of functional recovery after stroke: facts and theories," *Restorative Neurology and Neuroscience*, vol. 22, no. 3-5, pp. 281–299, 2004.

[65] M. Cutkosky, "On grasp choice, grasp models, and the design of hands for manufacturing tasks," *IEEE Transactions on Robotics and Automation*, vol. 5, pp. 269–279, June 1989.

[66] H. M. Schambra, A. Parnandi, N. G. Pandit, J. Uddin, A. Wirtanen, and D. M. Nilsen, "A Taxonomy of Functional Upper Extremity Motion," *Frontiers in Neurology*, vol. 10, Aug. 2019. Publisher: Frontiers.

[67] M. Laffranchi, N. Boccardo, S. Traverso, L. Lombardi, M. Canepa, A. Lince, M. Semprini, J. A. Saglia, A. Naceri, R. Sacchetti, E. Gruppioni, and L. De Michieli, "The Hannes hand prosthesis replicates the key biological properties of the human hand," *Science Robotics*, vol. 5, p. eabb0467, Sept. 2020. Publisher: American Association for the Advancement of Science.

[68] F. Stival, S. Michieletto, M. Cognolato, E. Pagello, H. Müller, and M. Atzori, "A quantitative taxonomy of human hand grasps," *Journal of NeuroEngineering and Rehabilitation*, vol. 16, p. 28, Dec. 2019.

[69] "SHAP: Southampton Hand Assessment Procedure."

[70] J. D. Howard, J. D. Hoit, R. M. Enoka, and Z. Hasan, "Relative activation of two human elbow flexors under isometric conditions: a cautionary note concerning flexor equivalence," *Experimental Brain Research*, vol. 62, pp. 199–202, Mar. 1986.

[71] J. C. Jamison and G. E. Caldwell, "Muscle synergies and isometric torque production: influence of supination and pronation level on elbow flexion," *Journal of Neurophysiology*, vol. 70, pp. 947–960, Sept. 1993. Publisher: American Physiological Society.

[72] A. Holobar and D. Zazula, "Multichannel Blind Source Separation Using Convolution Kernel Compensation," *IEEE Transactions on Signal Processing*, vol. 55, pp. 4487–4496, Sept. 2007.

[73] C. A. Taylor, B. H. Kopicko, F. Negro, and C. K. Thompson, "Sex differences in the detection of motor unit action potentials identified using high-density surface electromyography," *Journal of electromyography and kinesiology : official journal of the International Society of Electrophysiological Kinesiology*, vol. 65, p. 102675, Aug. 2022.

[74] S. Avrillon, F. Hug, S. N. Baker, C. Gibbs, and D. Farina, "Tutorial on MUedit: An open-source software for identifying and analysing the discharge timing of motor units from electromyographic signals," *Journal of Electromyography and Kinesiology*, vol. 77, p. 102886, Aug. 2024.

[75] A. S. Hassan, E. H. Kim, O. U. Khurram, M. Cummings, C. K. Thompson, L. M. McPherson, C. Heckman, J. P. Dewald, and F. Negro, "Properties of Motor Units of Elbow and Ankle Muscles Decomposed Using High-Density Surface EMG," *Conference proceedings : ... Annual International Conference of the IEEE Engineering in Medicine and Biology Society. IEEE Engineering in Medicine and Biology Society. Annual Conference*, vol. 2019, pp. 3874–3878, July 2019.

[76] F. Hug, S. Avrillon, A. Del Vecchio, A. Casolo, J. Ibanez, S. Nuccio, J. Rossato, A. Holobar, and D. Farina, "Analysis of motor unit spike trains estimated from high-density surface electromyography is highly reliable across operators," *Journal of Electromyography and Kinesiology*, vol. 58, p. 102548, June 2021.

[77] X. Hu, W. Z. Rymer, and N. L. Suresh, "Reliability of spike triggered averaging of the surface electromyogram for motor unit action potential estimation," *Muscle & Nerve*, vol. 48, no. 4, pp. 557–570, 2013. _eprint: https://onlinelibrary.wiley.com/doi/pdf/10.1002/mus.23819.

[78] E. Martinez-Valdes, F. Negro, C. M. Laine, D. Falla, F. Mayer, and D. Farina, "Tracking motor units longitudinally across experimental sessions with high-density surface electromyography," *The Journal of Physiology*, vol. 595, pp. 1479–1496, Mar. 2017.

[79] C. Chen, Y. Yu, S. Ma, X. Sheng, C. Lin, D. Farina, and X. Zhu, "Hand gesture recognition based on motor unit spike trains decoded from high-density electromyography," *Biomedical Signal Processing and Control*, vol. 55, p. 101637, Jan. 2020.

[80] D. Enrico, I. Ceroni, H. V. Cabral, F. Negro, and M. Semprini, "Evaluation of Hand Gesture Classification Based on Motor Units Activation for Prosthetic Application," *Annual International Conference of the IEEE Engineering in Medicine and Biology Society. IEEE Engineering in Medicine and Biology Society. Annual International Conference*, vol. 2025, pp. 1–7, July 2025.

[81] B. Hudgins, P. Parker, and R. Scott, "A new strategy for multifunction myoelectric control," *IEEE Transactions on Biomedical Engineering*, vol. 40, pp. 82–94, Jan. 1993.

[82] A. Phinyomark, P. Phukpattaranont, and C. Limsakul, "Feature reduction and selection for EMG signal classification," *Expert Systems with Applications*, vol. 39, pp. 7420–7431, June 2012.

[83] D. Farina, I. Vujaklija, M. Sartori, T. Kapelner, F. Negro, N. Jiang, K. Bergmeister, A. Andalib, J. Principe, and O. C. Aszmann, "Man/machine interface based on the discharge timings of spinal motor neurons after targeted muscle reinnervation," *Nature Biomedical Engineering*, vol. 1, p. 0025, Feb. 2017. Publisher: Nature Publishing Group.

[84] C. Chen, Y. Yu, X. Sheng, J. Meng, and X. Zhu, "Real-Time Hand Gesture Recognition by Decoding Motor Unit Discharges Across Multiple Motor Tasks From Surface Electromyography," *IEEE transactions on bio-medical engineering*, vol. 70, pp. 2058–2068, July 2023.

[85] T. Kapelner, I. Vujaklija, N. Jiang, F. Negro, O. C. Aszmann, J. Principe, and D. Farina, "Predicting wrist kinematics from motor unit discharge timings for the control of active prostheses," *Journal of NeuroEngineering and Rehabilitation*, vol. 16, p. 47, Apr. 2019.

[86] K. Englehart and B. Hudgins, "A robust, real-time control scheme for multifunction myoelectric control," *IEEE transactions on bio-medical engineering*, vol. 50, pp. 848–854, July 2003.

[87] R. A. Fisher, "THE USE OF MULTIPLE MEASUREMENTS IN TAXONOMIC PROBLEMS," *Annals of Eugenics*, vol. 7, pp. 179–188, Sept. 1936. Publisher: John Wiley & Sons, Ltd.

[88] N. Cristianini and J. Shawe-Taylor, *An Introduction to Support Vector Machines and Other Kernel-based Learning Methods*. Cambridge: Cambridge University Press, 2000.

[89] X. Glorot, "Understanding the difficulty of training deep feedforward neural networks," *Journal of Machine Learning Research - Proceedings Track*, vol. 9, pp. 249–256, Jan. 2010.

[90] S. C. Lemon, J. Roy, M. A. Clark, P. D. Friedmann, and W. Rakowski, "Classification and regression tree analysis in public health: methodological review and comparison with logistic regression," *Annals of Behavioral Medicine: A Publication of the Society of Behavioral Medicine*, vol. 26, pp. 172–181, Dec. 2003.

[91] M. Pelikan, "Bayesian Optimization Algorithm," in *Hierarchical Bayesian Optimization Algorithm: Toward a new Generation of Evolutionary Algorithms* (M. Pelikan, ed.), pp. 31–48, Berlin, Heidelberg: Springer, 2005.

[92] A. E. Hoerl and R. W. Kennard, "Ridge Regression: Biased Estimation for Nonorthogonal Problems," *Technometrics*, vol. 12, no. 1, pp. 55–67, 1970. Publisher: [Taylor & Francis, Ltd., American Statistical Association, American Society for Quality].

[93] J. H. Friedman, "Regularized Discriminant Analysis," *Journal of the American Statistical Association*, vol. 84, no. 405, pp. 165–175, 1989. Publisher: [American Statistical Association, Taylor & Francis, Ltd.].

[94] D. Farina, A. Holobar, R. Merletti, and R. M. Enoka, "Decoding the neural drive to muscles from the surface electromyogram," *Clinical Neurophysiology: Official Journal of the International Federation of Clinical Neurophysiology*, vol. 121, pp. 1616–1623, Oct. 2010.

[95] G. Purushothaman and R. Vikas, "Identification of a feature selection based pattern recognition scheme for finger movement recognition from multichannel EMG signals," *Australasian Physical & Engineering Sciences in Medicine*, vol. 41, pp. 549–559, June 2018.

[96] M. A. Dimyan and L. G. Cohen, "Neuroplasticity in the context of motor rehabilitation after stroke," *Nature Reviews. Neurology*, vol. 7, pp. 76–85, Feb. 2011.

[97] A. R. Luft, S. McCombe-Waller, J. Whitall, L. W. Forrester, R. Macko, J. D. Sorkin, J. B. Schulz, A. P. Goldberg, and D. F. Hanley, "Repetitive bilateral arm training and motor cortex activation in chronic stroke: a randomized controlled trial," *JAMA*, vol. 292, pp. 1853–1861, Oct. 2004.

[98] R. C. Sîmpetru, D. I. Braun, A. U. Simon, M. März, V. Cnejevici, D. S. de Oliveira, N. Weber, J. Walter, J. Franke, D. Höglinger, C. Prahm, M. Ponfick, and A. Del Vecchio, "MyoGestic: EMG interfacing framework for decoding multiple spared motor dimensions in individuals with neural lesions," *Science Advances*, vol. 11, p. eads9150, Apr. 2025. Publisher: American Association for the Advancement of Science.

[99] R. C. Sîmpetru, M. März, and A. Del Vecchio, "Proportional and Simultaneous Real-Time Control of the Full Human Hand From High-Density Electromyography," *IEEE Transactions on Neural Systems and Rehabilitation Engineering*, vol. 31, pp. 3118–3131, 2023.

Appendix A

Fingertip position prediction based on dry EMG bracelet

During a 4 months visiting period at the N2 Lab (Friedrich-Alexander-Universität, Erlangen) I explored the feasibility of predicting the kinematic of a virtual hand from a 32-channels dry EMG bracelet.

A.1 Materials and Methods

I collected EMG data from the dominant forearm of five healthy individuals performing 9 hand gestures (Figure A.1A). Each gesture lasted 30 seconds and was guided by a virtual hand displayed in a monitor (98). The fingers of the virtual hand were moving from complete extension (value of 0) to complete flexion (value of 1) following a sinusoidal trajectory. Both the raw EMG and a low-pass filtered (20 Hz cutoff) representation of EMG were used as input for the prediction. EMG and virtual kinematic data were chunked in windows of 180 ms with a 9 ms step. The mean kinematic over each window was used as ground truth. The dataset was split into a training set (70%), testing set (30%) and validation set (10% of testing). A deep learning model was adapted from a previous work (99). It combines a convolutional neural network (CNN) with a multilayer perceptron (MLP). I derived two versions of this model by modifying its structure and adapting its hyperparameters. In the first version, the MLP had two hidden layers of 128 neurons and 5 outputs to predict the kinematic of the 5 fingertips simultaneously (Figure A.1C). In the second version, the MLP had three hidden layers of 1024, 512 and 128 neurons and only one output predicting the kinematic of one single fingertip (Figure A.1D). In this case, five identical models have been trained to predict the five fingertips. In the first version the loss function was the mean absolute error, while in the second version the Huber loss was used.

A.2 Results

While the first version of the model does not allow to robustly identify single finger movements (Figure A.1E), the second version consistently detects movement onset across all hand gestures (Figure A.1F), which is promising for possible real-time applications of this version of the model.

A.3 Discussion and Conclusion

The deep learning model used in this exploratory study previously demonstrated high performance in predicting real hand kinematics from high-density EMG recordings acquired with multiple electrode grids (99). In the present work, we investigated whether a similar approach could be applied using a more practical acquisition setup based on a 32-channel dry EMG bracelet, which is easier and faster to deploy and therefore potentially more suitable for assistive technology applications.

In this configuration, the regression performance was lower than that reported in the previous study. This difference may be explained by the reduced spatial resolution of the bracelet compared to high-density EMG grids, the potentially lower signal quality associated with dry electrodes, and the use of virtual hand kinematics as ground truth, which may not provide sufficient variability for the model to learn detailed EMG–kinematic relationships.

Despite these limitations, the second model configuration was able to consistently detect movement onset across gestures, suggesting potential for applications requiring coarse motion detection. In the context of the ongoing collaboration with the N2 Lab, further experiments combining the graphical interface with motion capture measurements are planned to better assess the applicability of this approach in more realistic conditions.

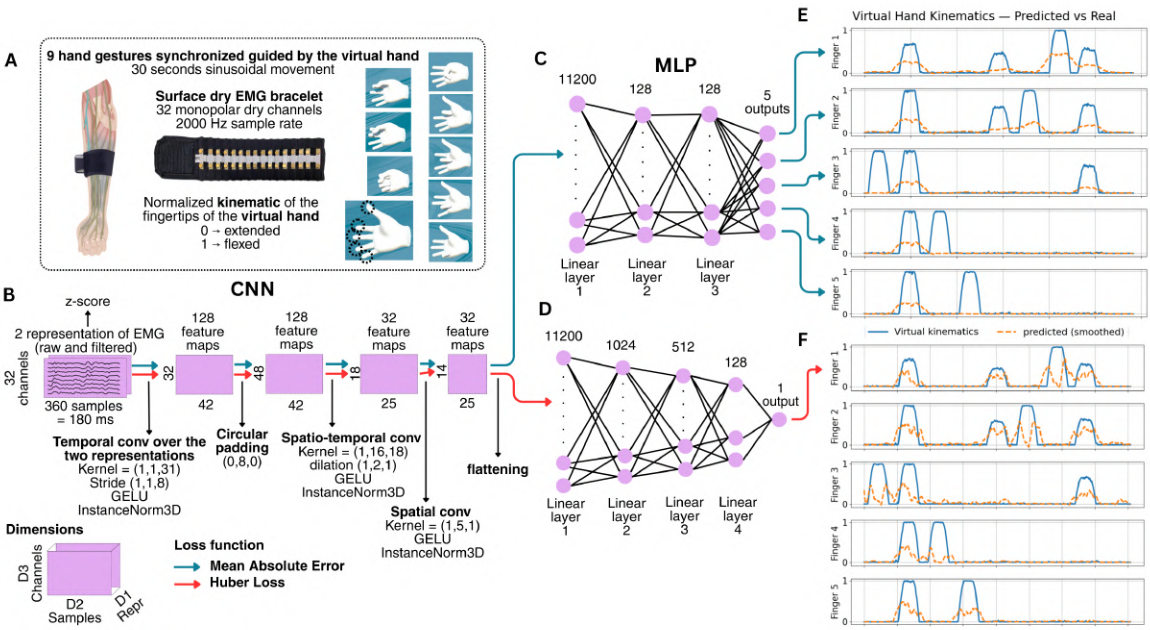

Figure A.1 Results of fingertip position regression for a pilot subject. A) Data acquisition protocol. B) Convolutional neural network structure. C) First version of the multilayer perceptron. D) Second version of the multilayer perceptron. E, F) Results on one pilot subject for the two versions of the neural network.